CENTER *for* MUSCULOSKELETAL RESEARCH

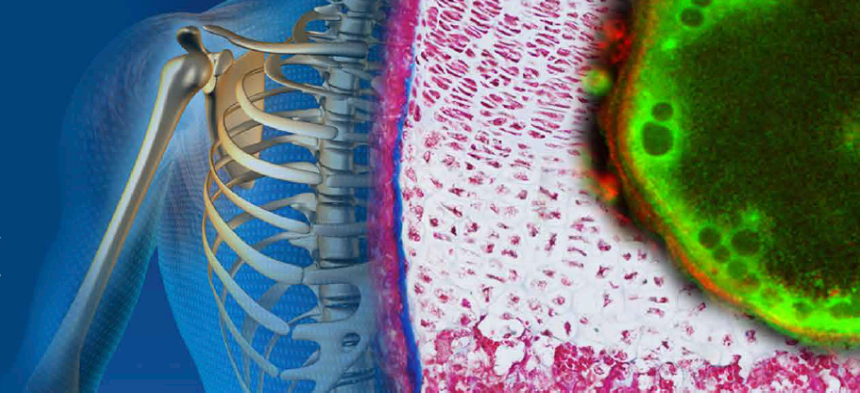

11th Annual CMSR Symposium

Wednesday, October 27, 2021

Sponsored By

Department of Orthopaedics and Rehabilitation
University of Rochester Medical Center
&
National Institute of Arthritis and Musculoskeletal and Skin Diseases (NIAMS) Grant T32 AR076950

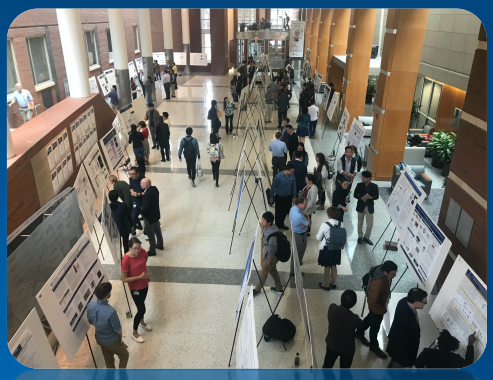

MEDICINE *of* THE HIGHEST ORDER

UR MEDICINE

ROCMSK Training Program

The Annual CMSR symposium is the center piece of the NIH/NIAMS funded T32 program entitled “Rochester Musculoskeletal (ROCMSK) Training Program” at the University of Rochester Medical Center. This program is designed to provide interdisciplinary didactic and research training in musculoskeletal science.

The overarching goal of ROCMSK Training Program is to develop future generations of interdisciplinary musculoskeletal scientists and leaders of innovations. The program is administered in The Center for Musculoskeletal Research (CMSR) at the University of Rochester and integrates 21 highly-collaborative faculty with primary appointments in 7 academic and clinical departments. The CMSR and associated training faculty represent a highly integrated group of Mentors that provide research training opportunities in Bone Biology and Disease, Cartilage Mechanobiology, Arthritis, and Regenerative Therapies, Tendon Development, Repair and Regenerative Engineering, Muscle Biology and Disease, Drug Delivery, Fracture Repair and Bone Tissue Engineering, Musculoskeletal Infection, Stem Cells and Musculoskeletal Development and Regenerative Biology, and Skeletal Cancer Biology and Therapeutics, as can be seen from the abstracts featured in this symposium.

The education program ensures a comprehensive understanding of musculoskeletal science that is seamlessly accessible to all CMSR trainees at every academic level. ROCMSK training emphasizes basic and translational science education. The training experience aims to build competency in areas ranging from the most basic molecular and genetic studies to the design and execution of human clinical trials. This year, ROCMSK awarded 2 pre-doctoral and 2 post-doctoral training seats.

This symposium is a celebration of the Trainees’ accomplishments.

Center for MusculoSkeletal Research

11th Annual CMSR Sympsoium

Wednesday, October 27, 2021

Zoom Registration Link https://urmc.zoom.us/webinar/register/WN_RVdp9ANIQHqQzeYRYI_s7g

Trainee Presentations Session - Class of 1962 Auditorium

	9:00 AM	Welcome & Opening Remarks	Awad, Rubery

Trainees Presentations

Post-Doc Rosier Awards Finalists	9:15 AM	Defining the epitenon cellular environment	Anne Nichols, PhD
	9:27 AM	Aged callus skeletal stem/progenitor cells contain an osteo-inflammatory subcluster with increased IRF-STAT pathways	Xi Lin, PhD
	9:39 AM	Novel strategies to purify murine mesenchymal stem cell (MSC) ex vivo reveal differential characteristics of bone marrow and bone derived stromal cells	Yuko Kawano, MD, PhD
Pre-Doc Rosier Awards Finalists	9:51 AM	Mitochondrial function controlled by the permeability transition pore/Cyclophilin D is an important regulator of bone phenotype and skeletal aging	Rubens Sautchuk Jr
	10:03 AM	Inducible depletion of Scx-lin cells disrupts tendon homeostasis and accelerates aging-associated compositional and structural changes in the extracellular matrix	Antonion Korcari
	10:15 AM	High-throughput semi-automated segmentation of murine hindpaw micro-CT datasets identifies the cuboid as a reliable longitudinal biomarker of arthritic progression in TNF-Tg mice	H. Mark Kenney
	10:27 AM	Semi-randomized zwitterionic peptides provide anti-fouling behavior to nanoparticles	Clyde Overby
	10:39 AM	Human Tissue-on-Chip (hToC) platform for modeling inflammation, fibrosis, and cell cycle regulation in fibrovascular tendon healing	Raquel Ajalik
	10:51 AM	Effects of elevated lactate levels in acute myeloid leukemia on the bone marrow microenvironment through polarization of leukemia-associated macrophages	Celia Soto
	11:03 AM	Health care disparities in complication and mortality rates following surgical management of cauda equina syndrome	Peter Joo
	11:30 AM	3MT (3-Minute Teasers) – Poster Award Finalists	
	12:15 PM	**Poster Session - Helen Wood Hall - Evarts Lounge**	

Plenary Session - Class of 1962 Auditorium

CMSR Faculty Spotlight

2:40 PM	**Roman Eliseev, MD PhD**	The role of mitochondria in bone health and disease
3:00 PM	**Calvin Cole, PhD**	Elucidating the Mechanism(s) of Skeletal Muscle Loss in a Murine Model of Pancreatic Cancer
3:20 PM	**Benjamin Frisch, PhD**	The dysfunctional microenvironment in the leukemic bone marrow
3:40 PM	**Jennifer Jonason, PhD**	All That's Certain in Osteoarthritis: Death and the SASP

Keynote Presentation

4:00 PM **Mary Bouxsein, PhD**

Fractures in Older Adults: Beyond BMD

5:30 PM **Dinner & Awards - Helen Wood Hall - Evarts Lounge**

MEDICINE of THE HIGHEST ORDER

UR MEDICINE

Keynote Speaker: Mary Bouxsein, PhD

Director, Center for Advanced Orthopaedic Studies,
Beth Israel Deaconess Medical Center
Professor, Department of Orthopedic Surgery,
Harvard Medical School
Associate Biologist, Department of Medicine, Massachusetts General Hospital
Member, NIAMS Advisory Council, National Institutes of Health

Dr. Bouxsein received her BS degree in General Engineering from the University of Illinois at Urbana-Champaign, and PhD in Mechanical Engineering from Stanford University, studying the effects of exercise on the skeleton with Dennis Carter, PhD and Robert Marcus, MD. She then completed a post-doctoral fellowship at the Orthopedic Biomechanics Laboratory at Beth Israel Deaconess Medical Center and Harvard Medical School under the mentorship of Wilson C. Hayes, PhD. She currently holds joint appointments as a Professor of Orthopedic Surgery at Harvard Medical School, adjunct Assistant Professor of Mechanical Engineering at Boston University, and is also a faculty member in the MIT-Bioastronautics Program.

Dr. Bouxsein has received more than 20 national and international honors, most recently the Adele Boskey Award from the American Society for Bone and Mineral Research. She has published over 330 peer-reviewed articles and more than 40 book chapters and invited editorials and reviews.

Dr. Bouxsein is world-renowned for her research, which has provided critical insights into the biomechanical factors that contribute to skeletal fragility with aging, as well as provided an improved understanding of how diet and exercise (or lack of exercise, i.e., disuse) impact bone metabolism, microarchitecture and strength.

Podium Abstracts

Disclaimer

Title: **Defining the epitenon cellular environment**

Presenting Author: Anne Nichols

Co-Authors: none

Lab PI / Mentor: Alayna Loiselle

Abstract (3500 characters or 500 words Limit)

Tendons are defined by their hierarchical structure which consists of bundles of collagen fascicles bound together by a thin sheet of connective tissue called the epitenon. Though thought to be a crucially important cellular source for tendon growth, healing, homeostasis, and adaptation, almost nothing is definitively known about the epitenon due to a lack of genetic markers with which to target epitenon cell populations. Through lineage tracing, we recently identified a novel cell population (GLASTLin) found in the epitenon of multiple tendons (including flexor, tail, and Achilles tendons) in adult mice, facilitating cell-based investigation of this important tendon structure for the first time. Our recent efforts have been focused on characterizing the cellular environment of the epitenon during homeostasis by examining GLASTLin cells using various imaging modalities and single-cell RNA-sequencing (scRNA-seq). In situ imaging revealed that not only are GLASTLin cells found in single cell layer on the surface of the tendon, but GLASTLin perivascular cells, adipocytes, and pericyte-like cells are also found in the epitenon space demonstrating both the heterogeneity of this cell population and complexity of the epitenon cellular landscape. To better understand the identity of GLASTLin cells, we performed scRNA-seq. In line with our in situ imaging observations, small numbers of GLASTLin cells were found in clusters representing ancillary cellular components of the epitenon niche including perivascular cells, muscle cells, nerves, macrophages, and T-cells, while the majority of GLASTLin cells (Tdtomato+ cells; 74.1%) were found in a distinct cluster which was subsequently defined as the primary epitenon cell population. As not all cells in this epitenon cell cluster were Tdtomato+, we explored potential cell subpopulations. Though all epitenon cells express common fibroblast markers, subsetting and reclustering revealed three previously unknown epitenon cell subpopulations: an immunoresponsive population (GLASTLin), a matrix-producing population (non-GLASTLin), and an intriguing new potential GLASTLin progenitor cell population. Identification of genetic markers for epitenon cells is a significant step towards understanding their role in tendon health and function. Here, we have combined the use of a genetic reporter (GLASTLin) with scRNA-seq to not only define the GLASTLin cellular environment but also to identify potential new functions and markers for three completely novel epitenon cell subpopulations. Together, our results suggest that the epitenon is much more complex than previously appreciated, with potential roles not only in the maintenance of tendon homeostasis through production of a protective extracellular matrix on the tendon surface, but also in facilitating the tendon immune response. Most interestingly, our results suggest the epitenon may serve as a niche for the historically elusive tendon progenitor cell population and identifies markers by which this population may be identified and traced. Ongoing fate mapping studies using scRNA-seq will comprehensively define the trajectory of all epitenon cell populations during tendon healing and will identify the cellular players and molecular programs responsible for driving these responses. A better understanding of epitenon cell behavior during homeostasis and healing will greatly enhance our ability to target specific cell populations to improve overall tendon health.

Title: **Aged callus skeletal stem/progenitor cells contain an osteo-inflammatory subcluster with increased IRF-STAT pathways**

Presenting Author: Xi Lin

Co-Authors: Hengwei Zhang, Jiatong Liu, Chia-Lung Wu, Andrew McDavid, Brendan F. Boyce, Lianping Xing

Lab PI / Mentor: Lianping Xing

Abstract (3500 characters or 500 words Limit)

Background. Skeletal stem/progenitor cells (SSPCs) are critical for fracture repair by providing osteo-chondro-precursors in the callus. Recent studies report that aged SSPCs have inflammatory and senescent phenotypes, which contribute to impaired fracture healing in aging mice. However, most of these studies use SSPCs from long bones or bone marrow. Thus, the molecular signatures of callus SSPCs and their potential influence on fracture healing during aging remain to be explored.
Methods. Single-cell RNA sequencing (scRNA-seq) was performed on 5648 young (3-m-old) and 7197 aged (20-m-old) FACS-sorted CD45-CD31-Ter119-Dapi- SSPCs isolated from mouse callus 10 days after tibial fracture. Doublets and cells with <200 gene counts and >8% mitochondrial genes were removed prior to bioinformatics analysis.
Results. Initial unsupervised clustering revealed 4 clusters. The expression of putative markers indicated that clusters 1-3 expressed Acta2, a gene commonly used in scRNA-seq studies of SSPCs, and Runx2, the master regulator for osteogenesis. Specifically: cluster1 expressed the osteoblast marker, Col5a1; cluster3 expressed the adipocyte marker, Lpl; and cluster4 expressed B cell genes. No chondrocyte-related genes (Sox9, Col2) were detected. Heatmap of top Differentially expressed genes (DEGs) and pathway analysis showed: 1) high levels of inflammatory (Retnlg, Cxcr2) and matrix degradation (Mmp8,9) genes, and inflammatory pathways in cluster1; 2) increased Mki67, Top2a, histones and upregulated cell-cycle pathways in cluster2; 3) a miscellany of oncogene Crip1, matrix-related Fn1, inflammatory S100a4, and stem-cell marker Ly6e in cluster3; and 4) B cell genes and pathways in cluster4. Thus, combining unsupervised clustering, putative makers, and DEGs/pathway analyses, we annotated clusters 1,2,3 as the osteogenic population, proliferating-progenitors, and adipogenic population, respectively. 124 B-cell gene-expressing cells in Cluster4 were excluded from subsequent analysis because they are likely contaminants during cell harvest. By performing trajectory analysis to detect various differentiation states of clusters1-3, it is possible to annotate cluster3 proliferating-progenitors as the trajectory root that has the potential to differentiate into osteogenic and adipogenic lineages. Exploring differences in the molecular signatures between young and aged, we detected 117 and 784 upregulated genes in young and aged SSPCs, respectively. Pathway analysis revealed that aged SSPCs have increased inflammatory pathways, while young SSPCs have increased protein processing pathways. UMAP revealed a clear separation of young and aged cells in cluster1 osteogenic cells, which were further sub-clustered into cluster1.1 and 1.2. These were decreased and increased in aged callus, respectively. DEGs of cluster1.1 were matrix-related genes (Syne1, Zmpste24) and cluster1.2 were inflammatory genes (Slpi, S100a6). The master regulators identified by RcisTarget analysis for cluster1.1 were the Sox family transcription factors, implying matrix-related functions of cluster1.1. In contrast, master regulators for cluster1.2 belonged to the IRF-STAT pathway, suggesting interferon-mediated inflammatory functions of cluster1.2.
Conclusion. We identified 3 major clusters in CD45-CD31-Ter119- SSPCs, confirming their heterogeneity. More importantly, we found decreased matrix-producing and increased inflammatory subclusters in the aged callus osteogenic population.

Title: **Novel strategies to purify murine mesenchymal stem cell (MSC) ex vivo reveal differential characteristics of bone marrow and bone derived stromal cells**

Presenting Author: Yuko Kawano

Co-Authors: Hiroki Kawano, Stephanie Busch, Allison J. Li, Chummo Chen, Mary Georger, Mitra Azadniv, Mark W. LaMere, Elizabeth A. LaMere, Michael W. Becker, Jane L. Liesveld, Laura M. Calvi

Lab PI / Mentor: Laura M. Calvi

Abstract (3500 characters or 500 words Limit)

Mesenchymal stromal cells (MSCs) in the bone marrow microenvironment (BMME) support the hematopoietic stem cell pool as well as cancer cells, and are enriched for skeletal stem cells capable of regenerating bone, cartilage and adipose tissues. Isolation of mouse bone and bone marrow (BM)-derived MSCs is essential to explore the functions of MSCs. However current protocols rarely test degree of MSC purification. Moreover, whether purity and function of MSCs depends on tissue of origin (bone vs bone marrow) is poorly understood. Therefore, we carefully evaluated the phenotypes of these cells with established flow cytometry analysis protocols, and surprisingly found abundant macrophage contamination in the MSC cultures (40-60% of cells in vitro) from BM and bone associated cells (BACs) liberated by collagenase-I digestion. To optimize MSC isolation, we performed stringent flow cytometric sorting or magnetic beads separation to exclude macrophages and their precursors using specific macrophage and monocyte markers, F4/80 and Ly6C in addition to CD45. This strategy unexpectedly identified CD45- macrophage progenitors concealed in the CD45-/CD31-/Sca-1+/CD51+ population, which are considered phenotypically as MSCs. Having successfully generated highly purified MSCs from BM and BACs, we found that BM-derived MSCs obtained by our novel strategy demonstrated stem cell characteristics in terms of proliferation, differentiation, and hematopoietic cell supporting capacity, while BAC-derived MSCs were more differentiated and heterogeneous. Cre activity targeted by the SOX9 promoter was previously shown to identify undifferentiated mesenchymal precursors in adult mice that can differentiate to osteoblasts, chondrocytes, adipocytes and CXCL12-expressing stromal cells. Therefore we utilized the SOX9-GFP reporter mouse as an alternative method to identify MSCs in our culture systems. Consistent with our data and previous reports, Sox9 expression was present in BACs but very rare in BM cells in vivo, and was expressed in cells identified as MSCs by flow cytometry. Most of the purified and plated BM-derived MSCs were SOX9-GFP positive, consistent with their immature MSC identity. SOX9-GFP+ cells expression was also high in BAC-derived MSCs but had high variance, which is consistent with heterogeneity of BAC-derived MSCs. Next we performed functional assay to see the influence of macrophage contamination in the MSCs in vitro. Comparing depleted and non-depleted MSC cultures, we found that the macrophages significantly reduced Sox9 expression in MSC populations and impaired their ability to support normal BM, especially in BAC-derived MSCs. Collectively, our novel strategy to purify MSCs cells in culture demonstrated high levels of macrophage contamination in conventional primary BM and BAC derived MSCs, which indicates the perpetuation of macrophage contamination likely due to residual CD45- macrophage progenitors. Moreover, the presence of macrophages significantly alters the cell fate of cultured MSCs, which could provide further understanding of MSC-macrophage interactions. Finally, the tissue source of MSCs contributes to differential characteristics, in spite of identical expression of surface markers in vitro. Our studies highlight the importance of assessing the purity of primary MSC culture systems, and they enable the isolation of highly purified MSCs to further study their role at homeostasis and in disease.

Title: **Mitochondrial Function Controlled By The Permeability Transition Pore/Cyclophilin D Is An Important Regulator of Bone Phenotype and Skeletal Aging**

Presenting Author: Rubens Sautchuk, Jr

Co-Authors:

Lab PI / Mentor: Roman A Eliseev

Abstract (3500 characters or 500 words Limit)

Bone maintenance is achieved by the appropriate balance between bone formation and resorption. During aging, osteoblast (OB) decreased activity, bone marrow stromal cell (BMSC) senescence and cellular pool exhaustion shift this balance in the direction of bone resorption. Our lab and others have demonstrated that during OB commitment, BMSCs must increase their use of oxidative phosphorylation (OxPhos). This process is compromised in aging. Conversely, higher OxPhos activity increases the probability of mitochondrial permeability transition pore (MPTP) opening due to higher levels of ROS and oxidative stress. MPTP opening is positively regulated by the mitochondrial matrix protein Cyclophilin D (CypD) and leads to loss of integrity of the inner mitochondrial membrane, membrane potential (Δψm), and OxPhos function. Therefore, to maintain BMSCs commitment to osteogenic lineage, MPTP inhibition is required to preserve Δψm, support OxPhos, and desensitize mitochondria to higher ROS levels. We found that BMP/Smad signaling transcriptionally represses CypD during OB differentiation. To characterize the effect of CypD regulation in OBs on bone development and maintenance we created an OB-specific CypD gain-of-function (GOF) mouse model expressing constitutively active CypD (caCypD). Constitutive Col1-Cre;caCypD newborn mice were analyzed for bone formation which was found to be deficient. Moving to a potential translational application, inducible OB-specific GOF mice (Col1-Cre^{ERt2};caCypD) were used to mimic the higher MPTP activity seen in aging. Tamoxifen-induced recombination was prompted at 2 mo and samples collected at 4 and 12 mo. The effects of mitochondrial dysfunction on bone were analyzed by bone formation assays, in vivo imaging, metabolomics, histology, µCT, and biomechanical testing. We found that isolated caCypD OBs have defective mitochondria presenting with lower Δψm and decreased OB activity. Newborn CypD GOF mice presented decreased bone and hypertrophic zone length in long bones. Postnatally tamoxifen-induced CypD GOF mice at 4mo and 12mo showed decreased OB activity measured by BoneTag *in vivo* imaging and via P1NP levels, decreased bone parameters measured by µCT analysis, and lower bone strength in biomechanical testing for both vertebrae and femur. Additionally, bone metabolomic analysis at 4mo revealed metabolic profile consistent with mitochondrial dysfunction and premature aging. To confirm our results, we re-expressed CypD in the model where CypD was initially deleted leading to improved bone maintenance and bone strength in aging. We used OB-specific CypD deletion (Col1-Cre^{ERt2};$CypD^{f/f}$) induced in 2 mo old mice aged to 22 mo while maintaining CypD deletion with bimonthly tamoxifen boosts. CypD expression was rescued via AAV2-CRE-DIO-caCypD vector delivery through intra-bone marrow injection in the tibiae of 22 mo-old mice. Contralateral tibiae were injected with sterile PBS solution as an intra-mouse control and specimens collected for analysis 2 mo later. We found that CypD rescue reversed the beneficial effects of its deletion on bone phenotype in aging. Altogether, our data present strong evidence that CypD expression and mitochondrial function are important factors regulating osteogenic signaling and bone homeostasis, and position mitochondria as important hubs mediating bone phenotype and skeletal aging.

Title: **Inducible Depletion of ScxLin Cells Disrupts Tendon Homeostasis and Accelerates Aging-associated Compositional and Structural Changes in the Extracellular Matrix**

Presenting Author: Antonion Korcari

Co-Authors: Alayna Loiselle

Lab PI / Mentor: Alayna Loiselle

Abstract (3500 characters or 500 words Limit)

During adulthood, tendon homeostasis is maintained via ongoing turnover of extracellular matrix (ECM) components. During aging, progressive deficits tendon of structure, composition, and mechanics are observed. The specific cell populations and ECM components that maintain homeostasis, or that are lost with aging are unknown. Scleraxis-lineage (ScxLin) cells are the predominant population of resident fibroblasts in the heterogeneous tendon cell environment. We hypothesized that long-term depletion of ScxLin cells will lead to progressive deficits in ECM structure, organization, composition, and mechanical integrity and will accelerate phenomena that happen during natural FT tendon aging.

We generated Scx-Cre+; Rosa-DTRF/+ mice to deplete ScxLin cells in the FDL tendon and also utilized Scx-Cre-; Rosa-DTRF/+ mice as controls. For the depletion, 20ng of diphtheria toxin (DT) was locally injected into the hindpaw of 10-13 weeks old mice for 5 consecutive days. Paraffin sections from 6, 9, 10, 12, 13, and 31 month old mice were rehydrated and DAPI stained to visualize cell nuclei. Cell density was calculated as the number of nuclei (DAPI) normalized by the area using ImageJ. Uniaxial displacement-controlled stretching of 0.1% strain per second until failure was applied. Structural and material mechanics were determined. Biomechanical properties were analyzed using a student's t-test. Significance level: $p < 0.05$

We found that ScxLin,DTR young adult tendons maintain ~60% tendon cell depletion efficiency during long-term homeostasis and their cell density resembles that of aged tendons. Next, we found that ScxLin,DTR tendons had reduced elastic modulus during homeostasis and their material quality also resembled that of aged WT tendons. Strikingly, our proteomic analysis revealed that ScxLin,DTR young tendons exhibited a loss of primarily high turnover rate ECM molecules, suggesting that ScxLin cells are required for the synthesis of such proteins during homeostasis. To our surprise, our proteomic analysis on WT tendons during natural aging also revealed that aged WT tendons exhibited loss of primarily high turnover rate ECM molecules, suggesting that our depletion model recapitulates mechanisms of ECM degeneration taking place during natural aging. Finally, proteomic analysis between the young ScxLinDTR tendons and aged WT tendons revealed idential levels of high turnover rate ECM molecules, further validating that depletion of ScxLin cells accelerates an ECM-related aging phenotype.

In this study, we showed that ScxLin cells are required during long-term homeostasis to maintain both tendon structure and function via constant synthesis of high turnover rate ECM proteins. We found that several ECM molecules that have not previously been implicated in tendon homeostasis are crucial for maintenance of tendon structure, function, material quality, and composition. Finally, we demonstrated that the proteome shift that occurs during natural aging was very similar to that observed following ScxLin depletion in young tendons. Collectively, these data identify ScxLin cell depletion as a potential model of accelerated tendon aging based on identical decrements in cell density and mechanical properties and shifts in ECM composition between aged C57Bl/6J and Cre-controls compared to ScxLin cell depletion in young animals

Title: **High-Throughput Semi-Automated Segmentation of Murine Hindpaw Micro-CT Datasets Identifies the Cuboid as a Reliable Longitudinal Biomarker of Arthritic Progression in TNF-Tg Mice**

Presenting Author: H. Mark Kenney

Co-Authors: H. Mark Kenney, Yue Peng, Kiana L. Chen, Raquel Ajalik, Lindsay Schnur, Ronald W. Wood, Edward M. Schwarz, Hani A. Awad

Lab PI / Mentor: Drs. Edward Schwarz and Hani Awad

Abstract (3500 characters or 500 words Limit)

Micro-computed tomography (μCT) is a valuable imaging modality for longitudinal quantification of bone volumes to identify disease or treatment effects for a broad range of conditions that affect bone health. Complex structures, such as the hindpaw with up to 31 distinct bones in mice, have considerable analytic potential, but quantification is often limited to a single bone volume metric due to the intensive effort of manual segmentation. Herein, we introduce a novel high-throughput, semi-automated method for segmentation of murine hindpaw μCT datasets to identify bone-specific erosions as reliable imaging biomarkers for the progression of inflammatory-erosive arthritis in tumor necrosis factor-transgenic (TNF-Tg) mice.

All animal studies were performed in accordance with protocols approved by the University of Rochester Committee for Animal Resources. In vivo μCT was performed on TNF-Tg mice and wild-type (WT) littermate controls on a C57BL/6J background (n=4-8 mice/group). The DICOMs were exported to Amira software (v2020.2; ThermoFisher Scientific) for the semi-automated watershed-based segmentation. Corresponding paraffin embedded ankle sections were stained with H&E-OG and segmented in Visiopharm (v2019.07) to quantify bone and pannus area.

The semi-automated segmentation method utilizes the original data (edge detection), binary mask (set threshold) and bone-specific markers that expand to the full volume of the bone using watershed algorithms. Automated workflows in Amira were generated to produce the mask and markers; the markers require quick-fix user corrections in approximately 6 bones/ankle (20%). Compared to the standard manual segmentation using Scanco at the University of Rochester, the semi-automated approach produced similar raw bone volumes (R^2=0.938; -0.038mm^3 avg difference). When the same datasets were analyzed twice by a user, the semi-automated method showed excellent internal reliability (R^2=1.000; -5.7x$10^{-5}$$mm^3$ avg difference). The semi-automated segmentation also demonstrated a significant reduction in segmentation time per dataset (2 ankles) for both experienced and novice (3 graduate students with no prior Amira experience) users compared to standard manual segmentation (experienced 19.3±5.3 & novice <44.5±16.0 vs manual 190.6±30.4min, n=6 datasets p<0.0001). Intraclass correlation coefficients between experienced and novice users were >0.9 (excellent reliability) for all but 3 bones, which were also the bones with the most segmentation errors before correction. Analysis of the midfoot bones identified the cuboid as the most severely eroded tarsal in TNF-Tg mice, which is accelerated in TNF-Tg females (4-months: cuboid -24.1±7.2 vs all other tarsals >-9.0±5.9% change from 2-month volume, p<0.01). Histologic validation revealed significantly reduced bone area (cuboid 37.6±5.8 vs talus 60.7±6.6mm^2) and increased pannus invasion (cuboid 56.1±5.6 vs talus 31.1±3.1mm^2) of 5-month TNF-Tg female cuboid vs talus as the gold-standard.

The described semi-automated segmentation approach provides remarkable inter- and intra-user reliability and throughput advantages. Application of the segmentation method allowed for high-throughput longitudinal data analysis of 188 ankles (5,726 total bones) from WT and TNF-Tg mice by a single user. This analysis identified the cuboid as a primary biomarker of arthritic progression in the midfoot region that can be utilized in future pre-clinical and clinical investigation.

Title: **Semi-Randomized Zwitterionic Peptides Provide Anti-Fouling Behavior to Nanoparticles**

Presenting Author: Clyde Overby

Co-Authors: Baixue Xaio, Tiana Salomon

Lab PI / Mentor: Danielle S.W. Benoit

Abstract (3500 characters or 500 words Limit)

Nanoparticles (NP) are a clinically proven siRNA delivery platform [1]. However, recent data indicate that NPs exhibit poor systemic delivery characteristics due to protein adsorption, which accelerates NP clearance via opsonization and macrophage uptake [2]. Anti-fouling NP modifications such as poly(ethylene glycol) (PEG) and zwitterionic (ZI) polymers and peptides have been shown to be highly efficacious but are susceptible to immunological reactions due to consumer product exposure and repeated chemical structures [2]. As an alternative, we propose the use of computationally designed semi-randomized ZI peptides (srZIPs) synthesized via controlled random amino acid (AA) incorporation in a single sequence to produce libraries (10^3-10^6) of related peptides to modify NP. We hypothesize that srZIPs will provide anti-fouling characteristics to NP and also be immunologically unique, hindering adaptive immune reactions. To investigate these hypotheses, the design, synthesis, and characterization of srZIP-NPs in vitro and in vivo was explored.

Materials and Methods: srZIPs of various AA lengths were generated in silico and scored using an algorithm based upon a peptide-peptide interaction model (PASTA) [3] for lowest interaction potential (ΔG = 2.5 kJ/mol). srZIPs were synthesized via solid phase peptide synthesis, with mixtures of AA precursors for semi-randomization, and confirmed through mass spectrometry. NPs were assembled from diblock copolymers of a poly(dimethylaminoethyl methacrylate) (DMAEMA) first block and 25% DMAEMA, 50% butyl methacrylate, and 25% propylacrylic acid second block synthesized via reversible addition fragmentation chain transfer (RAFT) polymerization [4]. srZIP or 5 kDa PEG, a typical size used in micellar NPs, were conjugated to NP via carbodiimide chemistry and confirmed via fluoraldehyde assay and NMR. NP aggregation in serum and plasma was evaluated via dynamic light scattering (DLS); adsorbed protein was quantified using the bicinchoninic acid assay. NP-mediated siRNA knockdown of GAPDH in mouse mesenchymal stem cells (MSCs) was assessed via RT-PCR. Macrophage and MSC uptake of NP was evaluated by flow cytometry and in vivo pharmacokinetics were characterized via intravital fluorescent microscopy of Cy7 labeled NPs.

Results and Discussion: NP functionalization by srZIPs did not alter size in PBS while serum protein adsorption is reduced by 65% and 35% compared to unfunctionalized NP and PEG-NPs, corresponding with a 14-fold reduction in size versus NP in serum (~40 nm versus >300 nm). srZIP-NP uptake by macrophages is reduced by 30% and MSC uptake increased by 55% compared to NPs, similar to PEG-NPs. siRNA GAPDH knockdown in MSCs by srZIP-NP is equivalent to or greater than NP in all conditions tested, correlating with reduced aggregation [5]. srZIP-NP circulation time increased 5-fold over NPs, exhibiting a half-life of 32 minutes.

Conclusions: Data suggest that srZIP functionalization reduces protein adsorption of NPs, reduces macrophage uptake, and enhances systemic circulation time without affecting siRNA delivery to MSCs. Future work will focus on evaluating in vivo biodistribution of and adaptive immune response to srZIP-NPs.

Refs: 1. David, A. et al. NEJM 379(1) (2018). 2. Verhoef, J.F., et al. Drug Discov. Today 19.12 (2014). 3. Trovato, A., et al. PEDS 20.10 (2007). 4. Convertine, A.J. & Benoit, D.S.W., et al. J. Control. Release 133.3 (2009). 5. Malcolm, D.W., et al. Bioeng transl med 1.2 (2016).

Title: **Human Tissue-on-Chip (hToC) platform for modeling inflammation, fibrosis, and cell cycle regulation in fibrovascular tendon healing**

Presenting Author: Raquel Ajalik

Co-Authors:

Lab PI / Mentor: Drs. James McGrath & Hani Awad

Abstract (3500 characters or 500 words Limit)

Human microphysiological systems (hMPS), also known as tissue- and organ-on-chips, are versatile in vitro tools that incorporate human cells to model diseases and accelerate therapy discovery. Based on our previous work, we hypothesized that direct and paracrine interactions between injured tendon's resident macrophages and tenocytes mediate transvascular infiltration of circulating macrophages and their subsequent activation to secrete inflammatory cytokines and factors, including TGF-β1. This ultimately leads to activation of myofibroblasts, senescent fibroblasts and the release of senescence-associated secreted proteins (SASP), which perpetuate feedback signaling leading to chronic inflammation and a fibrovascular scar. To model this, we designed a 3D multicompartmental human tendon-on-chip (hToC) to investigate cellular signaling between Endothelial Cells (EC), circulating monocytes (CM), tissue-resident macrophages (M), and primary tenocytes (TC) in the context of healing tendon's fibrovascular scar.

The hToC comprises a tenocyte-laden collagen hydrogel separated from a top vascular barrier by an ultra-thin dual scale (nano-micro-) porous silicon nitride membrane. Two acrylic, modular components adhesively combine to form a bottom channel with rigid anchors that provide directional strain and cell alignment to the hydrogel, and a top component housing the membrane, EC and CM. The TC/M culture is suspended in 2.7mg/ml TeleCol-3 at a final density of 1×10^6 TC/mL and 11:1 ratio. Upon culturing in the presence and absence of 10 ng/ml TGF-β1 to activate the fibrotic phenotype, bulk tissue contraction, α-SMA expression as a marker of activated myofibroblasts ,and γH2AX as a marker of senescent fibroblasts via immunofluorescence were analyzed. Additionally, CMs were added to the luminal side of the EC to establish a complete tri-culture microphysiological vascular tendon scar hydrogel with tissue-resident and infiltrating M to mimic the inflammatory response. Secreted cytokines in the tri-culture supernatant were measured and analyzed with an 8-panel Luminex detection assay.

In the EC/TC co-culture, TGF-β1 treatment accelerated the contraction of the hydrogel and increased expression of α-SMA compared to control ($P<0.001$), indicating elevated myofibroblast activation. TGF-β1 treatment also upregulated the ratio of γH2AX foci colocalized to the myofibroblast nuclei ($P<0.005$) indicating an increase in DNA damage characteristic of the senescent phenotype in fibrotic healing. The combination of macrophages and TC induced hydrogel contracture to the same extent as with exogenous TGF-β1. MCP-1 and IL-6 were expressed in mono-culture of TC +/-TGF-β1 treatment and were somewhat decreased in TC/M co-cultures. Additionally, the concentrations of secreted CXCL10, IL-1β, and TNF-α were significantly increased in tri-cultures of monocytes, TC, and EC ($P<0.0001$).

Our experiments demonstrated the feasibility of modeling the tendon-vascular interface and the induction of fibrosis through TGF- β1 treatment and similar results were observed by co-culturing with macrophages. Interestingly, the secretion of key inflammatory cytokines were only increased in tri-culture conditions of TC, M, and ECs, underscoring the importance of including EC in in vitro models of inflammatory fibrovascular tendon healing.

Title: **Effects of Elevated Lactate Levels in Acute Myeloid Leukemia on the Bone Marrow Microenvironment through Polarization of Leukemia-Associated Macrophages**

Presenting Author: Celia Soto

Co-Authors: Dr. Joshua Munger, Maggie Lesch

Lab PI / Mentor: Dr. Ben Frisch

Abstract (3500 characters or 500 words Limit)

Acute myeloid leukemia (AML) has one of the lowest cancer survival rates due to a rapid progression, relapse following treatments, and loss of hematopoiesis secondary to alterations of the bone marrow microenvironment (BMME). The BMME is composed of many cellular and molecular components and is at the core of hematopoietic regulation. The metabolic state of cancer cells is constitutively glycolytic (Warburg effect) and produces metabolic byproducts, such as lactate. In the solid tumor microenvironment, high levels of lactate secreted by cancer cells contribute to the polarization of macrophages to an alternative “M2-like” immunosuppressive phenotype, called tumor-associated macrophages (TAMs), and an increase in TAMs correlates with poor prognosis in multiple cancers. Similarly, leukemia-associated macrophages (LAMs) have been found in AML and shown to promote disease progression; however, the mechanisms by which they are polarized and how they function in leukemia have not been defined. Therefore, we hypothesized that leukemic cells secrete high levels of lactate to the BMME during AML, polarizing macrophages to LAMs that promote leukemic progression and reduce support for normal hematopoiesis. We found elevated lactate levels in the bone marrow serum of human AML patients compared to healthy controls ($n = 5$, $p < 0.001$). The use of a murine AML model for subsequent studies has been verified to reproduce the metabolite profile detected in human disease. We have found that LAMs express high levels of mannose receptor (CD206), and that lactate contributes to bone marrow-derived macrophage polarization in vitro. Lactate acts as an extracellular ligand to the G-protein-coupled receptor GPR81. In GPR81-/- recipients of our murine model of AML we demonstrated that lactate signaling through GPR81 alternatively polarizes LAMs in vivo (mean MFI of CD206 on macrophages in wt vs GPR81KO mice = 5784 vs 2633, SE of diff. = 946.7, $p < 0.05$). Leukemic burden was reduced in the spleen and peripheral blood of GPR81-/- recipients when measured at a late stage of disease. Furthermore, the loss of hematopoietic support in AML can be reproduced through exposure to elevated levels of lactate, using in vitro coculture of HSPCs with macrophages and mesenchymal stem cells (MSCs) (CFU-Cs =12.17 at 0 mmol/L lactate vs 1.167 at 5-10 mmol/L lactate, SE of diff. = 3.23, $n = 3$). In additional cocultures of macrophages and MSCs, lactate treatment reduces MSC proliferation and differentiation to osteoblasts in a dose-dependent manner (mean area of alkaline phophatase stain in pixels = 330146 at 0 mmol/L lactate vs 146325 to 18502 at 10-15 mmol/L lactate, SE of diff. = 17746, $n = 3$). The observed block in osteoblastic differentiation is consistent with a phenoytpe identified in human MSCs islolated from AML patients. This research identifies, for the first time, the role of lactate in AML pathophysiology, and identifies GPR81 as a potential therapeutic target for the treatment of this devastating disease.

Health Care Disparities in Complication and Mortality Rates Following Surgical Management of Cauda Equina Syndrome

Peter Joo MPH[1], Weijian Li MS[1], Amy Phan BS[1], Caroline Thirukumaran MBBS, MHA, PhD[1], Jiebo Luo PhD[1], Emmanuel Menga MD[1], Addisu Mesfin MD[1]
[1]University of Rochester Medical Center, Rochester, NY

INTRODUCTION:
Timely evaluation of cauda equina syndrome (CES) is important to prevent symptom progression and potentially restore neurologic function. Missed diagnoses and delays in treatment may lead to permanent neurologic deficits and significant ramifications for patients' quality of lives. While health care disparities related to race and ethnicity are well reported for non-emergent conditions, the literature on disparities in outcomes for emergent spinal conditions such as CES remains sparse. The objective of this study is to identify disparities in complication, mortality, and readmission rates following surgical intervention for CES based on race.

METHODS:
The Statewide Planning and Research Cooperative System (SPARCS), a comprehensive all payer database for all hospitalizations within New York State, was used for this study. Patients with CES treated surgically between the years 2000-2015 were identified based on diagnosis and procedural codes. Patient demographics (age, sex, race, comorbidities, and insurance status) and hospital characteristics (size as defined by hospital bed number quartiles) were evaluated. Primary outcomes of interest were all-cause postoperative complications, mortality rates, and 30-day readmissions.

Descriptive statistics of patient characteristics were reported and compared using chi-square and paired-sample t-tests for categorical and continuous variables, respectively. Multivariate logistic regression analysis was performed to analyze the association of race and outcomes variables, controlling for age, sex, comorbidities, length of stay, insurance, and hospital characteristics. Significance was set at $p<0.05$.

RESULTS:
Overall, 2,114 patients that underwent lumbar surgery for CES were identified. Patients underwent lumbar decompression (821, 38.8%), fusion (746, 35.3%), or both (547, 25.9%). African American patients consisted of 8% (177), Caucasian patients 79% (1680), and Asian patients 12% (257) of the overall population.

On multivariate analysis, the odds of 30-day mortality were 2.98-fold greater in African American patients than other patients ($p=0.029$). By 180 and 360 days, odds of mortality were 4.27 and 3.05-fold greater in African American patients than other patients, respectively ($p<0.001$ each). Thirty-day readmissions were 1.87-fold greater in African American patients compared to the others ($p=0.004$). No difference in overall complication rate was found between African American patients and all other race groups ($p=0.306$).

DISCUSSION/CONCLUSION:
We demonstrate that in patients included in the New York State SPARCS database, health disparities in the surgical management of CES exist. African American patients were found to have higher and increasing rates of mortality from 30 days to 1 year and greater readmission rates compared to other race groups.

Poster Abstracts

Disclaimer

#	Presenting Author	Title	PI
1	Ackerman, Jess	Lineage tracing and spatial transcriptomics illustrate the role of myofibroblasts during fibrotic tendon healing	Loiselle
2	Adjei-Sowah, Emmanuella	Tendon-Targeted Delivery of a p65 Inhibitor via Peptide-Functionalized Nanoparticles to Improve Tendon Healing	Benoit
3	Alenchery, Rahul	PAI-1 is critical for TGF-_1-induced mTOR signaling and myofibroblast activation in murine tenocytes	Awad
4	Alzamareh, Diana	CD11c+ Expression Associates with IFN-_ Responsiveness in Human B cells with clinical implications for SLE	Anolik/Barnas
5	Basu, Sayantani	Transcriptome Analysis of Autograft Mediated Bone Healing: Efficient Design of Tissue Engineering Approaches	Benoit
6	Bui-Bullock, Tina	Impact of altering gut microbiota metabolism on osteomyelitis severity in obesity-related type 2 diabetes	Gill
7	Chen, Chunmo	Osteoblast efferocytosis induces osteoblast senescence and apoptosis	Calvi
8	Chen, Kiana	Variable Effects of Testosterone on Male Versus Female Derived Macrophages in Inflammatory Arthritis	Rahimi
9	Chirokikh, Alexander	Non-invasive Assessment of the Ulnar Nerve Around the Elbow and Diagnosis of Cubital Tunnel Syndrome using Ultrasound	Ketonis
10	Denasty, Adwin	The Role of Demographic and Academic Characteristics on Industry Payments Received by Orthopedic Spine Surgeons in 2019 and 2020	Mesfin
11	El-Atawneh, Ihab	Fabrication of Cylindrical MSC-Sheets With Tunable Notch Signaling as Engineered Periosteum	Awad
12	Escalera-Rivera, Katherine	Cartilage-synovium crosstalk in osteoarthritis: role of NR4A1 signaling	Anolik/Jonason
13	Fraser, David	Hydrogel Swelling Induces Cell Alignment at Dentin Interfaces	Benoit
14	Hansen, Victoria	Spatial transcriptomics reveal unique molecular fingerprints of chondrogenesis during embryonic limb development	Wu
15	Heckman, Connor	Utilization of Novel Oxygen Reporting Molecule PtTAPIP and its Derivatives for Intravital Imaging of Oxygen Tension	Zhang

16	Hwang, Alan	Racial, Ethnic, and Income-Based Disparities in the Surgical Treatment of Rotator Cuff Tears	Thirukumaran
17	James, Nick	Dissecting the role of DNA double-strand breaks in osteoarthritis pathogenesis	Jonason
18	Jiang, Chen	In Vivo Engineered Extracellular Matrix as Scaffolding Materials for Biomimetic Periosteum	Zhang
19	Kawano, Hiroki	Mitochondrial transfer from donor to host utilizing ex vivo culture of mouse hematopoietic stem cells	Calvi
20	Kotelsky, Alexander	Differential Expression of Piezo1 and p-mTOR in Articular Chondrocytes of ACL-injured Mice	Lee
21	Kuhns, Benjamin	Validated Whole-Genome RNA Sequencing of Femoral Head Impingement Cartilage Identifies FGF-18 As A Biomarker in Hip Osteoarthritis Progression	Ackert-Bicknell/Wu
22	Lanham, Aubrey	Alginate hydrogels as alternate lung inflation media may improve tissue culture and RNA Isolation	Benoit
23	Lenhard, Nicholas	Optimization of Concurrent Osteogenesis and Angiogenesis in Bone Marrow Culture Utilizing a Reporter Mouse Model Labeling Both Osteoblasts and Sprouting Endothelial Cells	Zhang
24	Liu, Jiatong	Molecular signatures distinguish callus senescent cells from inflammatory cells	Xing
25	Mandalapu, Aniruddh	Radiographic and clinical findings associated with Klippel-Feil Syndrome: A case series	Mesfin
26	March, Alyson	Elucidating Design Parameters to Improve Tissue Engineered Periosteum Mediated Allograft Healing	Benoit
27	Massie, Christine	Anatomical site and BMI affect optimal source-detector offsets for transcutaneous Raman assessment of human hand bone quality assessment	Awad
28	Mereness, Jared	Tuning Engineered Hydrogel Matrix Degradation and Epitope Presentation for Salivary Gland Tissue Mimetic Culture	Benoit
29	Muscat, Samantha	CCR2 identifies tendon-resident T cell and macrophage populations while CCR2-/- impedes late tendon healing	Loiselle
30	Neumaier, Mackenzie	Analyzing the Impact of Comorbidity Indices on Patient Reported Outcomes Following Total Hip Arthroplasty	Ginnetti

31	Nguyen, Phong	Stage-specific healing behaviors are observed in a novel embryonic tendon explant model	Kuo
32	Nguyen, Phong	Mechanical properties of embryonic tendon are enhanced with lysyl oxidase upregulation	Kuo
33	O'Neil, Meghan	Characterization of RAGE expression to inhibit myofibroblast persistence during tendon healing	Loiselle
34	Pacar, Ivana	Characterizing efferocytic activity in multipotent stromal cells (MSCs) using confocal time-lapse imaging	Calvi
35	Peng, Yue	Evlaulation of Lymphatic Muscle Cell Damage and Peri-Vascular Mast Cells on Popliteal Lymphatic Vessel Function in TNF-Tg Mice with Inflammatory-Erosive Arthritis	Schwarz
36	Qi, Beibei	Automatic Vascular Imaging Analyses Using Deep Neural Networks	Zhang
37	Qiu, Bowen	Biomechanical Comparison of Stemless Humeral Components in Total Shoulder Arthroplasty	Voloshin
38	Quarato, Emily	High levels of efferocytosis by mesenchymal stromal cells induce senescence	Calvi
39	Ramirez, Gabriel	Does centralization of revision total hip and total knee arthroplasty affect patient travel distances/times in vulnerable patient populations?	Thirukumaran
40	Ren, Youliang	Development of bisphosphonate-conjugated antibiotics to target Staphylococcus aureus biofilm within the osteocyte lacuno-canalicular network of infected cortical bone in chronic osteomyelitis	Xie
41	Saito, Motoo	IL-27 suppresses Staphylococcal abscess formation in Staphylococcus aureus implant-associated osteomyelitis	Schwarz/Muthukrishnan
42	Salama, Noah	IGF-1 in the Bone Marrow Microenvironment Regulates Mesenchymal Stromal Cell Efferocytosis	Calvi
43	Schilling, Kevin	Intravital Imaging of Oxygen Tension and Energy Metabolism at the Site of Cranial Bone Defect Repair via 2-photon Based Phosphorescence and Fluorescence Lifetime Imaging	Zhang/Brown
44	Schloemann, Derek	Botulinum Toxin A in Mouse Model of Raynaud Phenomenon Ischemic Tissue Loss	Korman
45	Sharipol, Azmeer	Acute Myeloid Leukemia on a chip	Frisch/Benoit

46	Smolyak, Gilbert	PROMIS Scores Correlate to Treatment Selection for De Quervain Tenosynovitis	Ketonis
47	Srivatsava, Arvind	Investigating the Effect of PEG Hydrogel Substrate Stiffness on Retinal Pigment Epithelial Cell Adhesion and Barrier Function	Benoit
48	Wise, Brian	Exploring the biologic sequelae of Achilles tendon impingement using a novel murine hind limb explant platform	Buckley/Lee
49	Xiao, Baixue	Modulating macrophage function with drug delivery approaches to enhance fracture healing	Benoit
50	Yan, Ming	3D Printable Carboxymethyl Chitosan-Amorphous Calcium Phosphate Nanoparticles(CMC/ACP NPs) Enhance Osteogenesis and Regulate Macrophage Polarization	Awad
51	Yu, Chen	Crosstalk Between CypD/mPTP and Adipogenesis in Bone Marrow Stromal Cells	Eliseev
52	Zhang, Hengwei	Icam-1-inhibited M2 M_ infiltration is a new molecular mechanism for delayed fracture repair in splenectomized mice	Xing
53	Zhang, Hengwei	Senescent cells promote the disease progression of multiple myeloma from its asymptomatic precursor stages	Zhang/Lipe
54	Zhang, Jane	Pharmacological Inhibition of the TAM Receptors Decreases Mesenchymal Stromal Cell Efferocytic Ability	Calvi
55	Zhang, Victor	Investigating the effects of type III/I collagen ratios in hydrogel models of tendon injury	Awad/McGrath
56	Knapp, Emma	Cantilever Bending of Murine Femoral Necks	Awad
57	Schnur, Lindsay	MicroCT Core	B^2MTI Core
58	Fox, Jeffrey	HBMI Core	HBMI Core
59	Knapp, Emma	Biomechanical Testing Core	B^2MTI Core

Title: **Lineage tracing and spatial transcriptomics illustrate the role of myofibroblasts during fibrotic tendon healing**

Presenting Author: Jessica E. Ackerman

Co-Authors: Katherine T. Best, PhD, Chia-Lung Wu, PhD

Lab PI / Mentor: Alayna E. Loiselle PhD

Abstract (3500 characters or 500 words Limit)

Acute tendon injuries represent a major clinical burden, in part due to tendon's fibrotic healing process. Complete restoration of functional properties is prevented by the excessive scar tissue, and this is commonly thought to be due to dysregulation of specialized fibroblasts, termed myofibroblasts. While required for matrix production and wound contraction, persistence or abnormal functioning of myofibroblasts can drive pathological fibrosis. Therefore our goal is to investiage myofibroblast fate and function throughout tendon healing to determine the contribution of these cells to the fibrotic healing process.

Myofibroblasts are recognized by their α-smooth muscle actin (αSMA) stress fibers, but targeting these cells genetically is problematic, as αSMA is also expressed in the vasculature. To that end, we chose to focus on periostin, a matricellular marker that has been shown to represent activated myofibroblasts in cardiac fibrosis. Through extensive lineage tracing, using inducible Postn; Ai9 reporter mice in our murine acute flexor tendon injury model, we determined that Postn-Lin cells only transiently co-express αSMA early (D7) healing, yet persist in the granulation tissue to secrete abundant periostin into the extracellular space. Confocal imaging and in vitro work demonstrated that secreted periostin creates a matrix in the healing tissue that promotes myofibroblast differentiation of resident tenocytes. Current studies aim to determine how depletion of these cells, and therefore this matrix/myofibroblast niche, may alter the course of fibrotic tendon healing.

Given that Postn-Lin cells do not reliably label myofibroblasts in the context of fibrotic tendon healing, instead appearing to have an important matrix-specific role, we turned to Scleraxis-Lin cells to better understand myofibroblast fate and function. Our lab has previously shown that Scx-Lin cells contribute to the myofibroblast fate in a spatiotemporal pattern, and so we utilized spatial transcriptomics to define the different cellular/molecular programs guiding fibrotic tendon healing. Tendons from Scx; Ai9 reporter mice were harvested at homeostasis (control), along with those at D14 and D28 for fresh frozen sectioning onto gene expression slides, which are coated with millions of barcoded reverse transcription primers. From this, a cDNA library was created, sequenced, then mapped back to the tissue section. Gene expression data from the tendon/healing tissue was subsetted from each timepoint and integrated into a combined dataset, revealing five distinct cellular/molecular programs dictating the course of tendon healing. Differentially expressed genes along with spatial localization were used to annotate these programs, and pseudotime analysis conducted to define differentiation trajectories. Examination of the trajectory from basal tendon to highly reactive tissue (involved in matrix production/remodeling) revealed that Scx-Lin cells follow this path, and we were further able to determine transcription factors regulating this trajectory. These experiments offer new insights into the healing process and identify a variety of targets for modulation with the goal of regenerative tendon healing.

Title: **Tendon-Targeted Delivery of a p65 Inhibitor via Peptide-Functionalized Nanoparticles to Improve Tendon Healing**

Presenting Author: Emmanuella Adjei-Sowah

Co-Authors: none

Lab PI / Mentor: Danielle Benoit, PhD; Alayna Loiselle, PhD

Abstract (3500 characters or 500 words Limit)

Tendon regeneration following acute injury is marred by a fibrotic healing response that impairs complete functional recovery. Despite the frequency of tendon injuries and complications associated with fibrosis, including increased risk of re-injury and limited range of motion, there are currently no pharmacological approaches to improve the healing process. Together with others, we have recently shown that the canonical nuclear factor kappa B (NF-kB) signaling cascade, via p65, drives both inflammatory and pro-survival gene expression, resulting in increased myofibroblast content and matrix deposition, thus identifying p65 knockdown as a promising therapeutic approach to improve tendon healing. Despite the proven efficacy of p65 inhibitors, such as Helenalin, in reducing fibrosis, the application of these small molecules to improve tendon healing is limited by poor tendon-specific targeting of systemic treatments. Moreover, drug delivery via direct injection into the healing tendon reactivates the inflammatory response and disrupts tendon healing. Thus, the ability to specifically target the tendon via systemic delivery would substantially enhance translational feasibility of newly discovered disease modifying treatments, since systemic inhibition of NFkB is not feasible. We have recently demonstrated that introducing TRAP (tartrate resistant acid phosphatase) Binding Peptide (TBP) to our poly(styrene-alt-maleic anhydride)-b-poly(styrene) (PSMA-PS) nanoparticle drug delivery system results in high affinity targeting of TRAP+ cells in vitro and in vivo. Furthermore, exciting preliminary data demonstrate robust TRAP activity in the healing tendon during the late inflammatory and early proliferative stages of healing, thereby defining the optimal therapeutic window for TBP-NP drug delivery. Most notably, in a pilot study, we demonstrated substantial accumulation of TBP-NPs at the tendon repair site, relative to control NPs, however, we have yet to identify specific timing, frequency, and dosage required for efficient TBP-NP delivery. Future studies will aim at determinig the temporal-spatial targeting of TBP-NPs during the tendon healing process. We will investigate the appropriate frequency, dosage, and time-point(s) for optimally delivering fluorescently labelled TBP-NPs to take advantage of the enhanced permeation and retention (EPR) effect as well as the high levels of TRAP+ cells in healing tendons. Accumulation and systemic distribution will be assessed via in vivo imaging and histology. Control NPs functionalized with scrambled TBP will be used as controls. Furthermore, we will investigate the efficacy of TBP-NP mediated delivery of the p65 inhibitor, Helenalin, in promoting regenerative tendon healing.
While TBP-NPs can be used to effectively deliver a large spectrum of drugs, we are particularly interested in Helenalin because of its proven efficacy in reducing tendon adhesion by modulating proliferation, inflammation and apoptosis. TBP-NPs without drug and free Helenalin will be used as controls. The degree of p65 inhibition and changes in NFkB activation will be assessed via Western Blot, as well as functional and morphological changes which will be assessed from D14-63 post-surgery. Establishing a targeted delivery system with the potential to efficiently deliver various drugs will greatly increase our chances of improving tendon health in a plethora of ways.

Title: **PAI-1 is critical for TGF-β1-induced mTOR signaling and myofibroblast activation in murine tenocytes**

Presenting Author: Rahul Alenchery

Co-Authors: Raquel Ajalik, Firaol Midekssa, Sylvia Zhong

Lab PI / Mentor: Hani Awad

Abstract (3500 characters or 500 words Limit)

Introduction: Plasminogen Activator Inhibitor 1, encoded in mice by the Serpine1 gene, is a putative senescence marker, which is directly upregulated by TGF-β1 and implicated in several tissue fibrosis disorders including skin, lung, liver, kidney, heart and tendon. Our lab has been investigating the pathobiological effects of TGF-β1/PAI-1 signaling in tendon injury using a zone II injury to the deep digital flexor tendon in mice. We identified the activation of PTEN signaling and the inhibition of FOXO-associated biological processes in healing flexor tendons in PAI-1 null (PAI-1 KO) mice as antifibrotic pathways, which provides a possible mechanistic link to mTOR signaling. We previously reported the activation of mTOR signaling in C57Bl/6J mouse tenocytes *in vitro* upon treatment with TGF-β1, which was associated with increased myofibroblast activation through the pleiotropic protease inhibitor, PAI-1. Therefore, our central hypothesis is that TGF-β1/PAI-1 mediated inhibition of PTEN in tenocytes alters fibrotic tendon pathobiology through the PI3K/AKT/mTOR pathway.
Methods: Following euthanasia, flexor tendons were excised from healthy PAI-1 KO and wild type (WT) littermates for enzymatic tenocyte isolation. TGF-β1 (10 ng/ml) treated samples were analyzed using semi-quantitative Western blot analysis and qRT-PCR probing for TGF-β1 and mTORC1 signaling proteins and genes normalized to beta-actin. Cell samples were also stained for immunofluorescence to assess α-SMA in differentiated myofibroblasts.
Results: As hypothesized, TGF-β1 treatment increased phosphorylation of SMAD3 in both WT and PAI-1 KO tenocytes, which was associated with increases in phosphorylated AKT and 4E-BP1 levels in response to TGF-β1 treatment regardless of the genotype. Associated with the increased phosphorylation of AKT, phosphorylated PTEN was significantly decreased in PAI-1 KO tenocytes and reduced upon TGF-β1 treatment in WT tenocytes. Interestingly, the phosphorylation of 4E-BP1 downstream of mTORC1 in response to TGF-β1 treatment was reduced in PAI-1 KO tenocytes compared to WT controls. These results demonstrate that PAI-1 regulates the phosphorylation of key signaling proteins upstream and downstream of mTORC1 in response to TGF-β1 treatment.
These signaling changes were associated with significantly increased activation of α-SMA positive myofibroblasts when tenocytes were treated with TGF-β1, in both WT and PAI-1 KO tenocytes, as determined by immunofluorescence staining and qRT-PCR. Interestingly, the activation of myofibroblasts in response to TGF-β1 treatment was reduced in PAI-1 KO tenocytes. These findings are further corroborated by TGF-β1 induced activation of collagenous ECM genes (*Col1a1*, *Col3a1*, and *Serpinh1* (hsp47)) and inactivation of matrix metalloproteinases (*Mmp2*, *Mmp3*, *Mmp9*) compared to WT control. Interestingly, we also observed a drastic decrease in the expression of cell cycle regulators (*Cdkn2a* (p16), *Tp53* (p53), *Rb*, and *Bcl2*) in PAI-1 KO tenocytes compared to WT control.
Discussion: Previously, we demonstrated that TGF-β1 is secreted in injured mouse flexor tendons through a set of positive feedback mechanisms enhanced by inflammatory signaling. Our results indicate PAI-1 to regulate PI3K/AKT activation of mTORC1 and 4EBP1 to induce fibrosis. Furthermore, these results implicate the TGF-β1/PAI-1/mTOR axis to closely regulate adhesion, remodeling, and cell cycle genes. Accordingly, inhibition of mTOR signaling or PAI-1 may serve as a targeted therapeutic approach to ameliorate fibrosis.

Title: **CD11c+ Expression Associates with IFN-λ Responsiveness in Human B cells with clinical implications for SLE**

Presenting Author: Diana Alzamareh

Co-Authors: Jennifer Albrecht, Nida Meednu, Cameron Baker, Andrew McDavid, R. John Looney, Jennifer H. Anolik, Jennfer L. Barnas

Lab PI / Mentor: Anolik/Barnas

Abstract (3500 characters or 500 words Limit)

Type I interferon (IFN), such as IFN-α, and B cell aberrations contribute to systemic lupus erythematosus (SLE) pathogenesis. Type I IFN receptor blockade was recently approved for treatment of SLE. Type III IFN (IFN-λ) produce a gene signature currently indistinguishable from that of type I IFN in responsive cell types. IFN-λ utilize a unique receptor (IFNLR1) and thus are not blocked by type I IFN receptor blockade. Type III IFN are appreciated to have an important role in viral infection at epithelial barriers where IFNLR1 is strongly expressed. The effects of IFN-λ on immune cells remain understudied and are different between human and murine models. CD11c+ age/autoimmunity B cells (ABC) are a target of interest as recent studies suggest they are poised for plasma cell differentiation and enriched in autoreactivity and thus have the potential to contribute to SLE pathogenesis. Here, we study the effects of type I and type III IFN on human ABC.
Methods: Patients meeting 1997 ACR systemic lupus erythematosus classification criteria (n = 8) and healthy donors (HD, n = 5) had blood drawn under IRB-approved protocol. The transcriptome of sorted IgD+ CD27- naïve and IgD- CD27- (DN) B cells was measured by bulk RNA sequencing for differential expression and gene set enrichment analysis. Serum IFN-λ1 and all subtype IFN-α are measured by ELISA in HD (n=6) and SLE (n=26). HD B cells are stimulated in vitro with IFN-α2 and IFN-λ1. RT-PCR is performed for interferon stimulated genes (n=4). Cell phenotype and STAT1 phosphorylation (pSTAT1, n=10) was measured by flow cytometry.
Results: Naïve and DN cells display a prominent type I IFN gene expression profile in SLE. Transcript for type I, type II, and type III IFN receptors (IFNAR1, IFNAR2, IFNGR1, IFNGR2, IFNLR1, and IL10RB) are detected in HD and SLE B cells. CD11c+ CD21- frequency increased in DN compared to naïve B cells for SLE and HD (both $p< 0.001$). The mean and range of CD11c+ CD21- frequency was higher in SLE DN (30.7± 9.5%, mean±SEM; range 4.8-74.7%) compared to HD DN (7.6%±1.0%,3.6-9.4%). IFN-λ is detected in the serum of human SLE patients and correlates with IgD- CD27- CD21- CD24- (DN2) B cells, a compartment which contains ABC. Increased IFNLR1 transcript correlated with CD11c+ CD21- B cell expansion ($r2=0.922$, $p<0.0001$). IFN-λ1 stimulates IFIT1, IFI27, ISG15 and USP18 mRNA expression in B cells. Increased pSTAT1 after IFN-α2 treatment is found in monocytes, T cells, and B cells, but only increases in the B cells after IFN-λ1 treatment. Naïve, DN, switched, and unswitched memory HD B cells are responsive to type I and type III IFN, but demonstrated a higher pSTAT1 fold change with type I IFN treatment compared to type III IFN. In all B cell subsets, CD11c+ cells had a higher pSTAT1 baseline and fold change after IFN-λ1 stimulation than did CD11c- B cells. In HD with well-defined populations of CD11c+ DN cells, pSTAT1 fold change for IFN-λ approached that of IFN-α2.
Conclusions: All human B cell subsets defined by CD27 and IgD respond to IFN-α and IFN-λ, but those expressing CD11c+ have increased responsiveness to IFN-λ. CD11c+ cells expand in SLE and associate with autoreactive plasma cell development. Thus, the role of IFN-λ may take on increased clinical significance in the setting type I IFN receptor blockade. These results suggest IFN-λ may be an underappreciated driver of the IFN signature and B cell aberrations in SLE.

Title: Transcriptome Analysis of Autograft Mediated Bone Healing: Efficient Design of Tissue Engineering Approaches

Presenting Author: Sayantani Basu

Co-Authors:

Lab PI / Mentor: Danielle Benoit

Abstract: (3500 characters or 500 words Limit)

Bone grafts are the second most frequent tissue transplantation surgeries after blood transfusions with approximately two million bone graft surgeries performed in the US annually. Autografts are the gold standard for bone grafting, but their widespread use is hindered by donor site morbidity, limited tissue volumes, and complexity of tissue-harvesting procedures. Bone allografts are the clinical alternative, however, compared to autografts, allografts are associated with substantial 60% failure rate at 10 years post-implantation due to poor host integration. Healing deficiencies observed in allografts are due to the absence of periosteum, the thin layer of vascularized and innervated tissue that surrounds all bone tissue. The periosteum acts as a reservoir of multiple cell types including stem cells and osteoprogenitors that releases key paracrine factors to drive fracture repair. Previous literature has identified the various cell types in periosteum and performed transcriptomic analyses at different stages following fracture, but none have focused specifically on defect periosteal cells. Additionally, very little is known about the shift in periosteal cell populations and temporal paracrine factor profiles during autograft healing. Therefore, to investigate the underlying mechanism of periosteum mediated healing and identify key paracrine factors to design regenerative therapies, femur autograft surgeries were performed on female C57BL/6 mice, which were allowed to heal for 1, 2, 5, 7, and 14 days. Femurs were harvested, bone marrow flushed, and cells from the fracture callus were isolated, analyzed by flow cytometry, and RNA was collected for sequencing. Flow results show a reduction in the macrophage ($CD45^+/F4/80^+/Lg6G^-/Ly6C^-$) population from 11% to 4.5% of total live cells from day 2 to day 7. Additionally, endothelial cell ($CD45^-/Ter119^-/CD31^+$) and mesenchymal stem cell ($CD45^-/Ter119^-/CD31^-/Sca\text{-}1^+/CD51^+$) populations exhibited a sharp increase from 0.7% to 4% and 13% to 24% of total live cells and $CD45^-/CD31^-$ cells respectively from day 1 to day 7. These results indicate a dynamic change in the cell populations, which likely contributes to dramatic shifts in paracrine factor profiles at different stages of autograft-mediated bone healing, which are currently being analyzed via RNA sequencing. Future studies are focused on single cell sequencing of periosteal cells after autograft transplantation from red fluorescent protein (RFP) expressing mice to differentiate between the graft and host cells in the defect microenvironment during the early stages of healing. Data gathered from sequencing analyses will guide us towards the successful design of tissue engineering approaches for superior allograft healing.

Title: **Impact of altering gut microbiota metabolism on osteomyelitis severity in obesity-related type 2 diabetes**

Presenting Author: Tina I. Bui-Bullock

Co-Authors: Ann L. Gill, Robert A. Mooney

Lab PI / Mentor: Steven R. Gill

Abstract (3500 characters or 500 words Limit)

Staphylococcus aureus is an opportunistic pathogen causing osteomyelitis through hematogenous seeding or contamination of implants and open wounds following orthopedic surgery. S. aureus-mediated osteomyelitis is particularly problematic in obesity-related type 2 diabetes (obesity/T2D) due to systemic chronic inflammation impairing both adaptive and innate immunity. This inflammation is linked to obesity and associated gut dysbiosis. Interestingly, high fiber diets that modify the gut microbiota have demonstrated efficacy in reducing symptoms and complications of obesity/T2D. However, our understanding of the mechanisms by which modifications of the gut microbiota alter host infection responses is limited. Here, we monitored implant-associated S. aureus infections in obese/T2D mice following treatment with the dietary fiber, oligofructose. Oligofructose significantly decreased abscess formation and bacterial burden in infected bone and tissue in obese/T2D mice but not in lean controls. Oligofructose also decreased hyperinflammation following infection in obese/T2D mice, indicating at least partial restoration of immune homeostasis. For example, plasma inflammatory cytokines (TNF-α, IL-6) and chemokines (IP-10, KC, MIG, and MCP-1) were decreased in this group at 14 days post-infection. To identify gut microbiota-related mechanisms, we examined changes in gut microbiota composition due to oligofructose. Notably, the anti-inflammatory bacterium, Bifidobacterium pseudolongum, was increased relative to lean controls. Further analysis of the cecum and plasma metabolome suggested polyamine production was increased, specifically spermine and spermidine. Oral administration of these polyamines to obese/T2D mice resulted in reduced infection severity similar to oligofructose supplementation, suggesting polyamines may mediate at least some of the beneficial effects of fiber on severity of S. aureus-mediated implant-associated osteomyelitis in obesity/T2D and may have therapeutic potential.

Title: **Osteoblast efferocytosis induces osteoblast senescence and apoptosis**

Presenting Author: Chunmo Chen

Co-Authors: Emily Quarato, Yuko Kawano, Noah A Salama, Allison Li, Hiroki Kawano, Michael W. Becker

Lab PI / Mentor: Laura M. Calvi

Abstract (3500 characters or 500 words Limit)

Myelodysplastic syndromes (MDS) are a heterogeneous group of clonal stem cell disorders with an inherent tendency for leukemic transformation. More than 10,000 new cases occur in US annually and the incidences increase with age. The limited therapies emphasize the need for more studies on pathology of MDS. Increased cellular apoptosis is commonly seen in MDS, but whether clearance of apoptotic cells by phagocytes plays a role in disease progression is not known. Our laboratory recently found that in MDS, bone marrow (BM) macrophages are highly defective, with decreased efferocytic rates and increased inflammatory mediators. Mesenchymal stromal cells (MSCs) and osteoblasts (OBs) function as non-professional phagocytic cells capable of engulfing apoptotic cells, also known as efferocytosis. The increased apoptotic burden and defective macrophages would be expected to recruit non-professional phagocytes in the bone and bone marrow. Therefore, we hypothesize that osteoblasts participate in the clearance of apoptotic cells in the bone marrow microenvironment (BMME), maintaining bone marrow homeostasis. The increased osteoblastic efferocytic burden in MDS contributes to osteoblasts senescence and/or apoptosis as a mechanism of MDS progression.

We utilized primary murine MSCs isolated from BM and bone-associated cells (BACs) isolated from Collagenase-I digested long bone fragments. BM-derived MSCs were differentiated into OBs using mineralization media. Osteocalcin concentration in the supernatant of undifferentiated BACs confirmed this population includes primary osteoblasts. End stage neutrophils are mature apoptotic neutrophils homing back to bone marrow. We expect the end stage neutrophils would cause BM inflammation and are the targets of efferocytosis. Both differentiated MSCs and BACs were incubated with end stage neutrophils for 24 hours. Microscopic images and flow cytometry data show that nearly 70% of both differentiated BM-derived MSCs and BACs are phagocytic. High levels of efferocytosis are associated with increased senescence and apoptosis in BACs and increased apoptosis in differentiated BM-derived MSCs. Efferocytosis assays are also conducted in two murine MDS model, NHD13 and IDH2. In MDS-like environment, the osteoblast efferocytosis capacity is increased than in normal environment. In conclusion, our data demonstrate that osteoblasts from different regions perform phagocytosis and lead to different cellular fates after high level efferocytosis.

Our data may define novel mechanisms to explain the excessive senescence seen in MDS. The excessive senescence is possible related to MDS progression. Future experiments will involve in modulating the efferocytosis rate by clinical drug targeting efferocytic receptors, contributing to a novel therapeutic approach for MDS patients.

Title: **Variable Effects of Testosterone on Male Versus Female Derived Macrophages in Inflammatory Arthritis**

Presenting Author: Kiana L. Chen

Co-Authors: Xi Lin, Lianping Xing, H. Mark Kenney, Richard D. Bell, Edward M. Schwarz, and Homaira Rahimi

Lab PI / Mentor: Homaira Rahimi

Abstract (3500 characters or 500 words Limit)

Background: Rheumatoid arthritis (RA) is a chronic inflammatory joint disease that is female predominant. The TNF-transgenic (TNF-Tg) mouse model of RA also develops a sexually dimorphic inflammatory arthritis with earlier disease appearing in female mice (1). While the mechanism of the sexual dimorphism is unknown, studies suggest androgens can provide a protective effect against inflammatory disease progression (2,3). We hypothesize that androgens' anti-inflammatory effects on myeloid cells in the joint may mediate inflammatory arthritis progression.

Methods: Orchiectomy and sham control procedures were performed on 4-week old male TNF-Tg mice (n=3 mice/group). Mice were sacrificed at 3-months of age for serum and tissue collection. Testosterone and TNFα levels in sera were compared between groups, and knee joints sections were H&E and TRAP stained for histomorphometry. Bone marrow-derived macrophages (BMDMs) plated from 3-month old male and female TNF-Tg mice (n=3 mice/group), were treated with 0.1μM, 0.5μM, and 1μM of testosterone propionate (T), followed by murine IFNɣ and LPS stimulation. After 48 hours, supernatant was assayed for murine TNFα via ELISA . Groups were analyzed using unpaired t-tests for orchiectomy studies, and two-way ANOVA for in vitro studies. Values are reported as the mean ± standard deviation.

Results: Orchiectomized (Orch) mice joints had significantly higher (i.e. worse) histology scores than sham controls for synovial inflammatory infiltrate, pannus invasion, and TRAP+ area (2 Orch vs 1 Sham, 1.6 Orch vs 0.7 Sham, 1.4 Orch vs 0.3 Sham, $p<0.05$). Orchiectomized TNF-Tg mice were confirmed to have low testosterone levels (0.078 ng/mL (0.054-0.12) ng/mL, normal=1.3 ± 0.4 ng/mL). Serum human (h) and mouse (m)TNFα levels remained unchanged between orchiectomized and sham TNF-Tg mice (827 pg/mL, range 271-1400 pg/mL Orch vs 841 pg/mL, range 613-1011 pg/mL Sham hTNF and 8.5 pg/mL, range 7-10 pg/mL Orch vs 8.8 pg/mL, range 8-9.8 pg/mL Sham mTNF). Male derived BMDMs did not have a significant change in mTNFα expression when treated with T at any concentration compared to untreated cells (74.84 ± 101.9 pg/mL T 0.1μM, 107.1 ± 97.05 pg/mL T 0.5μM, 71.92 ± 64.55 pg/mL T 1μM vs 73.56 ± 72.48 pg/mL Untreated, $p>0.05$). Remarkably, female derived BMDMs had increased mTNFα expression at a concentration of 0.1μM compared to untreated cells (544.06 ± 363.6 pg/mL T 0.1μM vs. 21.50 ± 22.48 pg/mL Untreated, $p<0.01$).

Conclusions: Here we show that reduced levels of testosterone from orchiectomies is associated with increased synovial inflammation in TNF-Tg males, yet does not affect systemic TNFα levels. In vitro studies of BMDMs indicate that macrophages from TNF-Tg mice have sex and testosterone concentration specific release of TNFα, suggesting a sexual dimorphism at the cellular level. Further studies of in vivo and in vitro T administration to both sexes are necessary to clarify local versus systemic immune responses in TNF-Tg mice.

1. Bell R.D. et al. Arthritis Rheumatol 71(9):1512-1523. 2019.
2. Traish A et al. J Clin Med 7(12):549. 2018.
3. Lashkari M et al. Electron Physician 10(3):6500-6505. 2018.

Title: **Non-invasive Assessment of the Ulnar Nerve Around the Elbow and Diagnosis of Cubital Tunnel Syndrome using Ultrasound**

Presenting Author: Alexander Chirokikh

Co-Authors: Courtney Marie Cora Jones, PhD, MPH & Constantinos Ketonis, MD, PhD

Lab PI / Mentor: Constantinos Ketonis, MD, PhD

Abstract (3500 characters or 500 words Limit)

Objective:
Assess the feasibility of ultrasound as an alternative to NCS/EMG for the diagnosis of cubital tunnel syndrome.

Background:
Cubital tunnel syndrome is characterized by compression of the ulnar nerve at the elbow. It is the second most common peripheral entrapment neuropathy behind carpal tunnel syndrome, with an estimated 72,000 cases per year in the United States. Currently, the gold standard for diagnosis of cubital tunnel syndrome is electrodiagnostic studies, comprised of nerve conduction study (NCS) and electromyography (EMG). The sensitivity of NCS/EMG however, can range from 37-86%, and therefore recently, ultrasound (US) emerged as a promising non-invasive modality for cubital tunnel diagnosis. Using US, the ulnar nerve can be visualized and its cross-sectional area (CSA) can be quantified. CSAs that exceed 10 mm2 indicate swelling within the nerve which suggests downstream nerve compression consistent with cubital tunnel syndrome.

Methods:
Fifty-one patients who presented to Clinton Crossings clinic (Rochester, NY) with symptoms consistent with cubital tunnel syndrome were enrolled in this prospective study after providing informed consent. The following data were collected: EMG/NCS, maximum CSA, grip strength, key pinch, and two-point discrimination in the ulnar distribution. Patients were also administered the following symptom-based questionnaires: PRUNE, PROMIS, and DASH. To assess classification differences between NCS/EMG and US, a McNemar's test was used to quantify agreement. PRUNE scores were compared between patients classified as abnormal and normal on both NCS/EMG and US using an independent samples t-test. Pearson's correlation coefficients were used to assess the associations of NCS/EMG and maximum CSA with various symptom measures. A p-value of <0.05 was considered statistically significant for all analyses.

Results:
Fifteen patients were classified as abnormal both by NCS/EMG and US, 14 were classified abnormal by US only, 2 were classified abnormal by NCS/EMG only, and 8 were classified normal by both NCS/EMG and US ($p=0.003$, $K = 0.23$). Mean PRUNE scores among those with abnormal and normal NCS/EMG were 49.00 ± 18.13 and 40.23 ± 20.30, respectively ($p=0.17$). Mean PRUNE scores among those with abnormal and normal US were 45.22 ± 19.19 and 40.65 ± 21.58, respectively ($p=0.53$). Of those with PRUNE scores above the 10th percentile, EMG/NCS classified 17 patients as abnormal and 18 as normal. However, US classified 27 patients as abnormal and 8 as normal. Sensory amplitude correlated weakly with PRUNE ($r=-0.27$, $p=0.11$), PROMIS-Physical Function ($r=0.36$, $p=0.03$), and DASH ($r=-0.37$, $p=0.03$). Motor conduction velocity across the elbow weakly correlated with PROMIS-Physical Function ($r=0.30$, $p=0.08$), PROMIS-Pain Interference ($r=-0.27$, $p=0.11$), and DASH ($r=-0.23$, $p=0.17$). Maximum CSA only correlated with PROMIS-Depression ($r=0.34$, $p=0.04$).

Conclusion(s):
US may be a more sensitive tool than EMG/NCS for cubital tunnel syndrome diagnosis, while EMG/NCS may be a stronger predictor of symptom severity. Future studies will investigate the prognostic value of US following cubital tunnel release surgery.

Title: **The Role of Demographic and Academic Characteristics on Industry Payments Received by Orthopedic Spine Surgeons in 2019 and 2020**

Presenting Author: Adwin Denasty, MD

Co-Authors: Sean Pickard BS, Peter Joo MPH, Kristen Radcliff MD, Addisu Mesfin MD

Lab PI / Mentor: Addisu Mesfin, MD

Abstract (3500 characters or 500 words Limit)

Background/Objective: In an attempt for transparency, industry payments from medical device and drug companies are now required to be disclosed to Centers for Medicare and Medicaid Services (CMS), according to the Physician Payment Sunshine Act of 2010. According to data from the CMS, from 2014 and 2019, a total of $1.79 billion dollars was paid to 108,041 orthopedic surgeons. Our objective is to: evaluate the role of demographic characteristics (gender and race/ethnicity) and academic characteristics (H-index, fellowship completed) have in relation to industry payments received by orthopedic spine surgeons in 2019 and 2020.

Methods: This study is a cross-sectional retrospective analysis of orthopedic spine surgeons in the United States. The authors utilized the Centers for Medicare and Medicaid Services (CMS) website in August of 2021 to gather information on all industry payments received by orthopedic spine surgeons in 2019 and 2020. In addition to payments, the following variables were subsequently identified for each surgeon: gender, race/ethnicity, practice setting, spine fellowship completed, years of practicing experience and scholarship/research productivity (measured by the H-index). The authors utilized Scopus Preview, Web of Science, and Google Scholar databases to determine the H-index for each surgeon. Surgeon websites were queried for all other variables. Surgeons who were either deceased or retired and have not received industry payments in both 2019 and 2020 were excluded from the study.

Results: A total of 1738 orthopedic spine surgeons were included in the study, 1703 men (97.9%) and 35 women (2.1%). Payments in 2019 and 2020 were compared among men and women. Potential confounding variables such as years in practice and H-index was controlled for. On linear regression, Asian surgeons made on average $126,082.58 more than White surgeons in 2019 (p=0.01), holding the other groups constant and controlling for gender, years in practice, H-index, and practice type.

The average H-index for men and women orthopedic spine surgeons were 7.23 and 4.21, respectively. Years in practice and H-index were independent predictors of higher payments. Surgeons graduating from the Washington University in St. Louis received the highest industry payments.

Conclusion: Demographic characteristics does play a role in the amount of industry payments received by spine surgeons. Women orthopedic spine surgeons on average received 21.5% of the payments that their male counterparts received in 2019, and 14.4% in 2020. Hispanic and pacific islanders received the least amount of industry payments in 2019 and 2020. There continues to be disparity in payments between surgeons of different race/ethnicity and gender.

Title: **Fabrication of Cylindrical MSC-Sheets With Tunable Notch Signaling as Engineered Periosteum**

Presenting Author: Ihab El-atawneh

Co-Authors:

Lab PI / Mentor: Hani Awad

Abstract (3500 characters or 500 words Limit)

Massive bone loss in extremities is a challenging clinical problem. The standard of care is reconstructing the extremity by utilizing processed decellularized allografts. With 2.2 million bone graft procedures worldwide, allografts are marred with complications, including infection and fractures, that render their survival rate at 5 years to 52%. Previous work on murine intercalary femoral allograft model exhibited poor healing compared to the vitalized autograft primarily due to the lack of the periosteum and its osteoprogenitors in the allograft. The absence of a periosteal osteoprogenitors in processed allografts results in deficits osteogenesis, angiogenesis, and osteoclastic remodeling. To address the challenges of extremity bone regeneration, we are employing the thermo-responsive behavior of poly-N-isopropyl acrylamide (PNIPAM) to engineer cylindrical pseudo-periosteal membranes with de novo cell-secreted ECM. PNIPAM properties allow the fabrication of a single intact cell layer of marrow-derived mesenchymal stem cells (MSC) while preserving their surface markers and expression of gene markers of stemness . When engrafted on allografts as periosteum and transplanted to reconstruct femoral diaphyseal defects in the mouse, MSC-sheets induced robust callus formation, improved graft incorporation, and enhanced the torsional strength reaching about 70% of the strength of normal bones in just 6 weeks . These findings led to our hypothesis that MSC sheets can regenerate massive bone defects within a clinically relevant time frame. Using human MSCs in tissue engineering has many limitations because of the loss of stemness and multipotency during cell expansion. Studies have shown that the activation of Notch signaling pathway in cultured hMSCs via surface-coated recombinant Jagged1 (JAG1) ligand promotes hMSC maintenance and expansion while increasing their skeletogenic differentiation capacity . In vivo, previous studies showed that the transient inhibition of gamma secretase using DAPT improved fracture repair in mice . Therefore, we hypothesize that modulating Notch using JAG1 and DAPT will optimize the production of hMSC sheets in vitro and potentiate osteogenesis in vivo upon grafting devitalized bone allografts to reconstruct a critical size defect in the extremity bone, respectively. The work will establish Notch as single bidirectional molecular switch to enhance hMSC expansion and osteogenic differentiation of hMSC sheets. Calcium phosphate scaffolds will facilitate transfer and grafting of the cylindrical sheets in a rat model of 3D printed scaffold reconstruction of a critical femoral defect.

Title: **Cartilage-synovium crosstalk in osteoarthritis: role of NR4A1 signaling**

Presenting Author: Katherine Escalera-Rivera

Co-Authors:

Lab PI / Mentor: Jennifer H. Anolik and Jennifer H. Jonason

Abstract (3500 characters or 500 words Limit)

Osteoarthritis (OA) is a degenerative joint disease that currently affects over 30 million United States adults, with aging and injury as two of its main risk factors. OA is characterized by irreversible articular cartilage damage but can affect all tissues within the joint including the synovium. As OA progresses, chondrocytes within the cartilage matrix start to secrete NF-kappaB-mediated cytokines and damage-associated molecular patterns, which are released into the joint synovial fluid. These molecules are recognized by synoviocytes and infiltrating immune cells, which activate the NF-kappaB pathway to start secreting inflammatory mediators, creating a continuous feedback loop between cartilage and synovium that constitutes the initiation of chronic inflammation. NR4A1 is a transcription factor rapidly induced by inflammatory stimuli and a negative regulator of NF-kappaB signaling in multiple cell types, including macrophages, commonly found in the inflamed synovium. However, the role of NR4A1 in regulating proinflammatory signaling in chondrocytes and in OA progression is not understood. Using Immunohistochemistry to measure NR4A1 protein levels in chondrocytes of the articular cartilage of mice, we find a significant decrease in NR4A1 in joints subjected to meniscal/ligamentous injury (MLI) when compared to sham joints. To elucidate the role of NR4A1 during post-traumatic OA (PTOA) onset and progression, we performed MLI in wild-type (WT) C57BL/6J and age-matched NR4A1 global knockout (KO) mice and harvested the knee joints 4 weeks later for histology. We found increased loss of articular cartilage in NR4A1 KO mice compared to WT mice. In vitro, loss of NR4A1 in a chondrogenic cell line led to increased transcription of NF-kappaB target genes. Our data lead us to propose that NR4A1 in chondrocytes normally prevents uncontrolled secretion of inflammatory cytokines, a homeostatic role that is disrupted by enhanced protein degradation following joint injury, promoting chronic inflammation of the synovium and OA progression.

Title: **Hydrogel Swelling Induces Cell Alignment at Dentin Interfaces**

Presenting Author: David Fraser

Co-Authors: Tram Nguyen, Alex Kotelsky, Danielle S.W. Benoit

Lab PI / Mentor: Danielle S.W. Benoit

Abstract (3500 characters or 500 words Limit)

Introduction: Insertion and alignment of collagen fibers at hard-fibrous tissue interfaces is critical for repair of multiple tissues, including the periodontium. Since cell alignment can precede oriented fiber production, various techniques have been applied for engineering materials that guide alignment of periodontal ligament cells (PDLCs) perpendicular to tooth root (dentin) surfaces. Poly(ethylene glycol) (PEG) hydrogels are a tunable, soft matrix that can be used to encapsulate cells and direct their activity. In this study, we created an in vitro model consisting of dentin blocks, PEG hydrogels, and PDLCs, uncovering a previously unreported relationship between hydrogel mechanics and cell activity and devising a novel method for controlling PDLC alignment at dentin interfaces.

Materials and Methods: Dentin blocks and PDLCs were obtained from extracted human teeth following informed consent. PDLCs were suspended in PEG hydrogel solutions containing a matrix metalloproteinase-degradable crosslinker and RGD peptide and placed in molds with dentin blocks prior to hydrogel formation. Constructs were cultured in vitro for up to 7 days before characterization. Finite element analysis (FEA) was also used to simulate dynamic hydrogel behavior.

Results. PDLC spread within hydrogels and aligned perpendicular to the dentin surface but showed random alignment in regions distant to the dentin blocks. FEA suggested that hydrogel swelling occurring next to the stiff, non-swelling dentin created tensile strain at the hydrogel-dentin interface. Hydrogels were then tuned to display a range of swelling behaviors, where hydrogel volume increased isometrically within the first 24 hours before reaching equilibrium. PDLCs in constructs with minimal swelling showed random alignment adjacent to dentin blocks, similar to PDLC morphology in dentin-free hydrogels. As hydrogel swelling increased, both the degree of PDLC alignment and the extension of PDLC alignment from the dentin surface also increased. Swelling-mediated PDLC alignment also altered expression of PDL matrix genes without impacting cell viability. This phenomenon was replicated using different mold dimensions, bone blocks, and other cell types, suggesting a wider applicability of this composite system.

Conclusions. Hydrogel swelling induced cell alignment at dentin interfaces through production of localized, tensile strain. PDLCs responded to this strain by remodeling the hydrogel matrix and aligning perpendicular to the dentin surface. Further work using this model may be instrumental in unraveling the biomechanics of cell alignment and engineering robust interfacial tissues.

Title: **Spatial transcriptomics reveal unique molecular fingerprints of chondrogenesis during embryonic limb development**

Presenting Author: Victoria Hansen
Co-Authors: Gulzada Kulzhanova, Helen Shammas, Jack Reuter
Lab PI / Mentor: Chia-Lung Wu

Abstract (3500 characters or 500 words limit)

Introduction: Cartilage is an aneural and avascular tissue with poor healing capacity. In this regard, tissue engineering and stem cell therapy may offer important means to restore degraded cartilage for arthritic patients. However, how to precisely guide stem cells toward desired cartilage phenotype without off-target differentiation remains challenging, largely due to complicated signaling pathways, gene regulatory network, and cell-cell interactions involved in chondrogenesis. Here, we propose that dynamic biochemical cues during embryonic limb development provide significant insights into developing bona fide cartilage tissue. Thus, we aim to elucidate underlying molecular mechanisms regulating embryonic chondrogenesis by spatial transcriptomics (Spatial-seq), a novel next-generation sequencing technique allowing us to decipher gene expression profiles of cells in a spatially-resolved manner.
Method: Hindlimbs were harvested from E18.5 mouse embryos. Samples were cryo-sectioned and submitted to the UR GRC for Spatial-seq (Visium, 10X Genomics). Space Ranger was applied to map the whole transcriptome onto the hindlimb section. Bioinformatics packages including Seurat, Monocle, RcisTarget, and CellPhoneDB were used to determine distinct cell populations, detect differentially expressed genes (DEGs), construct differentiation trajectories, and identify cell-cell interactions, respectively.
Results and Discussion: Initial unsupervised clustering reveals 12 clusters representing various cell populations in hindlimb tissues including skin, muscle, marrow, cartilage, bone etc. To investigate embryonic chondrogenesis, we re-clustered cells around the knee joint (including both femur and tibia) and identified 4 distinct cell populations in a spatially-resolved zonal structure of cartilage tissue: 1) Col6a1/Acan+ superficial chondrocytes, 2) Wwp2/Col2a1+ proliferative middle chondrocytes, 3) Spp1/Pth1r+ deep pre-hypertrophic chondrocytes, and 4) Tnmd/Kera+ tendon cells. DEG analysis detected 131 DEGs between superficial and middle chondrocytes with Snorc and several troponin genes enriched in middle chondrocytes, while superficial chondrocytes have high expression of Cpxm2 and Tgfbi. Using pseudotime ordering and DNA binding motif analysis, we found that Mef2 family, TFIID complex and Srf are putative transcription factors (TFs) modulating differentiation of superficial chondrocytes into middle zone proliferative phenotype. Interestingly, only 21 DEGs were detected between proliferative middle and pre-hypertrophic chondrocytes despite having their own unique signatures, implying an early transition phase of middle chondrocytes into pre-hypertrophic chondrocytes at E18.5 stage. We further identified that Klf family, Clock, Snai3, and Foxa2 are among top TFs potentially modulating chondrocyte hypertrophic maturation process. Furthermore, cell-cell crosstalk analysis reveals that DLK1-NOTCH2, PTN-PTPRS, and IGF2-IGF1/2R are conserved cell-cell interactions among chondrocyte populations. However, MDK-LRP1 (a signaling axis essential for chondrocyte proliferation) and IGF2-IDE are unique cell-cell cross-talks only detected in superficial-middle chondrocytes and middle-pre-hypertrophic chondrocytes, respectively.
Conclusion and Future direction: Using Spatial-seq, we have identified 3 distinct chondrocyte phenotypes and one tendon population in the developing knee of E18.5 embryos. DEGs, putative TFs regulating and cell-cell interactions governing chondrocyte maturation were also determined. We are currently analyzing Spatial-seq datasets acquired from E11.5, E13.5 and E15.5 hindlimbs. Multiple Spatial-seq datasets with corresponding single cell RNA sequencing from above-mentioned time points will be integrated to delineate temporal-spatial gene expression profiles controlling embryonic chondrogenesis with enhanced cellular resolution. We believe our findings will facilitate cartilage regenerative medicine toward therapeutic applications.

Title: **Utilization of Novel Oxygen Reporting Molecule PtTAPIP and its Derivatives for Intravital Imaging of Oxygen Tension**

Presenting Author: Connor Heckman

Co-Authors: Kevin Schilling

Lab PI / Mentor: Edward Brown and Xinping Zhang

Abstract (3500 characters or 500 words Limit)

Measurements of oxygen tension (pO2) at high spatiotemporal resolution in three dimension is crucial for understanding oxygen delivery and consumption in bone defect repair and bone tissue engineering. Utilizing a two-photon excitable platinum porphyrin–coumarin-343 (PtP-C343) phosphorescent nanoprobe, we previously demonstrated a two-photon based phosphorescence lifetime imaging (2P-PLIM) approach for high resolution and real-time measurement of pO2 at the site of cranial bone defect repair. While successful, PtP-C343 relies on long acquisition time and high power to produce a signal from which a pO2 can be derived. A unique class of porphyrinoids, specifically Pt tetraaryphthalimidoporhyrin (PtTAPIP), exhibits higher oscillator strengths and a red-shifted stronger red/near infra-red absorption than regular porphyrins, a key advantage that enables more efficient excitation of molecules in biological tissues. The goal of our current study is to determine this new class of porphyrinoids and their derivatives for efficient pO2 measurements via 2P-PLIM in vitro and in vivo. Two approaches were tested to deliver the oxygen-sensitive nanoprobes into the living animals, via encapsulation of hydrophobic PtTAPIP in nanofibers and via direct injection of a soluable high-performance nanoprobe Oxyphor 2P (OX2P) in circulation. Our data demonstrated that the new class of nanoprobes produced an average of 60-fold higher signal than PtP-C343 in vivo or in vitro. The enhanced sensitivity dramatically lowered the power and acquisition time of phosphorescent signals, markedly reduced tissue scattering, allowing for deeper measurements of pO2 within bone. Since OX2P and PtTAPIP can be optimally excited at two different wavelengths of 960nm and 900nm respectively, we tested their ability to produce 2-photon phosphorescent signals at each other's respective wavelengths. Our results showed that while OX2P produced similar 2-photon signals at 900nm and 960nm, PtTAPIP generated ~10-20 fold lower signals at 960nm. When encapsulated in nanofibers, PtTAPIP at 20uM showed nearly ~ 50 fold lower signals at 960nm. This difference suggests the possibility of using PtTAPIP encapsulated nanofiber and soluble OX2P for pO2 measurement at the different stage and different location during bone defect healing. PtTAPIP containing oxygen reporting fiber mesh could allow oxygen measurements prior to the formation of vessels at the site of defect, potentially differentiating oxygen signals within or outside the scaffold. Further in vitro and in vivo work are ongoing to explore various approaches utilizing PtTAPIP and its enhanced derivatives for 2P-PLIM based high spatiotemporal oxygen measurements in vivo.

Title: **Racial, Ethnic, and Income-Based Disparities in the Surgical Treatment of Rotator Cuff Tears**

Presenting Author: Alan Hwang, MD

Co-Authors: Linda Zhang, MD; Gabriel Ramirez, MS; Ilya Voloshin, MD; Caroline Thirukumaran MBBS, MHA, PhD

Lab PI / Mentor: Caroline Thirukumaran, MBBS, MHA, PhD

Abstract (3500 characters or 500 words Limit)

Background: Rotator cuff tears are a commonly encountered problem within orthopedic surgery and can be associated with pain and disability of the shoulder. Indications for surgical repair of rotator cuff tears are controversial and there is currently no agreed upon treatment algorithm in the literature. Race-based and income-based disparities are present within orthopedic surgery, including in the treatment of rotator cuff disease. The goal of this study is to determine the rate of operative rotator cuff repair in New York State, and to analyze the racial/ethnic and income-based disparities in receiving surgical treatment for a rotator cuff tear.

Methods: A retrospective review of the Statewide Planning and Research Cooperative System (SPARCS) Database of New York State was conducted to include patients with a new diagnosis of rotator cuff tear between July 1, 2017 and June 30, 2019, with at least 6 months follow-up. The key outcome of interest was whether a patient with a rotator cuff tear underwent surgical treatment or not. We conducted bivariate analysis using chi-square tests and est imated multivariate logistic regression models to determine racial/ethnic and income-based disparities in the use of surgical treatment with rotator cuff repair to control for confounders.

Results: A total of 87,660 patients were identified for analysis. Of these, 36,422 patients (41.5%) underwent surgical treatment with either open or arthroscopic rotator cuff repair. Rates of surgery peaked in the 60-69 age group. Multivariate analysis showed that male gender (Adjusted Odds Ratio [AOR]: 1.18; 95% Confidence Interval [CI]: 1.14 to 1.22; $p < 0.001$), Asian race (AOR: 1.27; 95% CI 1.00 to 1.62); $p = 0.048$), Workers' Compensation insurance (AOR: 1.12; 95% CI: 1.07 to 1.18; $p < 0.001$), and higher income quartile of home ZIP code (AOR: 1.19; 95% CI: 1.09 to 1.30; $p < 0.001$) were independently associated with higher rates of rotator cuff surgery; while black race (AOR: 0.78; 95% CI: 0.69 to 0.87; $p < 0.001$), Hispanic/Latino ethnicity (AOR: 0.91; 95% CI: 0.85 – 0.97); $p = 0.004$), and Medicaid (AOR: 0.75; 95% CI: 0.70 to 0.80; $p < 0.001$), or other government insurance (AOR: 0.82; 95% CI: 0.78 to 0.86; $p < 0.001$) were independently associated with lower rates of rotator cuff surgery. The effects of race were altered when accounting for the other covariates, suggesting that race alone does not account for the differences in rate of surgery for rotator cuff tear.

Conclusion: This analysis demonstrates significant differences in demographic factors in patients diagnosed with a rotator cuff tear who undergo operative repair versus those who do not. This supports existing evidence that there are racial and socioeconomic disparities that influence treatment of this common orthopedic problem. Efforts should be made to identify barriers in disadvantaged populations and lessen disparities in treatment.

Title: **Dissecting the role of DNA double-strand breaks in osteoarthritis pathogenesis**

Presenting Author: M. Nick James

Co-Authors: Jennifer H. Jonason

Lab PI / Mentor: Jennifer H. Jonason, Ph.D. and Danielle Benoit, Ph.D.

Abstract (3500 characters or 500 words Limit)

Osteoarthritis (OA), the most common and most costly form of arthritis, is characterized by progressive loss of articular cartilage, however, the exact molecular mechanisms responsible for OA onset are still unclear. Aging is known to be among the most important risk factors associated with OA development. While aging is thought to be a consequence of accumulated DNA damage, the relationship between DNA damage and OA is not clear. Our laboratory has found that aged articular chondrocytes have increased inflammatory NF-κB activation and that enhanced IKKβ/NF-κB activation in chondrocytes accelerates spontaneous OA development in relatively young mice. DNA double-strand breaks (DSBs), a particularly toxic form of DNA damage, are also known to activate IKKβ which, in turn, promotes inflammatory NF-κB signaling. Thus, we hypothesize that accumulation of DNA damage in aging leads to chronic proinflammatory signaling that ultimately results in degeneration of articular cartilage and OA onset. To investigate the inflammatory role of DNA damage in OA development, we treated ATDC5 chondroprogenitors with the topoisomerase inhibitor etoposide to induce DNA DSBs. We demonstrated that etoposide effectively produces accumulation of DNA DSBs in ATDC5 chondroprogenitors and increases NF-κB activation by western blot. In vitro etoposide treatment also increased expression of NF-κB and IRF gene targets including proinflammatory cytokines, catabolic matrix enzymes, and interferon-stimulated genes. For more physiologically relevant experiments we plan to utilize the intron-encoded endonuclease, IPpoI, which will allow inducible, cartilage-specific induction of DNA DSBs. However, as proof of concept before moving in vivo, we transfected ATDC5 cells with an expression vector encoding NLS-I-PpoI which resulted in increased proinflammatory and catabolic chondrocyte gene expression. With confidence in the IPpoI endonuclease, we started our investigation in vivo using tamoxifen to induce expression of an IPpoi-ERT2 fusion protein to create cartilage-specific DSBs. Although intraperitoneal tamoxifen injection did not lead to an overt change in the number of DNA DSBs, we did observe an increased number of apoptotic cells marked by TUNEL (n=1). While these results suggest that DNA damage-induced inflammation may play a role in OA development, we are currently investigating the tamoxifen regimen and timing of DSB assessment after induction to better understand chondrocyte response to DNA DSBs. Understanding the impact of DNA DSBs on OA pathogenesis could inform development of novel OA therapeutic strategies that interrupt signaling pathways which mediate inflammation in OA.

Title: **In Vivo Engineered Extracellular Matrix as Scaffolding Materials for Biomimetic Periosteum**

Presenting Author: Chen Jiang

Co-Authors: Nicholas Lenhard, Kevin Schilling

Lab PI / Mentor: Xinping Zhang

Abstract (3500 characters or 500 words Limit)

Structural bone allograft has been widely used to treating critical sized bone defects that need immediate support. Many tissue banks have developed methods to sterilize allografts to ensure safety. The improved donor screening/testing techniques and the additional oversights from organizations, including Food and Drug Administration (FDA) and American Association of Tissue Banks (AATB), have further facilitated the wide application of bone allografts. However, bone allografts have not achieved a similar level of efficacy as compared to autografts, mainly due to the lack of periosteum, which contributes to over 70% of bone formation at the early stage of autograft-mediated healing. The absence of periosteum in allografts is directly associated with a 60% failure rate in 10 years after implantation due to non-union, infection, and propagation of microcracks of the devitalized bone. To enhance allograft incorporation and remodeling, various synthetic materials have been used to fabricate biomimetic replacement of periosteum. While limited success has been achieved, periosteum fabricated by synthetic materials is not patient-specific and may elicit immune or foreign body reactions to comprise healing and osseointegration the allografts. To address these limitations, we proposed an in vivo bioengineering strategy to generate decellularized extracellular matrix (dECM) with microchannels for guided periosteum tissue engineering. By implantation of a 3-dimensional (3D) printed polylactic acid (PLA) microfiber template subcutaneously or at a femoral defect site, a fibrous scaffold with defined paral|eled microchannels was created following a series of steps of depolymerizaton and decellularization. MicroCT and multiphoton analyses demonstrated well-organized multilayered and multichanneled structures within the scaffolds. The fabricated dECM were tested in vitro using bone marrow isolated from transgenic mice that mark endothelial cells and osteoblasts with fluorescence protein. Our data showed that dECM scaffolds supported the attachment, proliferation and infiltration of osteogenic and angiogenic cells in vitro. Osteogenesis can be further enhanced following mineralization of dECM in simulated body fluid (SBF). Future work will be focused on testing these dECM as periosteum mimetics in vivo. Additionally, our research will compare the difference between subcutaneously derived dECM and femur defects derived dECM and investigate the effect of TGFβ deficient signaling on ECM formation. Our goal is to 1) demonstrate a novel strategy to yield ECM scaffolds for periosteum tissue engineering; 2) offer mechanistic information on soft tissue ECM synthesis at different implantation sites for regeneration.

Title: **Mitochondrial transfer from donor to host utilizing ex vivo culture of mouse hematopoietic stem cells**

Presenting Author: Hiroki Kawano

Co-Authors: Yuko Kawano, Charles O. Smith, Mark W. LaMere, Michael W. Becker, Roman A. Eliseev, and Laura M. Calvi

Lab PI / Mentor: Laura M. Calvi

Abstract (3500 characters or 500 words Limit)

Mitochondrial dysfunctions have been observed in various conditions that spans from metabolic syndromes to mitochondrial disease, such as the Leigh syndrome, which can be caused by mutations in the nuclear DNA- or mitochondrial DNA (mtDNA)-encoded mitochondrial genes. Mitochondrial organelle and mtDNA transfer has been an emerging mechanism that enables regeneration and repair of damaged cells or tissues. Hence, developing the technology that facilitates transfer of mitochondria and mtDNA from donor to host cells can be a promising strategy for the treatment of mitochondrial dysfunctions. Here, we utilized a previously reported ex vivo culture of mouse hematopoietic stem cells (HSCs) and succeeded in expanding HSCs efficiently. Sufficient donor HSC engraftment into host was attained in a donor cell number-dependent manner. Then, to assess the mitochondrial transfer from donor HSCs to recipient cells, we expanded HSCs from the mitochondrial-nuclear exchange (MNX) mice. These mice have the nuclei from the C57BL/6 strain and mitochondria from the C3H strain. Thus, the MNX mice have C57BL/6 immunophenotype and C3H mtDNA which is known to confer more efficient OxPhos function to mitochondria. Our hypothesis was that the more efficient mitochondria from the MNX donor cells will be transferred to host cells. The expanded MNX HSCs were transplanted into the irradiated hosts and the analyses done at six weeks post transplantation. We observed high engraftment of donor cells, which has been further evaluated in each hematopoietic progenitor or HSC. We have also shown that HSCs from the MNX mice can transfer mtDNA to host cells. This work highlights the utility of ex vivo expanded HSC to achieve the mitochondrial transfer from donor to host in the transplant setting.

Title: **Defining the Time-Dependent Requirement for Scleraxis-lineage Cells During Tendon Healing**

Presenting Author: Antonion Korcari

Co-Authors: Alayna Loiselle

Lab PI / Mentor: Alayna Loiselle

Abstract (3500 characters or 500 words Limit)

During healing, tendons produce a fibrotic tissue by deposition of abundant and disorganized extracellular matrix (ECM), resulting in permanent impairment of tendon function. Scleraxis-lineage (ScxLin) cells are the predominant cell population in the healing flexor tendon (FT). To determine the requirement of ScxLin cells during tendon healing, we depleted them during the proliferative healing and collected the samples during the remodeling phase. We hypothesized that ScxLin cells are required to successfully restore tendon mechanics and morphology and to maintain myofibroblasts cell content.
We generated Scx-Cre+; DTRF/+mice. To inducibly deplete ScxLin cells, 20ng of diphtheria toxin (DT) was injected into the hindpaw for 5 consecutive days. Scx-Cre-; DTRF/+ mice were also injected with DT and served as wildtype controls. Murine FT repair model: 10-12 week old mice underwent complete transection and repair of the FTs in the right hindpaw. Between the 14th and the 18th day post-surgery, DT was injected in the hindpaw to deplete ScxLin cells during the proliferative phase. All hindpaws were harvested at 14-, 28-, or 56-days post-surgery. Immunofluorescence: 5μm paraffin sections from 4 biological samples (N=4) harvested at the timepoints above were incubated with antibodies for α-SMA conjugated to Cy3. Histology: 5μm paraffin sections from 4 biological samples (N=4) were stained with Alcian Blue Hematoxylin Orange Green (ABHOG) to visualize newly produced collagen and glycosaminoglycans (GAGs). Uniaxial displacement-controlled stretching of 0.1% strain per second until failure was applied.
First, we found that depletion of ScxLin cells during the proliferative phase (D14-18) significantly impairs FT structural and material properties by D28 but shows partial restoration by D56. Next, we showed that at D28 post-surgery, depleted tendons had singificantly decreased myofibroblastic content, and impairments in the production and morphology of newly synthesized collagen matrix in the tissue bridging area.
We showed that depletion of ScxLin cells during the proliferative healing phase significantly impairs both structural and material properties during the remodeling phase. Based on the impairments of D28 ScxLin,DTR tendons, it is suggesting that ScxLin cells regulate the healing response by directly producing ECM molecules required for wound closure and/or differentiating to myofibroblasts and then producing ECM proteins required for wound closure. Interestingly, our data showed that the D28 ScxLin,DTR tendons had identical structural and material properties as well as similar morphology of newly synthesized bridging tissue compared to D14 WT repairs. Thus, considering that depletion started at D14 post-surgery, these data further suggest a potential stagnation of the healing response upon ScxLin cell depletion. Strikingly, we found that during the late remodeling phase (D56 post-surgery), ScxLin,DTR tendons showed partial restoration of their material quality with no differences in elastic modulus relative to wildtype control repairs. These data suggest that while ScxLin cells may play a central role in healing to ~D28, a different cell population may control long-term remodeling and restoration of mechanical properties. Ongoing studies are focused on distinguishing between the ScxLin cells that are targeted for depletion, and those cells that mediate the partial mechanical recovery of ScxLinDTR tendons from D28-D56.

Title: **Differential Expression of Piezo1 and p-mTOR in Articular Chondrocytes of ACL-injured Mice**

Presenting Author: Alex Kotelsky (or one of the co-authors, please consider this abstract for a poster presentation)

Co-Authors: Alexander Kotelsky, Brian Wise, Katie Broun, Hana Kalco, Sandeep Mannava

Lab PI / Mentor: Whasil Lee

Abstract (3500 characters or 500 words Limit)

Anterior cruciate ligament (ACL) tears destabilize knee joints, alter gait kinematics, and 50% of ACL patients eventually develop post-traumatic osteoarthritis (PTOA). Although etiology of PTOA is multifactorial, one possible factor is injury/death of articular chondrocytes that promote imbalanced metabolism driven by chondrocyte phenotype changes and death, and eventually lead to cartilage degradation. Piezo1 is a mechanically activated ion channel playing the essential role of sensing high-strain mechanical cues and leading to chondrocyte death from injurious mechanical trauma. Recently, we found that chemical activation of mechano-sensitive Piezo1 channels makes in-situ chondrocytes more vulnerable to mechanical loading in female, but not in male mice. Furthermore, we found that inhibition of mTOR with rapamycin equally rescues articular chondrocytes from mechanical injury in males and females. Based on these findings we hypothesize that in-situ articular chondrocytes with higher expression levels of Piezo1 channels and p-mTOR are more vulnerable to injurious loading. Additionally, we expect to observe a sexual dimorphism in Piezo1 expression levels, but not in levels of p-mTOR.

To test our hypotheses, we used a non-invasive bi-lateral ACL injury mouse model to analyze chondrocyte mechano-vulnerability and expression levels of Piezo1 and p-mTOR. Briefly, both knee joints of 8-9 week old male/female C57BL/6 mice were subjected to an axial force in a flexed position until the applied force was dropped. Uninjured mice were used as controls. Both male and female mice developed PTOA by 4 weeks post-ACL injury. To assess mechano-vulnerability of articular chondrocytes in bi-ACL-injured and control groups (n = 8/group), carefully dissected distal femurs with intact cartilage from mice sacrificed at 4-week post-injury were vitally stained and subjected to 1mJ impacts. Areas of injured cells were quantified. While there was no sex-dependent difference in cell vulnerability, areas of injured cells were significantly larger in bi-ACL-injury group (~2 fold). Immunofluorescence assay was used to detect the expression levels of p-mTOR and Piezo1 after harvesting, paraffin embedding and slicing 7um thick sections of the intact knee joints (n = 3/group). The expression levels were evaluated based on the relative intensity of anti-Piezo1 or anti-p-mTOR signal in ImageJ. As expected, we observed sexual dimorphism with higher expression levels of Piezo1 in females (both in control and in injured groups), and lack of sexual dimorphism in p-mTOR expression. Regardless of sexual dimorphism, we observed a consistent elevation in expression levels of both p-mTOR (2-fold) and Piezo1 (1.5-fold) in bi-ACL-injury group relative to controls in female and male mice.

Taken together, our findings revealed that increased vulnerability of in situ chondrocytes in bi-ACL-injury group may be associated with elevated expression levels of p-mTOR and Piezo1. A recent prostate cancer study demonstrated that downregulation of Piezo1 channels suppressed phosphorylation of m-TOR and prevented mTOR-dependent tumor growth, suggesting that mTOR and Piezo1 are related. Interestingly, chondrocytes of female mice had higher Piezo1 expression levels than male mice. These findings will guide future studies investigating therapeutic strategies with a potential of targeting both mTOR and Piezo1 to delay PTOA progression due to ACL-I.

Title: Validated Whole-Genome RNA Sequencing of Femoral Head Impingement Cartilage Identifies FGF-18 As A Biomarker in Hip Osteoarthritis Progression

Presenting Author: Benjamin Kuhns MD

Co-Authors: John M. Reuter BS, Victoria L. Hansen PhD, Gillian Soles MD, Jennifer H Jonason PhD, Chia-Lung Wu PhD, Cheryl Ackert-Bicknell PhD, Brian Giordano MD

Lab PI/Mentor: Ackert-Bicknell/Wu

Background: The Cam type femoral morphology that defines femoroacetabular impingement (FAI) has been clinically associated with the development of early osteoarthritis (OA), however specific molecular mechanisms underlying this relationship remain poorly understood. The purpose of this study was to use whole genome RNA sequencing to characterize differences in gene expression between articular cartilage samples isolated from patients undergoing surgery for FAI and OA and validate expression differences of selected targets. We hypothesized that FAI and OA samples would have distinct expression profiles and differential expression in multiple pathways related to osteoarthritis.

Methods: 37 subjects undergoing either hip arthroscopy for FAI or total hip arthroplasty for end-stage osteoarthritis were included in the study. 20 gender matched patients (10 OA, and 10 FAI) were in the sequencing cohort while 17 patients (11 FAI and 6 OA) were in a subsequent validation cohort. All patients had radiographic evidence of a Cam deformity with an Alpha Angle (AA) greater than 60 whilepatients with dysplasia (Lateral Center Edge Angle (LCEA)<25) or prior hip surgery were excluded.
Cartilage samples were obtained over the Cam deformity prior to femoroplasty in the FAI group with intra-operative cartilage assessment using the Outerbridge classification. For the OA cohort, cartilage samples were obtained over the anterosuperior femoral head-neck junction in the OA group following extraction of the femoral head. Where possible, additional samples were obtained for histologic analysisof cartilage quality using the Osteoarthritis Research Society International (OARSI) classification.
Following RNA isolation, whole-genome RNA sequencing was performed with differentially expressed genes (DEGs) identified by DESeq2 R software package. Gene targets of interest were then validated with quantitative real time-PCR (qRT-PCR) and immunohistochemistry.

Results: We identified a total of 3,531 DEGs between the FAI and OA cohorts with multiple targets for genes implicated in the canonical OA pathway (Figure 1). qRT- PCR validation confirmed increased expression of FGF18 and WNT16 in the FAI samples, while there was increased expression of MMP13 and ADAMTS4 in the OA samples (Figure 2). Expression levels of FGF18 and WNT16 were also higher in FAI samples with mild cartilage damage (OARSI grades 1-2) compared to FAI samples with severe cartilage damage or OA cartilage (OARSI grade 4-6). Histologic evaluation of FAI samples demonstrated a range of cartilage pathology (OARSI grades 1-5) with higher OARSI grading associated with increasing severity of femoral head cartilage lesions in the FAI cohort ($r=0.68$; $p=0.01$). Immunohistochemical evaluation identified increased FGF-18 staining in OARSI grade 1-2 FAI samples compared to OARSI grade 5-6 FAI and OA samples (Figure 3).

Conclusions: The results of the present study support our hypothesis that there are significant differences in gene expression between FAI and OA samples in multiple pathways that are implicated in osteoarthritis. RNA sequencing of cartilage of FAI and hip OA patients identified a negative association of FGF18 expression levels with cartilage damage severity, suggesting that FGF18 may be used as a marker for hip OA progression.

Title: **Alginate hydrogels as alternate lung inflation media may improve tissue culture and RNA Isolation**

Presenting Author: Aubrey Lanham

Co-Authors: Jared A. Mereness

Lab PI / Mentor: Danielle S.W. Benoit

Abstract (3500 characters or 500 words Limit)

Introduction: Preparation of lung tissue for research purposes often includes inflation with agarose to retain physiological structure and allow sectioning with precision and accuracy. For example, precision-cut lung slices (PCLS) are a highly physiologically-relevant model that have allowed researchers to test various drugs, viruses, and disease conditions [1]. However, agarose impedes a multitude of assay techniques, such as RNA isolation, and can be difficult to remove without damaging the tissue [1]. A possible alternative, sodium alginate can be crosslinked via divalent cations such as Ca2+ or Mg2+, has excellent biocompatibility and can be degraded enzymatically or via exposure to monovalent cations. We hypothesize that alginate lung inflation will improve RNA and PCLS culture due to its ease of degradation and removal from tissue [2].
Methods: Alginate gels ranging from 0.5 - 5% (w/v) low-viscosity sodium-alginate (g) were ionically crosslinked with divalent cations via the calcium carbonate ($CaCO_3$) - glucono-δ-lactone (GDL) system [2]. Gels were tested for working time and modulus by flow inversion and mechanical testing. Other characterization included observation of $CaCO_3$ precipitates in gels and gross fragility. To test degradation modalities, 40 ul, cylindrical gels (~4.5 mm diameter x ~2 mm height) in PBS alone, or with 5 mM Ethylenediaminetetraacetic acid (EDTA), 20 U/ml alginate lyase (AL), or the combination of EDTA and AL. Gel volume was quantified after 15, 30, 60, and 90 minutes. To test the feasibility of lung inflation with alginate gels, we performed murine lung inflations under physiological pressure (24 mm Hg) with gel precursor solution, containing 4% (w/v) alginate, 0.27% (w/v) $CaCO_3$, and 0.86% (w/v) GDL. The trachea was clamped with a hemostat, and inflated lungs were removed and stored in PBS at 4 °C overnight. Gel degradation in inflated lung tissue sections was tested by including 5 uM TRITC-labeled 70 kDa dextran in the precursor solution. After overnight storage at 4 °C, the left lung lobe was cut into 1 mm slices and placed in 500 ul bronchial epithelial growth media (BEGM) with or without 20 U/ml AL. The tissues were kept at 37 °C and imaged via fluorescent microscopy at 2, 4, 6, and 16 hrs.
Results and Discussion: Gels were synthesized with elastic moduli and swelling ratios ranging from 1.2 – 11 kPa, respectively. A 4% alginate solution with 1.5x $CaCO_3$ and 2.0x GDL yielded an average modulus of 8.5 kPa, and a working time of 30 min at 4 °C, characteristics that would likely yield successful lung inflation and sectioning of PCLS slices. Degradation studies showed that 40 ul gels could be completely degraded with EDTA or AL alone in less than 90 min. Fluorescent in-lung degradation studies showed that nearly all fluorescence was lost from lung tissue within 2 hrs in media containing AL. Ongoing work includes RNA isolation and tissue viability studies from alginate-inflated tissue.
References
[1] Niehof et. al. BMC research notes, 2017.
[2] Kuo and Ma. Biomaterials, 2001.

Title: **Optimization of Concurrent Osteogenesis and Angiogenesis in Bone Marrow Culture Utilizing a Reporter Mouse Model Labeling Both Osteoblasts and Sprouting Endothelial Cells**

Presenting Author: Nicholas Lenhard

Co-Authors: Jixiang Xia, Chen Jiang

Lab PI / Mentor: Xinping Zhang

Abstract (3500 characters or 500 words Limit)

Enhancing osteogenesis coupled angiogenesis is vital for successful bone tissue engineering applications. Given the fact that in vivo tissue cells need to be within 100-200μm of the nearest capillary for nutrition and oxygen, construction of a prevascularized bone tissue engineered construct with spatially and temporally controlled angiogenesis could be advantageous for guided and uniform bone regeneration. To the end of understanding the interplay between osteogenesis and angiogenesis, and more importantly to defining the optimal conditions for construction of a pre-vascularized bone tissue engineered constructs, a transgenic mouse line, AplnCreERT2; Ai14; Col (I) 2.3 GFP, which labels osteoblasts with green fluorescent protein (GFP) and sprouting endothelial cells with red fluorescent protein (RFP) was generated. This transgenic mouse line enables us to simultaneously imaging osteogenesis and angiogenesis in vitro and at the site of bone repair. By utilizing this mouse line, we examined the relationship between Apln+ vessel formation and osteoblast differentiation/mineralization in bone marrow cultures. To facilitate both osteogenic and angiogenic differentiation of the cells, media containing various proportions of aMEM and EGM2, which respectively promote osteogenic and angiogenic differentiation, was used. Our data demonstrated a varying degree of antagonizing effects of these two types of media on osteogenic and angiogenic differentiation of isolated bone marrow cells. While the increasing proportion of aMEM facilitated osteoblast differentiation, the increasing proportion of EGM2 suppressed the osteoblast's ability to differentiate. A strong inhibitory effect of EGM2 media occurred at mineralization stage of osteoblasts when ascorbic acid (AA) and β-Glycerophosphate (β-GP) were added. Even a small percentage (25%) of EGM2 media could completely inhibit the mineralization of the culture. Interestingly, we found that the growth factors added in EGM2 media promoted the Col (I)2.3GFP+ nodule formation in 75% aMEM and 25% EGM2 media but markedly suppressed the mineralization of these bone nodules. The removal of growth factors from EGM2 media immediately restored the mineralization of GFP+ bone nodules. Spatially, the Apln+ vessels and GFP+ osteoblastic nodules are mutually exclusive with collagen coated plate showed enhanced Apln+ vessels formation around GFP+ nodules. The addition of ascorbic acid (AA) and β-Glycerophosphate (β-GP) in aMEM suppressed the Apln+ vessel formation but this effect can be restored by collagen coating of the plate. By examination of the effects of media content on osteogenic and angiogenic differentiation of bone marrow cultures, our ultimate goal is to harness both osteogenic and angiogenic cells in bone marrow cultures for construction of an effective prevascularized multi-functional nano and microfiber-based tissue engineered construct mimicking vascularized periosteum for large bone defect repair and reconstruction.

Title: **Molecular signatures distinguish callus senescent cells from inflammatory cells**

Presenting Author: Jiatong Liu

Co-Authors: Xi Lin, Andrew McDavid, Hengwei Zhang, Brendan F. Boyce

Lab PI / Mentor: Lianping Xing

Abstract (3500 characters or 500 words Limit)

Cell senescence plays important roles in human diseases, including musculoskeletal disorders. Recently, we found that aged mice have markedly increased numbers of senescent cells (SCs) in fracture callus that exert a senescence-associated secretory phenotype (SASP). Clearance of SCs promotes fracture healing in aged mice. However, aging is associated with chronic low-grade inflammation that also causes elevated levels of pro-inflammatory factors. Distinguishing SCs from inflammatory cells (Infl-Cs) in aged callus is very important, not only because both of them are increased and produce inflammatory factors, but also because they require different drug treatments, e.g. senolytic drugs for SCs and NSAID for ICs. Here, we hypothesize that SCs and Infl-Cs express different types or/and different levels of pro-inflammatory factors within the fracture environment. To test this hypothesis, we applied single cell RNA sequencing (scRNA-seq) of callus cells from aged mice to study molecular signatures of SCs and Infl-Cs and their interactions. We focused on CD45-CD31-Ter119- stromal cells because ~70% of callus SCs are CD45- cells. Uniform manifold approximation and projection (UMAP) of aged callus stromal cells showed the distribution of cells expressing Rela/Relb and cells expressing the senescent genes, Cdkn1a, Cdkn2a or Cdkn2c, yielding 2,572 Rela/Relb-expressing cells and 905 senescence-associated cells. Among these cells, 304 cells expressed both Rela/Relb and senescent genes, which we named inflammatory senescent cells (Infl-SCs). A heat-map showed that SCs and Infl-SCs have a similar gene profile compared to Infl-Cs, expressing top differentially genes in oxidation-reduction (ROS) and DNA damage response, which was further supported by gene ontology analysis. To determine if Infl-Cs, Infl-SCs and SCs express different types or different levels of pro-inflammatory factors, we examined the expression levels of 22 SASP factors, including TGF beta1, pro-inflammatory cytokines, chemokines, and MMPs and found that only 6 of these factors (TNF, IL1 beta, Cxcl2, Ccl6, TGF beta1 and MMP9) were increased in aged callus and detected in our scRNAseq data set. A Violin plot showed that Ccl6 was the signature gene for Infl-Cs and Infl-SCs; TGF beta1 was the signature gene for Infl-SCs and SCs; MMP9 was the signature genes for Infl-Cs. We examined interactions among these three subsets and found that infl-SCs and SCs expressed higher levels of or more ligands that affect Infl-Cs than SCs, using CellChat. Our findings indicate that Infl-C are the target of SCs and Infl-SCs. Using Nichenet, a ligand/target pairing based R package, we identified Tnfsf13 and TGF beta1 as the two most highly-expressed ligands that were differentially expressed between Infl-SCs/SCs and Infl-Cs. Thus, our findings show that callus Infl-SCs and SCs not only express SASP factors, but also genes related to ROS and DNA damage, which distinguish them from Infl-Cs. Bioinformatic analyses revealed that Infl-Cs are the target of Infl-SCs and SCs and that they potentially influence the effects of Infl-SCs/SCs on themselves by expressing active ligands (Tnfsf13/TGF beta1). Further analysis of target genes in Infl-Cs is needed to elucidate the contribution of Infl-SCs/SCs to stromal inflammation in healing fractures in aged mice.

Title: **Radiographic and clinical findings associated with Klippel-Feil Syndrome: A case series**

Presenting Author: Aniruddh Mandalapu

Co-Authors: Andrew Megas D.O., Gabrielle Santangelo M.D., Addisu Mesfin M.D.

Lab PI / Mentor: Addisu Mesfin M.D.

Abstract (3500 characters or 500 words Limit)

Introduction: Klippel-Feil Syndrome (KFS), a congenital disorder involving the fusion of two or more cervical vertebrae, has historically been described with a prevalence of 1 in 40,000. However, a recent study from the University of Rochester noted a higher prevalence of congenital cervical fusion of up to 1 per 83 patients. KFS classically involves a short neck, restricted mobility of the upper neck, and low posterior hairline because of improper segmentation of the cervical vertebrae during development.

Objective: The primary objective of this study is to describe the distribution of sex, race, anatomic level, Samartzis classification, the prevalence of scoliosis, and surgical intervention within the Klippel-Feil patient population.

Methods: RSRB approval was obtained. The UR CTSI TriNextX was used to identify patients that may have KFS. The sample from TriNextX was further narrowed down by confirming the KFS diagnosis through imaging in patient records. The final 59 patient database was categorized by the patient characteristics, anatomic characteristics following Samartzis classification, presence of scoliosis, and surgical intervention. Samartzis type 1 include those with a single congenitally fused cervical segment, Type 2 multiple noncontiguous fused cervical segments and type 3 and multiple contiguous fused cervical vertebrae.

Results: In our cohort of patients with KFS, the most common levels of fusion were C2-C3 (27.1%) and C5-C6 (22%). More females than males (52.5% vs 47.5%) were affected. Following the Samartzis classification, Type I was the most common followed by Type III and then Type II (55.9%, 25.4%, and 13.6% respectively). There was a 35.6% prevalence of scoliosis. 23.7% of the KFS cohort patients underwent spine surgery. Of the spine surgeries, there were 2 scoliosis fusions, 5 posterior spinal fusions, 1 anterior spinal fusion, 3 unspecified spinal fusions, 2 laminectomies, 1 discectomy, and 3 other spinal procedures. Of the 14 surgeries among the KFS cohort, 64.3% were contiguous at or near the level of fusion while 35.7% were non-contiguous or unknown. A majority of the patients were Caucasian (72.9%), with the others African American (13.6%), Hispanic (3.4%), Asian (3.4%), or unknown (6.8%).

Conclusions: KFS was more common in females than males. Type I (single fused cervical segment) was the most common variety of KFS and the most common fusion level was C2-C3. The KFS cohort had a prevalence of scoliosis of 35.6% and 23.7% had a spinal surgery. A majority of the surgeries within the cohort, 64.3%, were contiguous and the most common surgery was posterior spinal fusion.

Title: **Elucidating Design Parameters to Improve Tissue Engineered Periosteum Mediated Allograft Healing**

Presenting Author: Alyson March

Co-Authors:

Lab PI / Mentor: Danielle Benoit

Abstract (3500 characters or 500 words Limit)

The gold standard for treatment of critical size bone defects is decellularized bone allografts. However, allografts have a high failure rate, with approximately 60% of allografts failing within 10 years after implantation. In contrast, bone autografts can achieve full healing but are limited volumetrically due to donor site morbidity. One key feature of autografts that allografts lack is the periosteum, a thin connective tissue that surrounds bone. The periosteum is a highly vascular and innervated tissue layer that promotes bone healing and host tissue recruitment through periosteal-cell derived paracrine signaling. Our lab has developed a tissue-engineered periosteum (TEP) using matrix metalloproteinase (MMP) degradable poly(ethylene glycol) (PEG) hydrogels with encapsulated mouse mesenchymal stem cells (mMSCs) and mouse osteoprogenitor cells (mOPs) to mimic periosteum-mediated paracrine signaling. Bone defects treated with TEP-modified allografts showed a 4-fold increase in maximum torque versus unmodified allografts at 9 weeks post-surgery, indicating improved allograft healing. Despite this improvement, healing is still inferior to autografts, as autografts had a maximum torque approximately 2-fold greater than the TEP-modified allograft. We hypothesize that modification of the TEP degradation rates and adhesive peptide composition will improve cell-matrix interactions to promote host tissue integration and subsequent allograft healing. To study the effect of degradation rate, PEG hydrogels will be fabricated with crosslinks having a range of susceptibility to MMP mediated cleavage, resulting in slow, medium, or fast degradation. The adhesive peptide sequences RGD, GFOGER, and YIGSR, which mimic the extracellular matrix proteins fibronectin, collagen, and laminin, respectively, will be investigated at three different concentrations. We will utilize a design of experiments (DOE) approach to evaluate the combinatorial effect of hydrogel degradation and cell adhesive peptide composition on host tissue infiltration and integration. As a surrogate for host tissue integration, an in vitro angiogenic assay based on sprouting from spheroids composed of human umbilical vein endothelial cells (HUVECs) and human mesenchymal stem cells (hMSCs) will be performed. Preliminary data show that in hydrogels that exhibit both slow and medium degradation rates, the presence of RGD promotes rapid cell sprouting and supports network formation over 5 days, while hydrogels degrading at a slow or medium rate show similar levels of cell sprouting and network formation. We anticipate further studies to optimize the TEP using a DOE approach will identify hydrogel formulations with high potential for host integration and graft healing. These results will guide in vivo experiments with TEP-modified allografts tuned to promote vascularization and bone healing.

Title: **Anatomical site and BMI affect optimal source-detector offsets for transcutaneous Raman assessment of human hand bone quality assessment**

Presenting Author: Christine Massie

Co-Authors: Keren Chen, Emma Knapp, Andrew J. Berger, Hani A. Awad

Lab PI / Mentor: Hani A. Awad

Abstract (3500 characters or 500 words Limit)

Osteoporosis is a multifactorial bone disease, characterized by reduced bone mass and bone strength. Osteoporosis is diagnosed by measuring the patient's bone mineral density (BMD) through dual-energy X-ray absorptiometry (DXA). However, DXA is not accessible to all patients and this may lead to failure in identifying patient's with a high risk of experincing a fragility fracture. However, non-invasively measuring the bone's biochemical composition could serve as a pre-screening tool. Raman spectroscopy is a non-invasive optical technique that measures a sample's biochemical composition. However, limited progress has been made in using Raman spectroscopy to assess bone quality in vivo on humans due to the unavoidable signal contributing to the overlaying soft tissue. By incorporating spatially offset Raman spectroscopy (SORS), the specificity to bone increases. Bone quality assessment through SORS in rodent models has been well established, but it remains unclear how to translate these SORS instruments to human specimens. Larger source-detector offsets will give a larger percentage of signal contributing to the bone layer, but at the same time will decrease the signal to noise ratio (SNR). Thus far, our lab has focused on measuring murine tibia transcutaneously, however a large clinical study demonstrated the ability to diagnose osteoporosis through X-ray images of metacarpal bones and prospectively predict femoral fragility fractures with high reliability and specificity. The objective of this study is to empirically determine the optimal source-detector separations for SORS performed on human hand and investigate the effects of body mass index (BMI) and anatomical site transcutaneous measurements in the metacarpals and phalanges.

Two cadaver hands were obtained through the Anatomy Gift Registry, one with a healthy BMI of 24 and the other with a severely obese BMI of 36. Raman spectra were collected from the midshaft of metacarpals and proximal phalanges using an 830 nm laser with 150 mW at source-detector offsets between 0-8mm.

By qualitatively comparing the transcutaneous data, we observed 1) larger offsets increased the relative percentage of bone spectral features present, 2) the healthy individual had a higher bone specificity when compared to the obese subject, and 3) the phalanges had a higher bone specificity when compared to the metacarpals. This data led us to the hypothesis that both BMI and the anatomical region will affect the optimal source-detector offset. To quantify the bone signal to noise ratio and study how this metric is dependent on source-detector offset, simultaneous over-constrained library-based decomposition (SOLD) was used to un-mix transcutaneous spectra and quantify the contributions from bone and soft tissue. Area under the phosphate peak in the weighted bone basis spectra were quantified to represent the bone signal. The square root of the total counts in the phosphate region was calculated to represent the noise amplitude. Maximum bone signal to noise ratio occurred at offsets 5-6mm for metacarpals and 3-4mm for phalanges, but there was no large effect on the optimal offset dependent on the sample's BMI.

Our preliminary work here advances the field by optimizing source-detector separations for future bone quality assessment using Raman spectroscopy. This sets the foundation for validating human bone quality assessment through Raman spectroscopy to aid in fracture risk assessment.

Title: **Tuning Engineered Hydrogel Matrix Degradation and Epitope Presentation for Salivary Gland Tissue Mimetic Culture**

Presenting Author: Jared Mereness

Co-Authors: Lindsay Piraino, Tracey Moyston, Yuanhui Song, Azmeer Sharipol, Matthew H. Ingalls, Lisa A, DeLouise, Catherine E, Ovitt, Danielle S.W. Benoit

Lab PI / Mentor: Danielle S.W. Benoit

Abstract (3500 characters or 500 words Limit)

Nearly 600,000 head and neck cancer patients diagnosed globally each year will receive radiation therapy. Chronic dry mouth, or xerostomia occurs in >50% of these patients due to off-target salivary gland damage, leading to loss of acinar cell secretory function. Xerostomia causes chronic sore throat, difficulty eating or talking, dry, painful oral and nasal passages, and chronic oral infections. However, development of radioprotective strategies has been hampered due to rapid loss of salivary gland cell (SGC) secretory phenotype in vitro. This loss has been attributed to disruption of the extracellular matrix (ECM) during gland dissociation, which eliminates cues required for proper cell function. To address this challenge, isolated SGCs were encapsulated and cultured in engineered ECM based on poly(ethylene glycol) (PEG) hydrogels. This system provides tunable control of the matrix microenvironment via enzymatically-responsive peptide crosslinkers and presentation of peptide mimetics of matrix epitopes. We combined this approach with microbubble (MB) array technology to develop a high throughput drug screening platform wherein cells are seeded in high density arrays of 15 nL spherical cavities molded in PDMS (polydimethylsiloxane). Within gel-MBs, SGCs organize into tissue mimetic structures which morphologically and functionally resemble acinar units of the salivary gland.

Methods: SGC clusters in hydrogel precursor solutions (2 mM 20 kDa 4-arm PEG-amide norbornene, dicysteine-functionalized peptide crosslinker, cysteine-functionalized matrix epitopes, and lithium phenyl-2,4,6-trimethylbenzoylphosphinate (LAP)) were seeded into 96-well MB chips, and photopolymerized under 365 nm, ~5 mW/cm2. Light microscopy images were taken at 0, 24, and 48 hr in culture to assess tissue morphology. Fluorescent calcium-flux response after treatment with 100 uM ATP or 1 uM carbachol, an indicator of secretory function, was measured at day 7, and tissue lysates were retained for gene expression analysis by quantitative real-time PCR.

Results: Crosslinkers with lower MMP2 degradation rate accelerated sphere formation, reaching nearly 70% MB with spheres at 48hr, up to 2-fold greater than faster-degrading linkers and increased size (area) by 2.7-fold over the fastest-degrading linker. Slower degrading linkers also reduced cell outgrowth from MBs after prolonged culture, and increased the maximum and duration of the calcium flux response after stimulation with secretory agonists. Gene expression analysis showed increased expression of the saliva protein prolactin-induced peptide (Pip) in cultures with slower degrading crosslinkers, while expression of smooth muscle actin (Acta2), a myofibroblast marker was elevated using the fastest-degrading linker. Compared to tissues in gels without epitope incorporation, which organize into larger, shperical structures with ubiquitous calcium-responsive character, epitope incorporation produced tissues with branched, lobular morphology displaying specific calcium-responsive regions that require additional investigation. Overall, these studies indicate that gel degradation rate and matrix epitopes present within the hydrogel matrix play a critical role in the organization and function of SGCs in the SGC-MB-gel system. Further characterization of the organization and functionality of tissues in epitope-containing matrices will yield new biological insights and a more physiologically-relevant tissue mimetic system.

Title: **CCR2 identifies tendon-resident T cell and macrophage populations while CCR2-/- impedes late tendon healing**

Presenting Author: Samantha Muscat

Co-Authors: Anne E.C. Nichols, Emma Gira

Lab PI / Mentor: Alayna Loiselle

Abstract (3500 characters or 500 words Limit)

Following tendon injury, healing begins with an influx of inflammatory cell types such as macrophages. Macrophages mediate myofibroblast differentiation and scar formation. The native properties of the tendon are never fully restored as a result of this fibrovascular scar. Chemokine receptor 2 (CCR2) facilitates monocyte/macrophage infiltration into injured tissues; thus, we targeted CCR2 to define the role of extrinsic monocytes/macrophages during tendon healing. CCR2 is also expressed by resident macrophages in many tissues. While macrophage depletion in neonatal tendon resulted in impaired functional healing, the impact of impaired CCR2+ macrophages on the adult tendon healing process is unclear. In the present study, we defined the identity of CCR2+ cells during tendon homeostasis, defined the functional effects of CCR2 deficiency and tracked changes in CCR2+ cell recruitment during tendon healing as a result of CCR2-/- to test the hypotheses that: (1) CCR2 is expressed by tendon resident marophages during homeostasis, (2) following injury CCR2 deficiency will reduce recruitment of extrinsic macrophages, and (3) that blunted macrophage recruitment impairs myofibroblast differentiation and impedes functional restoration after injury. We utilized CCR2 knock out (KO) mice, which has a GFP followed by a polyadenylation signal inserted into the CCR2 gene, abolishing CCR2 expression and impairing monocyte recruitment. CCR2-GFP/+ mice have expression of both GFP and CCR2. CCR2 WT mice have normal gene expression. Mice underwent complete transection of the flexor digitorum longus tendon in the hind paw. Mice were harvested at various timepoints to assess histology and biomechanical analysis. Uninjured tendons were harvested and underwent scSeq analysis. During homeostasis, CCR2-GFP+ cells were observed in uninjured CCR2-GFP/+ tendons, and co-IF indicated that most of these cells were F4/80+ macrophages.There was a nearly complete loss of CCR2-GFP+ cells and F4/80+ macrophages in CCR2-KO tendons. There was a subpopulation of CCR2-GFP+ F480- cells in CCR2-GFP/+, with this population completely absent in the CCR2-KO. Single cell sequence data identified these as T-cells and confirmed a resident CCR2+ macrophage population. Future work characterizing the role of CCR2 in T cells during tendon healing and homeostasis is needed. At all timepoints post-repair, CCR2-KO mice have reduced number of CCR2+ F4/80+ macrophages, but did not completely inhibit their recruitment. We observed reduced number of myofibroblasts in the CCR2-KO compared to CCR2-GFP/+ at all timepoints. This is consistent with the reduced number of macrophages, as these cells are known to create a positive biomechanical feedback loop. We see a functional deficit at 28 days post-repair: Max Load at Failure (38.63% decreased, $p=0.03$) and stiffness (50.19% decreased, $p=0.05$). We suggest that reductions in these cell populations dictate the functional deficits that are observed at 28 days post-repair, due in large part to macrophage functions related to wound debridement, and myofibroblast-mediated ECM remodeling. In the present study, we have shown that CCR2 identifies tissue resident macrophages and T-cells and CCR2-/- is insufficient to completely block macrophage recruitment during tendon healing and homeostasis. However, loss of CCR2 impedes healing; elucidating the role of macrophages and T-cells with impaired CCR2 recruitment will drive future therapeutic strategies.

Title: **Analyzing the Impact of Comorbidity Indices on Patient Reported Outcomes Following Total Hip Arthroplasty**

Presenting Author: Mackenzie Neumaier, M.D.

Co-Authors: Gabriel Ramirez, Caroline Thirukumaran, Ph.D., John Ginnetti, M.D.

Lab PI / Mentor: John Ginnetti, M.D.

Abstract (3500 characters or 500 words Limit)

Introduction/Purpose: Total hip arthroplasty (THA) has assumed a central focus in the development of reimbursement reform through models such as the Bundled Payment for Care Improvement and Comprehensive Care for Joint Replacement models. As part of these Medicare models, patient reported outcomes (PROs) are recorded, however not yet tied to reimbursement. Though there is speculation that this may soon change. In anticipation of this, there is a need to effectively risk stratify patients and build adjustment into these models to prevent healthcare discrimination against higher-risk patients that will likely not achieve the same response in PROs as their healthy counterparts. In the process of doing so, investigation of classic comorbidity indices have exposed the need for a more "orthopaedic-specific" index prompting the development of the Functional Comorbidity Index (FCI). The purpose of this study was to investigate the utility of the FCI as well as 3 classic indices (Charlson (CCI), Royal College of Surgeons (RCS) Charlson and Elixhauser (ELIX)) in defining PROMIS outcomes after THA.

Methods: Our institution's electronic medical record was queried for all patients between the ages of 21-85 who underwent primary total hip arthroplasty between 1/1/2015 and 12/1/2018. Those who underwent revision THA or who underwent THA for fracture were excluded. Baseline characteristics were collected and the comorbidity indices were calculated manually, each as originally described. Patient reported outcomes were recorded through PROMIS via the domains of Physical Function (PF), Pain Interference (PI) and Depression (DEP). These outcomes were recorded at the patient's final pre-operative visit, 3-6 weeks post-operatively, 3-6 months post-operatively and 1-2 years post-operatively. Minimum clinically important difference (MCID) was calculated via distribution-based technique, using half of the standard deviation. Statistical analysis was performed consisting of receiver operative curve (ROC) analysis, standardized coefficients and odds ratio (OR) analysis.

Results: 409 patients met criteria for inclusion. The average age was 65.3 years old and average BMI was 29.7 kg/m2, 58% of the cohort was female and there was an equal split between anterior and posterior approach. Mean CCI value was 1.39 (0-8), RCS was 1.05 (0-6), ELIX was 2.99 (0-10) and FCI was 3.6 (1-9). MCID was calculated to be 2.93 (PF), 3.28 (PI) and 4.99 (DEP). ROC analysis revealed AUCs ranging from 0.59-0.77 at 1-2 yr post-operatively. Values were weakest for PF (0.59-0.64), strongest for DEP (0.76-0.77) and similar across all indices. Standardized coefficient analysis demonstrated mixed results across all PROMIS domains at different time points. The RCS proved to be the most influential 4 times, which was the most frequent of the indices. ORs of failing to achieve MCID were significant ($p<0.05$) at the 3-6mo and 1-2yr time points for all indices for both PF and PI. RCS had the highest ORs at 1-2yr for both PF (1.65; $p=0.00$) and PI (1.41; $p=0.01$). No ORs were significant at any time points when looking at DEP.

Conclusion: Increased comorbidity index scores negatively impact the ability for a patient to achieve MCID, though no index has proved to be superior in defining this relationship.

Title: **Stage-specific healing behaviors are observed in a novel embryonic tendon explant model**

Presenting Author: Phong K. Nguyen

Co-Authors: Catherine K. Kuo

Lab PI / Mentor: Catherine K. Kuo

Abstract (3500 characters or 500 words Limit)

Healing of injured adult tendon results in fibrotic scar tissue. In contrast, injured fetal tendons in a sheep model have been reported to heal scarlessly. Yet, the underlying mechanisms are not completely understood. Our lab recently showed the chick embryo is a promising model to study embryonic mechanisms of tendon healing in vivo and in ovo. As a complement to the in ovo model, a tendon injury explant model would offer a platform for screening of putative therapeutic targets that we could subsequently test in ovo. Here, we report that 1) injured tendons are viable in vitro and started to heal through at least 120h, 2) injury leads to significantly higher cell apoptosis and mRNA levels of pro-inflammatory mediators (interleukin (IL)-1β, IL-1 receptor 1 (IL-1R1)), matrix metalloproteinases ((MMP)-3, 9, and 13), and mediators of lysyl oxidase (LOX)-mediated crosslinking (LOX, bone morphogenetic protein-1 (BMP1)), and 3) healing responses differ between younger and older embryonic tendons. Hamburger Hamilton stage (HH) 40 and HH43 calcaneal tendons were transected with micro-scissors to create an injury site in the middle of the tendons. Explants were cultured in Dulbecco's Modified Eagle Medium with 10% fetal bovine serum and 1% antibiotic-antimycotic. 20 μm-thick cryosections were stained with TUNEL and Hematoxylin and Eosin (H&E). Tendons underwent uniaxial displacement-controlled stretching at 1% strain/sec until failure. Reverse transcriptase polymerase chain reaction was performed to characterize mRNA levels of IL-1R1, IL-1β, MMP3, 9, and 13, LOX, and BMP1 relative to 18s. LOX activity levels were measured using LOX activity kit. We found that deposition of new ECM at the injury sites could be detected through at least 120h, suggesting embryonic tendon explants can heal after injury in vitro. By 48h, cell apoptosis was evident in injured tendons, suggesting cells were reactive to the wounded tissue microenvironment. IL-1β binding to IL-1R1 transduces pro-inflammatory signaling intracellularly. It is interesting that injured HH40 tendon upregulated IL-1R1 mRNA levels, whereas injured HH43 tendon upregulated IL-1β mRNA levels compared to non-injured controls. These findings suggest both HH40 and HH43 tendons exhibited pro-inflammatory behaviors in response to injury in vitro, but possibly to different extents or via different mechanisms. LOX and BMP1 mRNA levels did not change with injury in HH43 tendon but increased significantly in HH40 tendon, whereas LOX activity levels increased significantly with injury in HH43 tendon but stayed the same in HH40 tendon. These findings suggest HH40 and HH43 tendons underwent different healing mechanisms, which would be significant as many tissues lose their scarless healing abilities at later stages of embryonic or fetal development. Ongoing experiments include assessment of healing responses at additional timepoints and more comprehensive characterizations of the explant injury model, as well as perturbation of the MMPs and LOX to test their roles in embryonic tendon healing. Future studies will use this explant model to complement the in ovo model to investigate how embryonic tendon transitions from scarless to scarred healing and inform therapeutic strategies to promote adult tendon regenerative healing.

Title: **Mechanical properties of embryonic tendon are enhanced with lysyl oxidase upregulation**

Presenting Author: Phong K. Nguyen

Co-Authors: Catherine K. Kuo

Lab PI / Mentor: Catherine K. Kuo

Abstract (3500 characters or 500 words Limit)

Tendon-associated birth defects affect 1 in 100 live births each year. Abnormal tendon mechanical properties have been implicated in development of joint dislocations, stiffness, and contractures. Our lab has showed lysyl oxidase (LOX)-mediated crosslinking is important in the elaboration of embryonic tendon mechanical properties. In this study, we aimed to examine how upregulation of LOX-crosslinking affects tendon mechanical properties. We hypothesized treatment of tendon with recombinant LOX (rLOX) will enhance collagen crosslinking to increase elastic modulus of earlier and later embryonic stage tendons. Tendon bundles were extracted from Hamburger Hamilton stage (HH) 40 and HH43 calcaneal tendons and cultured for 72h in Dulbecco's Modified Eagle Medium with 1% antibiotic-antimycotic and 10% fetal bovine serum. 1.5 μg/mL of rLOX or HBSS vehicle control was added at 0h and 24h. Force Volume-Atomic Force Microscopy (AFM) was performed with 20 nm tips on 20 μm-thick cryosections. Cryosections were stained with hematoxylin and eosin (H&E) and picrosirius red (PSR). Cryosections were also imaged to measure LOX-crosslink density based on autofluorescence (AF) (780/390±20nm) and fibrillar collagen content and organization based on second harmonic generation (SHG) signal (780/445±20nm). Average pixel intensities of SHG images were quantified to determine collagen content and AF/SHG ratio was computed to determine crosslink density. We found that treatment with rLOX significantly increased elastic modulus of both HH40 and HH43 tendon bundles, suggesting LOX-targeted strategies could be used to manipulate embryonic tendon mechanical properties. Elastic modulus maps of HH43 tendon bundles showed greater heterogeneity compared to HH40 tendon bundles, reflecting the development and maturation of collagen fibers and other ECM structures in tendon, which was consistent with our previous studies. Qualitative assessment of H&E and PSR staining along with quantification of SHG imaging suggested collagen content and organization were unaffected by rLOX treatment, whereas increases in AF/SHG ratio suggested crosslink density increased with rLOX treatment. The latter outcome was specific to HH43 tendons, as HH40 tendons exhibited a non-significant increase perhaps because more biological replicates should be tested. The increases in AF/SHG ratio suggest the rLOX-induced increases in tendon elastic modulus were mediated by LOX-crosslinking. Due to the small size and fragility of tendon bundles (< 300 μm in cross-sectional diameter), AFM was chosen to characterize tissue elastic modulus. We have recently shown that nano-scale elastic moduli of chick embryo tendon during development follow the same trends as tensile elastic moduli, suggesting nano-scale elastic modulus may reflect changes in tendon macro-scale properties. However, future studies will benefit from tensile testing to confirm tensile mechanical property changes. Future studies will also test the ability to enhance tendon mechanical properties by promoting LOX-crosslinking in vivo. Taken together, our findings support the potential to use LOX-targeted therapies to manipulate mechanical properties of developing embryonic tendons, which could lead to future therapeutic approaches to treat tendon-associated birth defects in utero.

Title: **Characterization of RAGE expression to inhibit myofibroblast persistence during tendon healing**

Presenting Author: Meghan M. O'Neil

Co-Authors:

Lab PI / Mentor: Alayna E. Loiselle

Abstract (3500 characters or 500 words Limit)

Acute tendon injuries heal via a scar-mediated process that is often complicated by excessive scar tissue causing functionally impaired tendons. The myofibroblast (MF) is responsible for synthesizing and contracting matrix to promote proper tendon healing. We have shown that at D28 of tendon healing that MFs exhibit pro-survival signaling, thus identifying a population of persistent MFs. However, the persistence of MFs shifts the rate of matrix formation to be greater than the rate at which matrix is degraded, which forms excessive scar tissue. We hypothesize that one mechanism of MF persistence is via NF-kappaB dependent pro-survival signaling, which is activated by S100a4-RAGE signaling. To elucidate the role of S100a4-RAGE activation of NF-kappaB dependent pro-survival signaling in MFs we are proposing to inhibit the receptor RAGE in persistent MFs as a means of preventing excessive scar formation. To characterize the expression profile of RAGE in MFs, we assessed co-immunofluorescence of RAGE and alpha-SMA (marker of MF stress fibers) expression. We were able to see that early MFs at D14 do not express RAGE, however by D21 all MFs express RAGE. RAGE expression in MFs continues until at least D28. These data suggests that persistent MFs (D21 through D28) can be targeted by their RAGE expression. We plan to knock-out RAGE in MFs to inhibit downstream NF-kappaB dependent pro-survival signaling to prevent MF persistence as a means of improving tendon healing.

Characterizing efferocytic activity in multipotent stromal cells (MSCs) using confocal time-lapse imaging

Authors: Ivana Pacar[1,4], Emily R. Quarato[2,4,5], Yuko Kawano[3,4 5], Jane L. Liesveld[3,4], and Laura M. Calvi[3,4,5]

1. Department of Biomedical Engineering, University of Rochester, Rochester, NY; 2. Department of Environmental Medicine, University of Rochester Medical Center, Rochester, NY; 3. Department of Medicine, University of Rochester Medical Center, Rochester, NY; 4. Wilmot Cancer Institute, University of Rochester Medical Center, Rochester, NY; 5. Center for Musculoskeletal Research, University of Rochester Medical Center, Rochester, NY

Housed within the bone marrow microenvironment, multipotent stromal cells (MSCs) are known for their tri-lineage differentiation into chondrocytes, osteoblasts, or adipocytes and their ability to support hematopoiesis. While in the bone marrow macrophages serve as the primary agents of efferocytosis, a specialized form of phagocytosis in which apoptotic cells are cleared, recent discoveries in our lab have demonstrated that MSCs can also participate in facultative efferocytosis and that when macrophage efferocytosis is deficient during aging MSCs enhance their efferocytic ability. Thus we hypothesized that MSC efferocytic activity is regulated by macrophages. To identify the pathways involved in efferocytic activity by MSCs, RNA sequencing analysis was conducted and suggests that MSCs utilize the Axl, Tyro3, and Lrp1 receptor pathways in the activation of efferocytosis. Flow cytometry and confocal imaging have shown that loss of the efferocytic receptor Axl results in a decreased level of efferocytosis in bone marrow MSCs but not macrophages. Additionally, preliminary data in our lab suggests that there are time-dependent differences in levels of efferocytosis by MSCs, starting from as early as 3 hours. Using confocal time-lapse imaging we aim to better characterize the dynamics between phagocytes within the bone marrow microenvironment. Using WT and Axl -/- mice, we created two *in vitro* culture systems; one in which primary MSCs and macrophages were co-cultured and the second in which MSCs were isolated using tri-marker magnetic depletion (CD45+/F480+/Ly6C+) were fed end-stage neutrophils (PMNs). The confocal time-lapse imaging procedure is currently being optimized to confirm previously obtained results in primary murine (mMSCs) and to further characterize the dynamics of efferocytosis in MSCs. Thus far, both the dye type and concentration have been selected through a series of dose-response trials to minimize cell death while simultaneously optimizing the optical parameters to maximize image quality. Following the 24hr time-lapse using the optimized cellular and optical parameters, we started imaging analysis to quantify the number, type, speed, and duration of interactions between MSCs and apoptotic targets. Using a MATLAB operated script, we are selecting a region of interest (ROI) as a binary mask that is created based on the differences in the intensity gradient across the image. We are attempting to identify engulfment events through overlapping binary mask positivity for identical coordinates across the different channels. Currently, we are in the process of troubleshooting the script which should ultimately be able to identify engulfment events and quantify field of view positivity percentage. Using this strategy, we will dissect the dynamics of efferocytosis performed by bone associated cells and bone marrow-derived MSCs.

Title: **Evlaulation of Lymphatic Muscle Cell Damage and Peri-Vascular Mast Cells on Popliteal Lymphatic Vessel Function in TNF-Tg Mice with Inflammatory-Erosive Arthritis**

Presenting Author: Yue Peng

Co-Authors: H. Mark Kenney, Yue Peng, Karen L. de Mesy Bentley, Chad A. Galloway, Homaira Rahimi, Lianping Xing, Christopher T. Ritchlin, Edward M. Schwarz

Lab PI / Mentor: Edward M. Schwarz

Abstract (3500 characters or 500 words Limit)

Background: Lymphatic dysfunction is a factor in the onset and progression of joint inflammation and bone erosion in rheumatoid arthritis (RA). Our prior studies demonstrated reduced lymphatic clearance in the hands of symptomatic RA patients vs. healthy controls. We reported similar findings in the tumor necrosis factor transgenic (TNF-Tg) mouse model of RA, which exhibits reduced contractility of joint-draining popliteal lymphatic vessels (PLVs). Remarkably, anti-TNF therapy in flaring TNF-Tg mice recovers PLV contractions concomitant with amelioration of arthritis. Based on this result, we hypothesize that PLV dysfunction in TNF-Tg mice is caused by chronic inflammation induced: 1) lymphatic muscle cell (LMC) damage, and/or 2) accumulation of activated mast cells around joint draining lymphatic vessels that secrete paracrine factors (e.g. histamine) known to inhibit lymphatic contractions. Specifically, we hypothesize that: 1) alpha-smooth muscle actin (αSMA) PLV-LMC coverage and LMC turnover is reduced, while peri-PLV mast cell numbers are increased, in TNF-Tg mice with severe arthritis; and 2) anti-TNF therapy reverses these pathologies with recovery of PLV function and amelioration of inflammatory-erosive arthritis.
Methods: PLV function was assessed by in vivo near-infrared (NIR) imaging of 24-hour indocyanine green (ICG) clearance from the footpads. Bromodeoxyuridine (BrdU) (0.1mg/g/day/i.p.) was administered to 8-month-old wild-type (WT, n=8 mice) and TNF-Tg (placebo or anti-TNF therapy, n=5 mice each; i.p. 10mg/kg/week) mice for 6-consecutive weeks, followed by whole mount immunofluorescent microscopy for αSMA+ and BrdU+ PLV-LMCs. Talus bone volumes were measured by μCT longitudinally every 3-weeks as a biomarker of ankle arthritis. Preliminary scanning electron microscopy (SEM) was performed on WT PLVs (n=2 mice) to assess the feasibility of evaluating LMC coverage by ultrastructural analysis. Quantification of peri-PLV mast cells was performed on toluidine blue stained serial sections through the PLV, and degranulating mast cells were identified by numerous extracellular granules.
Resutls: αSMA+ PLV-LMC coverage was reduced in TNF-Tg placebo mice vs. WT littermates (61.32±23.47% vs 84.99±10.79%; p<0.0001). However, anti-TNF therapy failed to recover αSMA+ PLV-LMC coverage (68.86±20.41%), consistent with no change in LMC turnover (<2% BrdU+/αSMA+ cells for all groups). In contrast, anti-TNF therapy restored talus bone volume, and there was no relationship with αSMA+ PLV-LMC coverage and bone volume (R^2=0.1106; p=0.1519). "SEM of PLVs identified the TNF-induced peri-PLV inflammatory cells to be mast cells based on size and morphology. While no differences were observed between total mast cell numbers around WT and TNF-Tg PLV, we observed a significant correlation between the % of degranulated mast cells and PLV function (ICG clearance) (R^2=0.8616; p=0.0075).
Conclusions: TNF-Tg RA mice with severe arthritis have reduced αSMA+ PLV-LMC coverage. While 6-weeks of anti-TNF therapy reverses joint bone loss in TNF-Tg mice, this short-course does not enhance αSMA investiture or LMC turnover in damaged PLVs. Thus, anti-TNF therapy recovery of lymphatic function may not due to LMC repair or regeneration. Howeover, our finding that degranulated mast cells are associated with PLV dysfunction in TNF-Tg mice suggests that mast cell specific therapies (i.e. cromolyn sodium) may be useful, and experiments to test this are ongoing.

Title: **Automatic Vascular Imaging Analyses Using Deep Neural Networks**

Presenting Author: Beibei Qi

Co-Authors: Chenyu Lin

Lab PI / Mentor: Jiebo Luo and Xinping Zhang

Abstract (3500 characters or 500 words Limit)

Quantitative and morphological evaluation of vascular imaging obtained from multiphoton scanning of bone tissues in 3D format has been a persistent challenge due to large data sets as well as a high level of imaging noise coupled with the presence of complex and fine vascular structures from the harvested tissue samples or from intravital imaging. The goal of this project is to create a streamlined automatic imaging analysis protocol that can be used to perform unbiased analyses of the vasculature in soft tissue and bone. Deep neural networks have demonstrated successes in various natural and medical image recognition tasks including automatic identification, detection and segmentation of object of interest. Among available network architectures, U-Net has been widely used in medical image segmentation, while a more recent Ladder Net adds more paths of information flow for potentially better performance. In this project, we utilize these state-of-the-art methods for 3D blood vessel segmentation in multi-photon images where imaging noise makes it challenging to segment heavily entangled thin structures that correspond to blood vessels. To establish the ground truth for vascular structure segmentation, we carefully use ImageJ and Amira to semi-automatically remove noise and unwanted regions in thresholded binary masks while considering neighborhoods in the 3-dimensional volume. The stacks of cleaned masks are used as the ground truth to train several deep neural network models. In the training process, the U-Net models are fine-tuned in a two-stage process to obtain the best segmentation results consistent with the expert opinion. The best model using Ladder Net achieves an AUC of 0.998 and an F-1 score of 0.886 on a test dataset that contains representative samples of bone tissues. Perceptually, the segmentation results provide effective noise supression while preserving vascular structures. Future work will include testing and fine-tuning for image stacks with heavier noise following acquisition.

Title: **Biomechanical Comparison of Stemless Humeral Components in Total Shoulder Arthroplasty**

Presenting Author: Bowen Qiu

Co-Authors: Raymond E. Chen, Emma Knapp, Anthony Miniaci, Hani Awad

Lab PI / Mentor: Ilya Voloshin

Abstract (3500 characters or 500 words Limit)

Background: Stemless humeral components provide certain advantages compared to stemmed implants, including decreased stress shielding and preservation of bone stock. However, the ideal design of stemless components and the relationship between specific designs and proximal humeral BMD remains unknown.
Methods: Five humeral stem designs were included in this study: three stemless (Sidus, Simpliciti, OVOMotion), one short stem (50 mm) and one standard stem (130 mm). 50 cadaveric human humerii were obtained and divided into five groups. BMD within the humeral head was determined for all samples via DEXA scan. The 25 samples with the lowest and highest BMDs were categorized as "Low" and "High", respectively, with a BMD threshold of 0.35 g/cm2, creating BMD subgroups. Mean BMD was similar between groups. Each sample underwent axial loading followed by torsional loading. Sensors attached to the specimen recorded micromotion throughout testing. Axial loading consisted of cyclic loading for 100 cycles at 3 peak forces (220, 520 and 820 N). Torsional loading consisted of 100 cycles of internal/external rotation at 0.1 Hz at 6 peak torques, or until failure (+/- 2.5, 5, 7.5, 10, 12.5 and 15 Nm). Failure was defined as the torque at which any bone fracture, implant detachment from anchor/stem or an excess of 50□ internal/external rotation occurred.
Results: At maximal axial loading, Simpliciti demonstrated greater micromotion (540 μm) than OVOMotion (192 μm). Simpliciti and Sidus (387 μm) also had greater micromotion than Short stem (118 μm) and Standard stem (85 μm). These differences were accentuated at low BMD. Torsional testing demonstrated that Standard stem failed at greater torque (7.2 Nm) than Simpliciti (2.3 Nm), Sidus (1.9 Nm) and OVOMotion (3.9 Nm). When comparing torsional testing results of low BMD samples, both Standard stem and Short stem failed at greater torque than Simpliciti (p=0.02) and Sidus (p=0.03) but failed at a similar torque to OVOMotion.
Conclusion: Primary fixation of stemless and stemmed humeral implants depends on implant design and proximal humeral bone quality. Stemmed implants outperformed Simpliciti and Sidus in low BMD (<0.35 g/cm2) specimen during testing. OVOMotion (central screw and peripheral rim-fit design), demonstrated greater primary stability at low BMD when compared to Simpliciti (cylindrical center body and three solid fins, no rim-fit) and Sidus (four open fins, no center body, no rim-fit).

Title: **High levels of efferocytosis by mesenchymal stromal cells induce senescence**

Presenting Author: Emily R. Quarato

Co-Authors: Allison J. Li, Yuko Kawano, Noah Salama, Rubens Sautchuk Jr., Roman A. Eliseev, and Laura M. Calvi

Lab PI / Mentor: Laura M. Calvi

Abstract (3500 characters or 500 words Limit)
Aging has been shown to induce osteopenia, or bone loss, increasing the risk for fractures, morbidity, and mortality, and often leading to substantial healthcare costs. While the current literature has explored aging on the bone marrow as a whole, there are several critical gaps in our knowledge on the components of the bone marrow microenvironment, particularly mesenchymal stromal cells (MSCs), and how they lead to bone loss during aging. In aged mice, our lab found that bone marrow derived macrophages become deficient in their ability to phagocytose dead cells (efferocytosis). Previous studies have shown that MSCs can act as a facultative phagocyte cell population in embryos when macrophages are impaired. Our functional data indicate that 5% of MSCs in vivo and 30+% in vitro conduct efferocytosis. In vivo, we observed MSCs had increased efferocytic rates in aged mice, where macrophage efferocytosis is known to be defective. In vitro co-cultures demonstrated that MSC efferocytic activity is decreased by the presence of functioning macrophages, suggesting a correlation between macrophage number and function and MSC efferocytic activity. To identify the pathways involved in efferocytic activity by MSCs, RNA sequencing analysis was conducted and suggests that MSCs utilize the Axl, Tyro3, and Lrp1 receptor pathways in the activation of efferocytosis. Using an Axl KO mouse model, we confirmed that loss of Axl decreases, but does not completely block, MSC efferocytosis. Interestingly the RNA sequencing showed that the level of efferocytosis influences the pathways utilized by the MSCs. During low levels of efferocytosis we see upregulation of pathways associated with adhesion, proliferation, and mobility while during high levels of efferocytosis we see increased evidence of cellular senescence and apoptotic pathways. We generated the Bai1xPrxCre mouse model where MSCs have enhanced MSC efferocytosis. In vitro Bai1xPrxCre MSCs cultured with end stage neutrophils performed increased efferocytosis and shifted towards a senescent phenotype, that became more severe with higher neutrophil doses. Our initial analysis of Axl-/-, where MSC efferocytosis is reduced, showed increased bone density by DXA, suggesting that blocking MSC efferocytosis may improve bone health. Collectively, these data support that idea that MSCs can utilize established efferocytic pathways but during high levels of efferocytosis, MSCs become senescent. These data suggest that excessive MSC efferocytosis may represent a novel mechanism of MSC senescence and age-dependent bone loss. Since pharmacologic tools exist to modulate efferocytosis, these data may provide a novel approach to improve bone health.

Title: Does centralization of revision total hip and total knee arthroplasty affect patient travel distances/times in vulnerable patient populations?

Presenting Author: Gabriel Ramirez

Co-Authors: Caroline Thirukumaran, Benjamin RicciardiLab PI / Mentor: Caroline Thirukumaran

INTRODUCTION: Previous studies have shown an association between higher hospital volume and lower rates of adverseoutcomes after revision total join arthroplasty (TJA). This may motivate various strategies to centralize revision TJA care to higher volume centers in order to reduce adverse postoperative outcomes. The impact of centralization of revision TJA care on patients' travel distance, especially in vulnerable patientpopulations, is unknown. This study simulated centralizing revision TJA services to higher volume hospitals to determine if centralization significantly affected patient travel distance or travel time; or disproportionately affectedlow-income, rural, or racial or ethnic minority populations.

METHODS: New York State's (NYS) administrative Statewide Planning and Research Cooperative System database was queried using Medicare Severity Diagnosis Related Groups to identify inpatient episodes of revision hip and knee arthroplasty from 2008-2016 with NYS residential zip codes (n=33,493). The Open Source Routing Machine project was used to estimate driving distance and time using each patient's residentialzip code and the zip code of the facility providing that patient's revision TJA care. The first centralization scenario redirected patients in the lowest 25% by-volume hospitals to the nearest by-distance hospital in the remaining higher 75% by-volume hospitals. The second and third scenarios similarly centralized patients in the lowest 50, and 75% by-volume facilities to the remaininghigher 50, and 25% by-volume facilities respectively. Redirected patients travelling more than 60 miles or more than 60 minutes were considered adverselyimpacted with an increased travel burden; otherwise they were not considered adversely impacted. Patients not redirected were assumed not adversely impacted. The secondary outcome of interest was the impact of the aforementioned scenarios on lower income, non-white race, rural versus urban counties, and Hispanic ethnicity. Key predictors included patient race, ethnicity, and income.

RESULTS: These three scenarios resulted in 633 (2%); 3,050 (9%); and 9,323 (28%) centralized patient that resulted in any change of hospital, of which 1 (0%), 312 (1%), and 814 (2%) respectively for scenario 1, scenario 2,and scenario 3 were adversely impacted with increased travel distance or travel time. In scenarios 2 and 3 White patients (scenario 2: odds ratio [OR]=3.23, 95% confidence interval [CI]=1.54-6.67; scenario 3: OR=10.0, CI=6.67-14.3), Hispanic patients (scenario 2: OR=12.3, CI=5.04-30.2; scenario 3: OR=3.24, CI=2.24-4.68), low-income patients (scenario 2: OR=69.5, CI=17.0-283; scenario 3: OR 3.86, CI 3.21-4.64), rural patients (scenario 2: OR=98.0, CI=49.6-192; scenario 3: OR 11.7, CI 9.89-14.0), and patients withoutgovernment or private insurance (scenario 2: OR=3.51, CI=1.89-6.51; scenario 3: OR=1.65, CI=1.23-2.23)were significantly more likely be adversely impacted relative to their respective counterparts.

CONCLUSION: This study shows that hypothetical centralization policies in New York State would not result in increased travel burden for most patients. The most aggressive scenario, centralizing patients from the lowest 75% by volume hospitals, resulted in less than 10% of patients having increased travel burden, however this scenario may disproportionately increase travel burden for White, Hispanic, rural, and low-income patients. Any centralization policy for revision TJA care would need to be designed to minimize the impact on vulnerable patient groups.

Title: **Development of bisphosphonate-conjugated antibiotics to target Staphylococcus aureus biofilm within the osteocyte lacuno-canalicular network of infected cortical bone in chronic osteomyelitis**

Presenting Author: Youliang Ren

Co-Authors: Karen L. de Mesy Bentley, Thoma Xue, Motoo Saito, Frank H. Ebetino, Shuting Sun, Edward M. Schwarz, Chao Xie

Lab PI / Mentor: Chao Xie

Abstract (3500 characters or 500 words Limit)

INTRODUCTION: The recent discovery of Staphylococcus aureus (S. aureus) colonization of the osteocyte lacuna-canalicular network (OLCN) of live bone via transmission electron microscopy (TEM) analyses of infected bone has provided new insights into the problems of antibiotic therapy to treat bone infections. We demonstrated that standard of care (SOC) antibiotics delivered systemically and locally at high doses are very effective at killing planktonic bacteria on implants and soft tissue, but have no effect on established biofilm in bone. To address this, we developed bisphosphonate conjugated drugs that bind to metabolically active bone surfaces after systemic administration. After attachment to bone sites, the drug is released due to low pH levels, or by enzymatic cleavage, completing the "target-and-release" drug delivery. Importantly, our BP-conjugated drugs lack the amino group required for osteoclast apoptosis, and thus have no toxic effects on bone cells, bone formation or bone resorption. Based on sitafloxacin's remarkable efficacy against MRSA biofilm and small colony variants, we synthesized bisphosphonate-conjugated sitafloxacin (BCS) and hydroxybisphosphonate-conjugate sitafloxacin (HBCS) molecules, and demonstrated their efficacy in vitro. Here we tested the hypothesis that these drugs prevent osteolysis by killing S. aureus within the OLCN in an established murine model of implant-associated osteomyelitis.

METHODS: All animal studies were performed under protocols approved by the UCAR. 8-week-old female C57B/6 mice (n=4) received a transtibial implant contaminated with 10^5 CFU of bioluminescent MRSA (USA300-LAC::Lux), and were given placebo (saline), free sitafloxacin, BCS or HBCS on days 0, 1 & 2 post-op following established biofilm formation and OLCN invasion. Longitudinal bioluminescent imaging (BLI) was performed on days 3, 5, 7, 10 & 14. Infected tibiae were harvested on day 14 and processed for micro-CT, Brown & Brenn and TRAP stained histology and TEM as previously described. Data are presented as means +/- SD for each group, and statistical significance was determined using a one-way ANOVA where $p<0.05$ was considered significant.

RESULTS: Longitudinal BLI demonstrated that free sitafloxacin immediately decreases planktonic MRSA growth, while BCS and HBCS activity is delayed 3-7 days, consistent with the hypothesized target-and-release kinetics. Micro-CT analysis of peri-implant osteolysis revealed that only bisphosphonate conjugated sitafloxacin (BCS and HBCS) significantly inhibits bone loss, which was confirmed by TRAP stained histology. Brown & Brenn stained histology demonstrated reduced biofilm formation on necrotic bone fragments, while TEM of the infected bone demonstrated preliminary evidence of HBCS and BCS induced cytotoxicity (bacteria cell swelling with large numbers of vacuoles).

DISCUSSION: The inability of local high-dose antibiotic treatments to eradicate S. aureus within the OLCN of infected bone strongly suggest that bone-specific targeting of antimicrobials is needed. Here we explored the potential of bisphosphonate conjugated antibiotics that target reactive bone surfaces, and demonstrate proof of concept of "target-and-release" pharmacodynamics via BLI, and the resulting efficacy on osteolysis due to bacterial cytotoxicity. Formal studies with larger numbers of animals and quantitation of the MRSA cytotoxicity via TEM morphologic assessment are warranted.

Title: **IL-27 suppresses Staphylococcal abscess formation in Staphylococcus aureus implant-associated osteomyelitis**

Presenting Author: Motoo Saito

Co-Authors: Yugo Morita, Stephen L. Kates, John R. Owen, John L. Daiss, Edward M. Schwarz and Gowrishankar Muthukrishnan

Lab PI / Mentor: Edward M. Schwarz and Gowrishankar Muthukrishnan

Abstract (3500 characters or 500 words Limit)

NTRODUCTION: Interleukin-27 (IL-27) is a multifaceted cytokine, and its role in host immunity against bacterial osteomyelitis remains to be elucidated. In a clinical study, we found that IL-27 serum levels were remarkably elevated in S. aureus osteomyelitis patients, and further increased during sepsis. To elucidate the effect of IL-27 on S. aureus osteomyelitis, we tested the hypothesis that IL-27 mediates bacterial clearance during S. aureus osteomyelitis in mice.
METHODS: Vertebrate animals: All studies with mice were performed on IACUC-approved protocols. In vitro IL-27 induction assay: Primary bone marrow-derived murine macrophages, osteoclasts and osteoblasts were infected with S. aureus USA300 at MOI = 10 for 24 hours followed by collecting the cell culture supernatant to examine IL-27 secretion using ELISA. Implant-associated osteomyelitis model: WT and IL-27Rα-/- in the C57BJ/6 background mice were challenged with a S. aureus contaminated trans-tibial implant. The sterile implant were used for the control. The bone homogenate supernatant and serum were collected on day 1, 3, and 14 post-op, and local and systemic IL-27 levels were confirmed by ELISA. Induction of systemic IL-27 in mice: To induce exogenous IL-27 expression in mice, intramuscular injection with recombinant adeno-associated virus (rAAV) expressing IL-27 or GFP (control) were performed on WT and IL-27Rα-/- mice. The assessment of CFU (implant, surgical site soft tissue and tibia), peri-implant osteolysis (high-solution μCT), and histopathology (TRAP staining) were performed on day14 post-op. Differences between groups were determined by unpaired t-test or ANOVA.
RESULTS: IL-27 production in primary murine macrophage cultures was significantly elevated by S. aureus infection ($p<0.0001$), while in primary osteoclasts, IL-27 levels were undetectable regardless of infection. Interestingly, IL-27 production in primary osteoblasts was also significantly increased by S. aureus infection ($p<0.0001$). In vivo, local IL-27 levels were increased on day 1 post-infection compared to sterile implant controls, but no differences in IL-27 levels were observed on days 3 and 14. In IL-27Rα-/- mice, there was no significant difference between the two groups at all time points. Serum IL-27 levels were undetectable in all groups. Remarkably, systemic IL-27 induced by rAAV suppressed abscess formation at the surgical site compared to rAAV-GFP controls, and quantification of CFU in soft tissue at the surgical site confirmed this significant decrease ($p<0.0001$). μCT showed that peri-implant osteolysis was decreased in mice treated with rAAV-IL-27 compared to rAAV-GFP controls ($p<0.05$). In IL-27Rα-/- mice, these differences were no longer observed, suggesting that the effects of rAAV-IL-27 on S. aureus osteomyelitis in WT mice were due to IL-27/IL-27R signaling. Moreover, the number of TRAP positive cells around surgical site was reduced by treating with rAAV-IL-27 ($p<0.05$). These data are consistent with IL-27's direct inhibitory effects on osteoclasts.
DISCUSSION: Here we show that systemic IL-27 ameliorates surgical site soft tissue infection and osteolysis during S. aureus implant-associated osteomyelitis via IL-27/IL-27R signaling. In the natural course of implant-associated osteomyelitis model, we also demonstrated that IL-27 was induced locally only in the acute phase. Collectively, IL-27/IL-27R pathway could be a potential therapeutic target for S. aureus osteomyelitis.

Title: **IGF-1 in the Bone Marrow Microenvironment Regulates Mesenchymal Stromal Cell Efferocytosis**

Presenting Author: Noah A. S. Salama

Co-Authors: Emily R. Quarato, Chunmo Chen, Yuko Kawano, Daniel K. Byun, Allison Li, Roman A. Eliseev, Jane L. Liesveld, Michael W. Becker

Lab PI / Mentor: Laura M. Calvi

Abstract (3500 characters or 500 words Limit)

The bone marrow is a major site of cellular production but is also essential for cellular clearance, removing roughly 5-10X10^10 apoptotic cells/day. In order to clear these apoptotic cells (ACs) from the bone marrow microenvironment (BMME) without causing inflammation, professional phagocytes such as macrophages utilize efferocytosis. Imbalanced efferocytosis is seen in a variety of inflammatory conditions, and we demonstrated defects in efferocytic bone marrow macrophages induces accumulation of ACs and hematopoietic dysfunction. Non-professional phagocytes such as stromal, epithelial, and fibroblastic cells can assist with clearance, recruit professionals, but may also demonstrate altered phenotypes post efferocytosis. Our lab identified mesenchymal stromal cells (MSC) as an important non-professional phagocyte which assists bone marrow macrophages (bMΦs) in clearing of ACs from the BMME. However, our preliminary data show that MSCs performing efferocytosis have increased cellular senescence and apoptosis in a dose-dependent fashion, which could partially explain both impaired hematopoiesis and osteoporosis in aging, fracture repair, and myeloablation. Therefore, signals that regulate and coordinate the efferocytic responses from bMΦs and MSCs could be manipulated to decrease MSC efferocytosis and thereby reduce their senescence. We found increased efferocytosis in bone marrow MSCs from aged mice, where bone marrow macrophages were defective. Since studies on non-professional phagocytes in other systems have shown that IGF1 produced by MΦs restrains efferocytic activity by non-professionals, we hypothesized that the IGF1 axis could regulate MSC efferocytosis in the BMME. In support of this hypothesis, IGF1 transcripts were significantly decreased in bMΦs from aged (20-24 month old) versus young (3-4 month old) mice (Log2FoldChange -2.24, adjustedP=2.02x10^-9).
Cytokine arrays on bone associated cell (BAC) cultures from aged (>12 months) and young (2-3 months) mice, we identified the IGFBP family as major cytokines at baseline and after MSC where fed apoptotic neutrophils. Furthermore, BAC cultures collected from aged animals exhibited elevated IGFBP3, the primary inhibitor of IGF1, which decreases bioavailable IGF1. Cultures from aged mice had a > 20 fold decrease in bioavailable IGF1 (ratio of IGF1:IGFBP3) compared to young mice, consistent with the reduced IGF1 reported by other labs as a functional indicator of aged bone marrow. We next tested whether addition of IGF1 in vitro decreases MSCs efferocytosis. Using the ST2 bone marrow stromal cell line, IGF1 treatment significantly decreased rate and efficiency of MSC efferocytosis at 3- and 24-hours. These data suggest that reduced IGF1 from macrophages and excessive IGFBP3 from MSCs and BACs we observed in aged cultures would tip the system toward excessive efferocytosis by MSC, leading to increased senescence and apoptosis. By better understanding the relationship between bMΦs and MSCs in the BMME, we may identify novel therapeutic targets that balance the clearance of ACs while mitigating the detrimental impact on stromal support cells, suggesting a potential clinical approach to shift efferocytic burden toward bMΦ and away from MSCs. This strategy may be especially helpful in scenarios where large influxes of ACs will occur as a result of treatment with radiation, chemotherapy, or in pathologic states with increased burden of ACs, such as in myelodysplastic syndromes.

Title: **Intravital Imaging of Oxygen Tension and Energy Metabolism at the Site of Cranial Bone Defect Repair via 2-photon Based Phosphorescence and Fluorescence Lifetime Imaging**

Presenting Author: Kevin Schilling

Co-Authors: Yuankun Zhai, Zhuang Zhou, and Nick Lenhard

Lab PI / Mentor: Edward Brown and Xinping Zhang

Abstract (3500 characters or 500 words Limit)

Tissue oxygenation is one of the key determining factors in bone repair and bone tissue engineering. Adequate tissue oxygenation is essential for survival and differentiation of the bone-forming cells and ultimately the success of bone tissue regeneration. Currently available methods for measurement of tissue oxygen levels in repair are invasive, prohibiting analysis of unperturbed oxygen landscapes within regenerative niches. In this thesis, we have developed and demonstrated an approach termed two-photon phosphorescence lifetime imaging (2P-PLIM) in conjunction with multiphoton laser scanning microscopy (MPLSM) for mapping and interrogation of oxygen tension (pO2) at high resolution during bone defect healing. To understand the impact of local oxygen levels on the activities and behaviors of bone and vessel forming cells at the site of bone defect repair, we further developed two-photon-based NAD(P)H and FAD autofluorescence lifetime imaging (2P-FLIM) that allows the delineation of redox state and cellular metabolism of the healing tissue in living animals. Combining these advanced optical techniques with transgenic animals that differentially labels osteoblasts, sprouting endothelial cells (ECs) and arterial ECs, we examined the oxygen distribution as well as the cellular metabolism at the osteogenic and angiogenic interface of cranial bone defect repair. Our study shows that: 1) oxygen distributions in capillary vessels and repair tissue at the site of healing are heterogeneous as well as time and location-dependent; 2) injury-induced hypoxia could significantly impact cellular metabolism of osteoblasts; and 3) ECs and osteoblasts could utilize different metabolic pathways at the site of healing, with osteoblasts using more OxPhos and consuming more oxygen at the site of repair.The findings in this study have contributed new information to a deeper understanding of osteogenic and angiogenic coupling during cranial bone defect healing. With the information presented here, future work will focus on the design of effective bone tissue engineering strategies aimed at manipulating osteoblast energy metabolism or the hypoxia pathway for enhanced bone healing outcomes. With the establishment of the various high resolution and state-of-the-art optical imaging techniques, this thesis further laid the foundation for future studies aimed at better understanding of stem/progenitor cell behavior and the healing microenvironment during skeletal repair and regeneration.

Title: **Botulinum Toxin A in Mouse Model of Raynaud Phenomenon Ischemic Tissue Loss**

Presenting Author: Derek T. Schloemann, MD

Co-Authors: Warren C. Hammert, MD and Benjamin D. Korman, MD

Lab PI / Mentor: Warren Hammert and Benjamin Korman

Abstract (3500 characters or 500 words Limit)

Raynaud's phenomenon (RP) is a clinical syndrome characterized by cold-induced vasospasm of the digits and affects up to 5% of healthy women. It is caused by a combination of vascular, neurogenic, and immunologic dysfunction. While many cases of RP are not clinically dangerous, a subset of patients have RP in the setting of a systemic disease (secondary RP), and these patients have substantially increased risk of morbidity including digital ischemia and ulceration, pain, and impaired hand function. Secondary RP is prevalent in systemic sclerosis (SSc, scleroderma), affecting over 95% of these patients, and causing a very high burden of ischemic complications. One major barrier to the study of ischemic Raynaud's is a lack of faithful model systems. While it has yet to be reproduced, a recent study demonstrated autoantibodies to cytokeratin 10 (K10) in serum from patients with ischemic RP, and passive immunization of mice with antibodies against K10 induced cold-induced ischemic tissue loss in the ear, which mimics the pathology seen in RP in SSc.
While a variety of treatment targets for RP exist, vasodilators are considered the gold standard, but are frequently ineffective in SSc patients. In these challenging cases, advanced therapies such as injections of botulinum toxin A and surgical treatment consisting of sympathectomy or arterial bypass have been used with variable success. Botulinum toxin, a neuromuscular blocking agent, is produced by Clostridium botulinum, and is used clinically for a variety of indications. In RP, botulinum toxin is thought to block sympathetic-mediated vasoconstriction, and has been reported to result in rapid pain relief that can last for months. Moreover, this can have additional benefits including improved digital transcutaneous oxygen saturation, nutritional blood flow, and healing of ulcers.

Our long-term goal is to better understand the mechanism of ischemic tissue loss in Raynaud's phenomenon (RP) and develop a system to assess the efficacy of treatment of this disease. To this end, we will test the hypothesis that ischemic tissue loss in the anti-K10 antibody murine model of RP is caused by loss of endothelial cells, and that this can be ameliorated by local administration of botulinum toxin A. Here we discribe our experimental approach to reproduce the published findings, and optimize this model for the Botulinum toxin studies. We will also assess whether histologic loss of endothelial cells can be used as a surrogate for tissue loss to assess the efficacy of treatment. We will then administer local botulinum toxin A to test the hypothesis that ischemic tissue loss is ameliorated by this therapy and that the reduction in tissue loss is associated with a reduction in the number of endothelial cells.

If successful, this work will establish the K10 immunization model as a useful system to screen medications for to treat ischemic RP and to further investigate the mechanism by which treatments prevent end

Title: **Acute Myeloid Leukemia on a chip**

Presenting Author: Azmeer Sharipol

Co-Authors: Maggie Lesch, Celia Soto

Lab PI / Mentor: Benjamin Frisch, Co-PI: Danielle Benoit

Abstract (3500 characters or 500 words Limit)

Acute myeloid leukemia (AML) is the most predominant and aggressive blood cancer in adults. Standard therapy results in an average 5-year survival rate of <30% with few new treatment options having been developed in the past 50 years. Due to the complex malignancies of AML, studies of pathophysiology and therapy have been limited to standard tissue culture, utilization of patient-derived xenograft mice models (PDX), or syngeneic animal models. None of these are capable of faithfully recapitulating the complex interactions within the human bone marrow microenvironment (BMME). It is well known that leukemic cells may interact with the BMME and affect cellular function, hematopoietic stem cell (HSC) fate, and disease burden. Particularly, our lab has shown that CCL3 signaling from leukemic cells can induce loss of osteoblastic function, which promotes leukemic cell survival in a murine model of AML. In addition, AML patients also show elevated levels of CCL3, suggesting a role of the pathway in human AML disease. To bridge the gap of research and increase throughput in drug discovery, our lab aims to generate a 3D in vitro model of murine and human AML able to recapitulate specific BMME interactions. We will couple our understanding of the cell-microenvironment interaction with a dynamic tissue engineering approach using microfluidics (Emulate Chip S-1) and fibrin hydrogel scaffolding. Briefly, we have cultured bone marrow stromal cells (BMSCs) isolated from C57BL/6J mice into the apical channel of Chip S-1 to create a supportive osteoblastic layer. Upon 14 days of culture under continuous flow rate of 30µl/hour with osteoblast differentiation media, robust mineralization was observed in chips as shown by positive Alkaline Phosphatase and Von Kossa staining. To recapitulate the 3D microenvironment, we encapsulated BMSCs and support cells from whole bone marrow in fibrin hydrogel on top of the differentiated osteoblastic layer and provided an endothelium monolayer on the basal side of chip membrane to emulate the vascular compartment. Sorted hematopoietic stem cells, HSCs (Lin- Sca+ cKit+), grown for two weeks in healthy BM chip shows maintenance at 0.29 ± 0.13% of total cells, frequencies that are similar to flow cytometric analysis of freshly isolated bone marrow at 0.15 ± 0.04%. In addition, chip grown HSCs were able to successfully engraft in a murine BM transplant model and gave rise to ~60% of total peripheral blood mononuclear cells (PMBCs) at 8- and 12-week post transplantation. This data is comparable to transplant of freshly isolated BM cells which resulted to more than 70% of total PMBCs at the same timepoints suggesting promising BMME recapitulation on chip. When leukemic cells were introduced in the chip, similar loss of osteoblastic function were observed by marked reduction of Osteocalcin I and Collagen I gene expression compared to healthy chip (98.8% and 94.82% decreased expression respectively) Overall, our findings suggest that the 3D culture conditions can provide a highly supportive microenvironment for HSC survival and hematopoiesis and, can replicate leukemic cell interaction with the BMME in vitro.

Title: **PROMIS Scores Correlate to Treatment Selection for De Quervain Tenosynovitis**

Presenting Author: Gilbert Smolyak

Co-Authors: Courtney Jones PhD MPH, Bowen Qiu MD, Constantinos Ketonis MD PhD

Lab PI / Mentor: Constantios Ketonis MD PhD

Abstract (3500 characters or 500 words Limit)

Introduction:
De Quervain Tenosynovitis (DQT), remains a common source of pain and loss of hand function. Despite conservative management, many patients continue to experience persistent pain in the affected hand. Currently, choice of treatment is largely empiric, but, Patient Reported Outcomes Management Information System (PROMIS) scores at the time of diagnosis might provide insight into success of non-operative management and predict necessity for surgical release.

Materials & Methods:
Patients presenting to a tertiary academic medical center from 2014-2019 with a sole diagnosis of DQT were identified. Patients <18 years old or that had other diagnosis were excluded. Patients were separated by treatment: physical therapy, injections, surgery or combinations thereof. Patients' status of undergoing surgery as an initial treatment and at any time before the end of the follow up period was also recorded. Chi-square analysis was performed to identify confounding variables or demographic factors that affect treatment strategy. A two-sided t-test was performed to identify differences in presenting PROMIS scores (PPS) between the initial and final operative status. Patient groups were then dichotomized by PROMIS score using predetermined cut-offs. Using logistic regression, odds-ratio of surgical intervention was determined based on each pertinent variable. Patients without a PPS were excluded from statistical tests involving PROMIS.

Results:
Of the 1529 patients that met inclusion/exclusion criteria, 685 had PPS. Notably, survey response rates were much higher from patients choosing more invasive interventions. Older patients tended to choose more invasive treatments as their initial management. For initial treatment, 2.9% of patients chose PT, 84.8% chose injection, and 12.3% chose surgery. By the end of the follow up period 87.0% of patients received an injection, with 21.3% of those patients requiring at least one additional injection, and 29.9% of the total cohort eventually undergoing surgery. There were no significant differences in PPS between patients of any initial treatment group. However, significant differences in scores were found between patients of different final treatment groups. Upon dichotomization of patients by PROMIS scores it was determined that patients with Physical Function (PF) scores less than 40 (OR = 1.62 [1.062-2.47]) or Pain Interference (PI) scores of greater than 60 (OR = 1.62 [1.051-2.496]) had significantly increased odds of undergoing surgery. Age 40-60 and female gender also had an increased odds of undergoing surgery. Furthermore, patients who had both a low PF and high PI were observed to utilize the surgical treatment at a rate double than patinets who had statistics below their respective thresholds.

Conclusions:
PROMIS survey results could be used to identify patients that are likely to fail non-operative intervention for DQT. While there were no differences in PPS between patients choosing PT, injection or surgery as their initial management, patients who scored lower than 40 for PF or higher than 60 for PI had significantly increased odds of eventually undergoing surgery. In light of this, the use of PROMIS scores could aid in patient-clinician discussion and facilitate shared decision-making leading to more effective and earlier handling of symptoms for individuals with DQT.

Title: **Investigating the Effect of PEG Hydrogel Substrate Stiffness on Retinal Pigment Epithelial Cell Adhesion and Barrier Function**

Presenting Author: Arvind R. Srivatsava

Co-Authors: Kannan V. Manian, Anthony Emanuel, Kevin Ling, Ruchira Singh

Lab PI / Mentor: Danielle S.W. Benoit

Abstract (3500 characters or 500 words Limit)

Retinal diseases affecting the macula, such as Age-Related Macular Degeneration (AMD) and Sorsby's Fundus Dystrophy (SFD), are widespread maladies that cause a progressive central vision loss. The specific outer retinal tissue, namely the Retinal Pigment Epithelium (RPE) – Bruch's Membrane (BrM) – Choriocapillaris (CC) complex, is often implicated in these diseases. However, the underlying mechanisms of tissue dysfunction are poorly understood. Our group has previously developed an in vitro model of the RPE-CC complex using peptide-functionalized poly(ethylene glycol) (PEG) hydrogels and induced pluripotent stem cell (iPSC)-derived cells. While we successfully developed CC-specific vasculature formation and disease-specific CC phenotypes, the model was limited in replicating key BrM features consistent with in vivo barrier formation. We hypothesize that tuning microenvironmental cues in the PEG hydrogel scaffold will lead to formation of a more robust RPE-BrM tissue, which can be used to better replicate human macular disease phenotypes. Previous studies have shown that in vitro RPE formation was improved when using substrates that mimicked native BrM stiffness (~1000 kPa). Therefore, we aimed to investigate iPSC-RPE monolayer integrity and BrM protein expression through culture on tunable PEG hydrogel substrates exhibiting a wide range of stiffness. This range (4 - 1000 kPa) was generated with hydrogels synthesized using 8 arm PEG-norbornene (20 kDa) crosslinked with MMP-degradable peptide sequence GKKC-GPQG↓IWGQ-CKKG or linear PEG-dimethacrylate (1 kDa). Hydrogels were either functionalized with 3 mM cell adhesive peptide GCRGDSG or acrylated-PEG-RGDS. iPSC-RPE were seeded on hydrogels and cultured for over two weeks, monitoring maturation as indicated by development of hexagonal morphology and pigmentation. Initial results show formation of a mature RPE monolayer on stiff (~1000 kPa) hydrogels with robust elastin expression, as assessed using immunostaining. In current experiments, substrates with a variety of elastic moduli are being explored to promote development of contiguous, and mature RPE layers with barrier integrity assessed using transepithelial resistance (TEER) meaurements and collagen IV, V, VI, laminin, and elastin expression and localization evaluated using immunostaining and confocal microscopy. Through this study, we aim to demonstrate the role of substrate elastic modulus on maturation and function of the RPE layer of RPE-BrM-CC complex. Moving forward, our goal is the development of a more physiologically relevant in vitro RPE-BrM-CC complex, which will be explored by tuning in vivo-relevant scaffold biochemical cues for retinal disease modeling.

Title: **Exploring the biologic sequelae of Achilles tendon impingement using a novel murine hind limb explant platform**

Presenting Author: Brian Wise

Co-Authors:

Lab PI / Mentor: Mark Buckley, Whasil Lee

Abstract (3500 characters or 500 words Limit)

Tendon impingement generates a disparate and multiaxial mechanical strain environment characterized by elevated compressive strain directed transverse to the longitudinal axis, which elicits a fibrocartilage-like tissue phenotype. Clinically, tendon impingement is understood to be an important extrinsic factor driving some of the most common tendinopathies. Despite these observations, the underlying mechanobiological mechanisms by which cells sense and respond distinctly to the unique mechanical demands of tendon impingement are understudied and poorly understood, which obscures our understanding of tendinopathy pathogenesis and results in inadequate treatment. Previously, our lab has developed a novel murine hind limb explant system to induce Achilles tendon impingement against the calcaneus during passive dorsiflexion, which provided in situ measurement of microscale deformations during impingement. Here, we paired this Achilles tendon impingement model with a tissue culture protocol to test whether this system can be deployed to study the biologic sequelae of tendon impingement over longer time scales. Explants were loaded into this experimental platform to apply static impingement or baseline tension to the Achilles tendon, and the terminal deoxynucleotidyl transferase dUTP nick end labeling (TUNEL) assay was performed to assess apoptosis. Nearly 100% cell viability within the tendon was maintained for at least 7 days of explant culture, suggesting that this platform can be used to interrogate biological output secondary to mechanical impingement over extended time periods. In our ongoing experiments, we are utilizing this model to investigate changes in gene expression with quantitative polymerase chain reaction (qPCR) following 3 days of static impingement by comparison to baseline tension, with a focus on i) key proteins comprising the extracellular matrix (ECM) and pericellular matrix (PCM); ii) tenogenic and chondrogenic transcription factors; and iii) signaling pathways hypothesized to be activated in response to tendon impingement including Indian hedgehog (Ihh)-mediated transcription of Gli1. Based on our preliminary strain measurements and finite element simulations, we hypothesize cells modify the composition and mechanical properties of their immediate PCM to modulate strain transfer to the cell in adaptation to tendon impingement, and we therefore anticipate changes in the expression of PCM proteins secondary to tendon impingement relative to baseline tension. These data will be supplemented with histological staining (hematoxylin-eosin, toluidine blue) to visualize gross morphological changes after 3 days of static impingement. We anticipate that this study will make progress toward identifying pathways that can be targeted to interfere with impingement-generated tissue alterations that drive debilitating tendinopathies.

Title: **Modulating macrophage function with drug delivery approaches to enhance fracture healing**

Presenting Author: Baixue Xiao

Co-Authors: Marian Ackun-Farmmer

Lab PI / Mentor: Danielle Benoit

Abstract (3500 characters or 500 words Limit)

Despite major advances in surgical procedures, there is still a high percentage (~10%) of fractures that do not heal, known as nonunion fractures. Underlying chronic inflammatory conditions, such as advanced age, rheumatoid arthritis, and diabetes have a high association with nonunion fractures, which are estimated to cost $9.2 billion/year in the US. Therefore, novel and minimally invasive approaches are urgently needed to prevent and/or treat debilitating and costly nonunion fractures. To this end, the Benoit Lab has developed a novel bone-targeting strategy based on tartrate-resistant acid phosphatase (TRAP) binding peptide (TBP)-functionalized nanoparticles (TBP-NPs). Wnt/beta-catenin agonists delivered via TBP-NP to treat mouse femur fractures showed 6-fold greater of TBP-NPs accumulation at fractures versus naïve bone, robust beta-catenin activation, and expedited fracture healing versus untreated controls. Despite these promising findings, the majority (~75%) of NPs at fractures were taken up by macrophages (MΦ) rather than regenerative cells types (e.g., osteoblasts or mesenchymal stem cells). Notwithstanding, MΦ have critical functions in fracture healing and dysregulated MΦ polarization, specifically more or persistent M1 MΦ and less or short-lived M2 MΦ, has been suggested to negatively impact healing process. Therefore, we hypothesized that preferential NP uptake by MΦ could be leveraged to enhance fracture healing via MΦ modulation. To test this hypothesis, in vitro drug screening was performed to identify drug candidates that promote M1-to-M2 polarization of MΦ. Specifically, bone marrow derived MΦ (BMDM) were harvested and differentiated to M0, M1, and M2 MΦ, followed by drug treatments for 1, 3, and 6 days. Then, drug-treated M0, M1, and M2 MΦ were tested for gene expression (PCR), cell surface markers (Flow Cytometry), and cytokine release (Luminex) to evaluate the impact of drugs on polarization. Following additional drug screening, we will deliver candidate MΦ polarization modulator with TBP-NP to murine fractures to investigate its impact on fracture M1-to-M2 transition and fracture healing. Altogether, this study seeks to leverage preferential NP uptake by MΦ and robust MΦ polarization modulation which will have widespread applicability in orthopaedics and beyond driven by aberrant MΦ polarization.

Title: **3D Printable Carboxymethyl Chitosan-Amorphous Calcium Phosphate Nanoparticles(CMC/ACP NPs) Enhance Osteogenesis and Regulate Macrophage Polarization**

Presenting Author: Ming Yan

Co-Authors:

Lab PI / Mentor: Hani Awad

Abstract (3500 characters or 500 words Limit)

INTRODUCTION: Amorphous Calcium Phosphate (ACP) has great potential as an orthopaedic implant material due to its ability to rapidly form bone-like crystals along collagen fibers. However, due to its amorphous state, the instability of ACP can hinder osteogenesis and evoke a pro-inflammatory response. Under physiological conditions, ACP is stabilized and transported by nanoparticles composed of non-collagenous proteins (NCPs). Carboxymethyl chitosan (CMC) has been explored as an engineered analog to NCPs when used as a nanocomplex with ACP to promote collagen fiber mineralization in vitro. We previously reported the development of an extrusion-based 3D-printable hyperelastic PCL bioink containing CMC/ACP NPs and demonstrated its cytocompatibility and antimicrobial properties. In this study, we investigate the dose-dependent effects of CMC/ACP NPs on the osteogenic differentiation of murine stromal progenitor cell (ST2) and on the polarization of Bone Marrow Derived Macrophages (BMDM).
METHODs: CMC/ACP NPs were synthesized by the dropwise method. ST2 cells were grown and treated with growth medium or osteogenic medium. The cells were either cultured without nanoparticles as controls, with low concentration of 50 µg/ml nanoparticles, or with high concentration of 500 µg/ml NPs for up to 7 days. Cell numbers, Alkaline phosphatase (ALP) and Alizarin Red staining and quantification were used to analyze the proliferation and mineralization. BMDM from C57Bl/6J mice were isolated, and were either induced into MΦ cells, M1, or M2 cells, or treated with a low or high concentration of NPs. After 24 hours, cells were used for flow cytometry or lysed for qPCR to evaluate gene expression of M1and M2 markers to quantify the effects of NPs treatment on macrophage polarization. Data were analyzed using one- or two-way ANOVA followed by Bonferroni-corrected multiple comparisons ($p<0.05$).
RESULTS: There were no significant effects of the NPs treatment on cell number or ALP levels. Treatment of ST2 cells with a high concentration of NPs significantly increased the mineralization in both growth and osteogenic media conditions by >2-folds, as early as day 3 of culture, which is generally not observed in control osteogenic culture of ST2 cells before day 7. When BMDM were treated with low or high concentrations of NPs, we observed dose-dependent increases in CD markers associated with M1 phenotype (MHC II and CD38) and M2 phenotype (CD 163 and CD206). This was further illustrated through double gating, which suggested that high concentrations of NPs activate a hybrid M1/M2 phenotype. Gene expression analysis also confirmed the induction of the hybrid M1/M2 phenotype upon NPs treatment. In cells treated with high concentrations of NPs, M1 markers gene expression generally decreased except for Il1b, while M2 markers gene expression increased except for Cd206. The data also show that High NPs increase the expression of Arg1, Cd163 and Ccl17, indicating a shift towards the M2 phenotype.
DISCUSSION: CMC-stabilized ACP was shown in this study to accelerate osteoblast mineralization while also promoting macrophage polarization in a mixed M1/M2 phenotype. Optimizing osteoinductive and anti-inflammatory NPs in 3D printed scaffolds can enhance the potential of this technology to stimulate bone regeneration in nonhealing defects.

Title: Crosstalk Between CypD/mPTP and Adipogenesis in Bone Marrow Stromal Cells

Presenting Author: Chen Yu

Co-Authors: Owen Charles Smith, Rubens Sautchuk, Roman A. Eliseev

Lab PI / Mentor: Roman Eliseev

Abstract (3500 characters or 500 words Limit)

Age-related bone loss is associated with decreased osteoblast-mediated bone formation, increased bone resorption and accumulation of bone marrow fat. During aging, differentiation potential of bone marrow stromal (a.k.a. mesenchymal stem) cells (BMSCs) is shifted towards adipogenic and away from osteogenic lineage. Our previous data has shown that activation of mitochondria is important during osteogenesis of BMSCs. A byproduct of such an activation is increased ROS, leading to oxidative stress and pathological opening of the mitochondrial permeability transition pore (mPTP) which results in mitochondrial dysfunction, oxidative phosphorylation (OxPhos) uncoupling, and in some cases, cell death. It is, therefore, beneficial for osteoinduced BMSCs to deactivate this pore. Cyclophilin-D (CypD) is a mitochondrial matrix protein that facilitates opening of the mPTP. We observed that CypD is downregulated during osteogenesis leading to lower mPTP activity and thus protecting mitochondria from ROS. However, the role of mitochondria and CypD during adipogenesis is unclear. Here, we are trying to characterize the potential role of CypD during adipogenesis of BMSCs. During adipogenesis, BMSCs do not activate mitochondrial respiration but increase glycolysis. Our preliminary data show that CypD is upregulated during adipogenesis of C3H10t1/2 mesenchymal cell and remains unchanged in human BMSCs. By performing CypD gene, Ppif, promoter analysis, we have identified multiple binding sites for adipogenic C/EBP and inflammatory NF-κB transcription factors. Using CypD gene, Ppif, promoter-reporter activity assay and ChIP-PCR, we found that C/EBP α, an essential regulator of adipogenesis, is involved in the transcriptional activation of CypD. Interestingly, overexpression of NF-κB p65 subunit shows synergistic effect with C/EBPα inducing Ppif promoter-luciferase reporter expression. This is important as inflammatory NF-κB signaling has been shown to be activated during adipogenesis. The interaction between C/EBP α and NF-κB p65 subunit is verified by co-immunoprecipitation (Co-IP) assay and western blot analysis. On the other hand, CypD overexpression in C3H10t1/2 cells enhances whereas CypD knockdown impairs adipogenic differentiation. Thus, there appears to be a reciprocity between CypD/mPTP and adipogenic signaling. For future experiment, to further elucidate the role of CypD/mPTP during adipogenesis: we will define mPTP activity and the crosstalk between C/EBP α and BMP/Smad signaling, especially Smad1, an osteogenic transcription factor negatively regulating CypD; elucidate the metabolic changes during adipogenesis using metabolic tracing and the effect of CypD on metabolism using Seahorse assay; determine the effect of CypD manipulation in BMSCs on bone marrow adiposity in vivo. In summary, this project will elucidate the potential role of CypD/mPTP during adipogenesis of BMSCs, facilitating the understanding of stem cell fate determination and molecular mechanism of age-related bone loss.

Title: **Icam-1-inhibited M2 MΦ infiltration is a new molecular mechanism for delayed fracture repair in splenectomized mice**

Presenting Author: Hengwei Zhang

Co-Authors: Tao Wu

Lab PI / Mentor: Lianping Xing

Abstract (3500 characters or 500 words Limit)

Introduction: Bone fractures caused by traffic accidents are commonly accompanied by abdominal injuries. A splenectomy procedure is vital to save patients' lives when spleen rupture occur. Delayed fracture repair is reported in splenectomized mice and human patients. A few reports show that the splenectomy decreases macrophages (MΦ), inflammatory cytokines and osteoblasts in callus. However, the underlying mechanism is not known. We found that splenectomized mice have decreased M2 MΦs and increased senescent cells (SCs) in the callus. M2 MΦ is beneficial to fracture repair. SCs from splenectomized mice significantly expressed a higher level of intracellular adhesion molecule-1 (Icam-1), an important component of senescence-associated secretory phenotype (SASP), which is reported to inhibit M2 MΦ polarization. Therefore, we hypothesize that delayed fracture repair in splenectomized mice is mediated by SCs via Icam-1 to inhibit M2 MΦ polarization.

Results: Mice received splenectomy showed decreased woven bone area, callus volume, bone strength, and decreased number of MPCs, osteoblast progenitor cells and blood vessels after fracture. Splenectomy decreased the total MΦ and M2 MΦ, but not M1 MΦ. Fractured mice with splenectomy treated with IL4/IL13 at D3 by local injection have increased M2 MΦs in the callus, callus volume and bone strength. Splenectomized mice have increased number of p16+ SCs in callus evidenced by qPCR and flow. qPCR screening of SASPs and Notch signal ligands associated with MΦ polarization showed that Icam-1 expression dramatically increased in p16+ callus SCs, but not in p16- callus cells. Fractured mice with splenectomy treated with Icam-1 inhibitor, methimazole at D3 have increased M2 MΦ number and genes expressions (Il4 and Arginase) in callus, decreased Icam-1 expression in p16+ cells, and increased callus volume and bone strength.

Disucussion: In present study, we confirmed that splenectomized mice have decreased MΦs, mainly M2 MΦs. M2 MΦ is well known to benefit the fracture repair by producing growth factor, cytokines and chemokines. To elucidate the importance of M2 MΦ in fracture repair of splenectomized mice, we induced the M2 MΦs in splenectomized mice by local injection of IL4/IL13 and found that IL4/IL13 treatment enhanced the fracture repair in them. To investigate the mechanism of decreased M2 MΦs, we screened the expression levels of SASPs and Notch ligands that are related to MΦ polarization and found that Icam-1 was the most increased gene in SCs, but not in non-SCs. Icam-1 from osteoblasts was reported to inhibit osteoclast recruitment in bone, but has not been studied in bone fracture yet. Importantly, Icam-1 is to inhibit M2 MΦ polarization. We demonstrate that Icam-1 inhibitor specifically suppressed the Icam-1 expression in SCs and subsequently increased M2 MΦ in callus and enhanced fracture repair. Thus, our data suggested that SC represents an important source of Icam-1 that impairs fracture repair by decreasing M2 MΦ infiltration in splenectomized mice. Although SCs were proved to be major source of Icam-1 in callus of splenectomized mice, we are not willing to deplete SCs by pharmatheutical or genetic approaches, because the overall contribution of SCs to injury healing is still controversial.

Title: **Senescent cells promote the disease progression of multiple myeloma from its asymptomatic precursor stages**

Presenting Author: Hengwei Zhang

Co-Authors: Thomas Conley, Kyle Strife, Lianping Xing

Lab PI / Mentor: Hengwei Zhang, Brea Lipe

Abstract (3500 characters or 500 words Limit)

Introduction: Multiple Myeloma (MM) is an incurable cancer of plasma cells causing significant morbidity and mortality. MM arises from asymptomatic precursor stages, monoclonal gammopathy of undetermined significance (MGUS) and/or smoldering MM (SMM). Plasma cell dyscrasias are aging related diseases and senescent cells (SCs) accumulate during aging, but neither the mechanisms by which SCs contributes to these diseases nor the mechanisms that drive disease progression to MM are fully known. We found that SCs not only promoted CD138+ plasma cells (CD138+ cells) survival, growth, and transition, but also induced bone erosion after co-transplantation with CD138+ cells. CXC chemokine receptor 2 (CXCR2) is a cancer stem cell-like marker. We found that CXCR2+ SCs were significantly increased in bone marrow of patients with progressed MGUS/SMM. Therefore, we hypothesize that CXCR2+ SCs in the bone environment of SMM/MGUS/MM patients could promote MM disease progression by supporting growth, expansion and transition of CD138+ plasma cells, which can be inhibited with senolytic drug.
Results: Co-culturing CD138- bone marrow stromal cells (CD138- cells) with CD138+ cells (10:1), both from MGUS/SMM patients, promotes the cell survival and growth of CD138+ cells in vitro. For the establishment of an in vivo pre-MM mouse model, sequential co-transplantation of CD138- and CD138+ (10:1) from patients with MGUS/SMM into 2 subsequent NSG mice results in clear bone erosion, a gold standard of MM-associated bone lesion, in tibias. RNAseq and qPCR revealed increased expression of cellular senescence gene (p16) in CD138- cells of SMM patients and SCs existence was further confirmed by SA-b-gal staining of cultured CD138- stromal cells from MGUS/SMM patients. p16 expression in our mouse model is closely correlated with the areas of bone erosion. To understand the cellular mechanism, a human mesenchymal stem cell line (hMSCs) induced by H_2O_2 for cell senescence promoted the survival and growth of CD138+ cells when co-cultured with CD138+ cells, and promoted the transition of CD138+ cells from CD138- cells when co-cultured with CD138- cells. Depletion of SCs by senolytic drugs in mice decreased bone erosion in tibias of our disease model. Recent scRNAseq analysis revealed two sub-clusters of SCs expressing CXCR2 with a high-secretory profile by bioinformatical analysis in the bone of aged mice. CXCR2+ SCs, but not CXCR2- SCs significantly increased in the stromal cells of mice from our animal model and highly expressed IL8 and IL10.
Discussion: We demonstrate the successful establishment of a pre-MM mouse model to study the mechanisms of disease progression of MM from MGUS/SMM. With our newly established animal model, our study investigated the mechanisms by which SCs promote MM and infer that the CXCR2+ SC sub-cluster may be responsible for the progression of MGUS/SMM to MM. Importantly, there is currently no approved therapy to treat MGUS/SMM. Our study indicates that depletion of SCs in MGUS/SMM patients may offer a new target to prevent this “transformation” to MM.

Title: **Pharmacological Inhibition of the TAM Receptors Decreases Mesenchymal Stromal Cell Efferocytic Ability**

Presenting Author: Jane Zhang

Co-Authors: Emily R. Quarato, Yuko Kawano, Noah Salama, Daniel K. Byun, Eric Zhu, Chunmo Chen, Jane L. Liesveld, Roman A. Eliseev, and Laura M. Calvi

Lab PI / Mentor: Laura M. Calvi/Emily R. Quarato

Abstract (3500 characters or 500 words Limit)

Bone marrow derived mesenchymal stromal cells (MSCs) are a population with multi-lineage differentiation capacity and play an important role in immunomodulation of the bone marrow niche. While macrophages are the primary phagocytes within the bone marrow, previous studies have shown that MSCs can act as facultative phagocytes in embryos when macrophages are impaired. Recently, our laboratory has further explored the role of MSCs as non-professional phagocytes and found that low levels of MSC efferocytosis are beneficial for bone formation, while high levels actually shift these cells towards a senescent phenotype. Because increased senescence is detrimental to MSCs and the bone marrow microenvironment, we aimed to block this activity. Through RNA sequencing, we found that MSC efferocytosis is regulated in part by the TAM receptors (Axl, MerTK, and Tyro3), a group of receptor tyrosine kinases that utilize bridging molecules such as Gas6 and Protein S. Since Axl expression was highest in MSCs and regulated by efferocytosis, we tested MSCs from mice lacking this receptor. Genetic Axl loss reduced but did not completely block levels of MSC efferocytosis, suggesting that while Axl is likely the dominant efferocytosis receptor in MSCs, other receptors are also involved.

We next aimed to assess the efficacy of a pharmacological inhibition of all TAM receptors. This approach not only could add to the mechanistic understanding of MSC efferocytosis, but also allow for clinical translation. Inhibitors for Axl (TP0903), MerTK (UNC2025), and all three TAM receptors (LDC1267, a pan-inhibitor) were chosen because of their specificities for the targeted receptors and feasibility of clinical translation. General viability after treatment was assessed on ST2 cells, a bone marrow-derived stromal cell line, and primary human MSCs (hMSCSs) using microscopy and flow cytometry. Cells were then incubated with primary end-stage neutrophils (PMNs) and viability and efferocytic capacity were assessed using fluorescent microscopy and flow cytometry. Drug treatment toxicity was low in the tested concentrations of TP0903, UNC2025, and LDC1267. In cultures treated with higher concentrations of the Axl inhibitor (TP0903) and Pan-TAM inhibitor (LDC1267), an increased amount of cell remnants and debris was seen in the media using microscopy in both ST2 and hMSC cultures. This accumulation may reflect a decreased ability of MSCs to clear debris and indicate that treatment may block efferocytic pathways. PMN uptake by MSCs was significantly reduced when cells were pre-treated with the highest concentration of LDC1267 for 48 hr. Mean Fluorescent Intensity (MFI), a measure of efferocytic efficiency, was also lower with the pan-TAM inhibitor (LDC1267) treatment. Our findings suggest that inhibition of the TAM receptors has the potential to pharmacologically reduce MSC efferocytosis in vitro, which may have important clinical significance in the treatment of states of excess MSC efferocytosis, such as myelodysplastic syndromes and response to myeloablative regimens. Future directions of this project include identifying a narrower range of drug concentrations to determine maximum efficacy, combining the pan-TAM inhibitor with the Axlko in vitro to assess the contribution of other receptors in MSC efferocytosis, and directly assessing the role of treatment on cellular senescence.

Title: **Investigating the effects of type III/I collagen ratios in hydrogel models of tendon injury**

Presenting Author: Victor Zhang

Co-Authors: Raquel Ajalik and Rahul Alenchery

Lab PI / Mentor: Hani Awad and James McGrath

Abstract (3500 characters or 500 words Limit)

Like many other tissues in the body, tendons exhibit complex responses to injury and wound healing. In tendon, proper regeneration of functional, pre-injury tissue requires the coordination of tissue and matrix remodeling, inflammatory responses, and vascular and neuronal responses, among other processes. Tendon remodeling heavily influences the levels of numerous extracellular matrix components including collagen, which comprises the majority of the dry weight of tendon. In healthy tendon, more than 90% of the collagen ECM is type I. However, during post-injury remodeling levels of type III collagen rise increasing the type III to type I collagen ratio. This rise in III to I ratio is well established and is characteristic of injured or pathological tendon. It is believed that in long-term pathological states such as tendinopathy, the III to I ratio remains increased as the normal remodeling of type III to type I collagen does not occur.

While this clinical correlation is widely accepted, the mechanism by which an altered collagen composition affects tendon healing and regeneration is poorly understood. Studies have demonstrated the molecular differences between type I and type III collagen while also providing insights into how they might affect each other in processes such as cross-linking and fibril formation. Still, the link between these fundamental properties of collagen and the eventual clinical presentations of tendinoapthy and fibrovascular scar following acute injury remain largely a mystery. We have planned several experiments to investigate this link between altered tendon collagen composition and its pathology. The goal being to further elucidate the changes in structure and property of a tendon-like hydrogel matrix with changing collagen III to I ratio in order to better understand how these changes might affect the biological processes involved in tissue regeneration such as cell signaling and immune cell recruitment and migration.

To investigate the basic structure of these gels, experiments are planned to roughly determine the hydrogel pore size and network structure. Using small, fluorescent beads we can achieve an estimate of the pores in the hydrogel by seeing what size beads the hydrogel captures and restrains while allowing smaller beads to move around. This data will be supplemented by information gathered from electron micrographs. These fluorescent beads will also be used to determine the viscoelastic properties of these hydrogels through microrheology techniques and particle tracking. Together, this information will provide a survey of the fundamental properties of these hydrogels and if they change with the type III to I ratio. This will inform further functional assays such as diffusion exerpiments utilizing fluorescence recovery after photobleaching (FRAP) and other techniques as well as experiments with primary human tenocytes seeded in the hydrogels. These experimnets will ultimately explore the effect of collagen III/I ratio on the processes involved with tendon healing and fibrovascular scar formation.

Title: **Cantilever Bending of Murine Femoral Necks**

Presenting Author: Emma Knapp

Co-Authors:

Lab PI / Mentor: Dr. Hani Awad

Abstract (3500 characters or 500 words Limit)

Fractures in the femoral neck are a common occurrence in individuals with osteoporosis. Many mouse models have been developed to assess disease state and therapies, with biomechanical testing as a primary outcome measure. However, traditional biomechanical testing focuses on torsion or bending tests applied to the midshaft of the long bones. This is not typically the site of high risk fractures in osteoporotic individuals. Therefore, we developed a biomechanical testing protocol that tests the femoral necks of murine femurs in cantilever bending loading to better replicate the types of fractures experienced by osteoporosis patients. Since the biomechanical outcomes are highly dependent on the flexural loading direction relative to the femoral neck, we created 3D printed guides to maintain a femoral shaft at an angle of 20° relative to the loading direction. The new protocol streamlined the testing, reduced variability in alignment (21.6° ± 1.5°, COV=7.1%, n=20) and improved reproducibility in the measured biomechanical outcomes (average COV=26.7%). The new approach using the 3D printed guides for reliable alignment of the specimen improves rigor and reproducibility by reducing the measurement errors due to specimen misalignment, which should minimize sample sizes in mouse studies of osteoporosis.


1850
MELIORA
UR
MEDICINE